

Technische Universität München
Fakultät für Medizin

Characterization of the radiation response of Glioblastoma cells with different radiosensitivities

Anna Kirstein

Vollständiger Abdruck der von der Fakultät für Medizin
der Technischen Universität München
zur Erlangung des akademischen Grades
einer Doktorin der Naturwissenschaften (Dr. rer. nat.)
genehmigten Dissertation.

Vorsitzende: Prof. Dr. Gabriele Multhoff

Prüfende der Dissertation:

1. Prof. Dr. Thomas E. Schmid
2. Prof. Dr. Björn Menze

Die Dissertation wurde am 25.08.2021 bei der Technischen Universität München
eingereicht und durch die Fakultät für Medizin am 12.04.2022 angenommen.

TABLE OF CONTENTS

Abstract	IV
Zusammenfassung	V
List of Abbreviations	VI
1. Introduction	1
1.1 Glioblastoma multiforme	1
1.1.1 Treatment of GBM	3
1.1.1.1 TMZ and MGMT	6
1.2 Lomeguatrib	9
1.3 Radiation	10
1.4 Radiation Biology	13
1.5 Aim	17
2. Materials and Methods	18
2.1 In vitro	18
2.1.1 Cell Culture	18
2.1.2 Cell irradiation	19
2.1.3 Lomeguatrib treatment	19
2.1.4 Doubling time calculation	20
2.1.5 Colony-forming assay (CFA)	20
2.1.6 Cell cycle flow cytometry	21
2.1.7 γ H2AX foci	22
2.1.8 Caspase 3/7 flow cytometry	23
2.1.9 Migration	23
2.2 Molecular biology	24

TABLE OF CONTENTS

2.2.1	MethyQESD.....	24
2.2.1.1	qPCR efficiency	25
2.3	Protein techniques	26
2.3.1	Harvesting of protein samples.....	26
2.3.2	Protein concentration determination.....	27
2.3.3	SDS-PAGE.....	28
2.3.4	Transfer.....	28
2.3.5	Immunological detection	29
2.4	In vivo experiments	29
2.4.1	Animal Model.....	29
2.4.2	Whole-body irradiation	30
2.4.3	Subcutaneous injection of tumor cells.....	30
2.4.4	Tumor volume measurement.....	31
2.4.5	Lomeguatrib administration and radiation therapy.....	31
2.4.5.1	Radiation therapy at Gulmay irradiation device.....	32
2.5	Statistics.....	33
3.	Results	34
3.1	Comparison of pre- vs. post-plating in clonogenic survival.....	34
3.2	Radiosensitivity of different GBM cell lines.....	36
3.3	MGMT promoter methylation and MGMT protein expression.....	37
3.4	MGMT protein inhibition using Lomeguatrib.....	39
3.5	Cell proliferation.....	40
3.6	Cell survival upon lomeguatrib treatment.....	41
3.7	Lomeguatrib on cell cycle distribution	42
3.8	MGMT expression, ionizing radiation, and lomeguatrib	43
3.9	Clonogenic cell survival upon combined lomeguatrib treatment.....	44
3.10	Cell cycle distribution after lomeguatrib and radiation.....	47

TABLE OF CONTENTS

3.11	DNA damage and DNA repair	51
3.12	Apoptosis.....	57
3.13	Migration capacity of GBM cell lines.....	59
3.14	Tumor growth delay.....	62
4.	Discussion	74
4.1	Identification of MGMT expressing cell lines.....	75
4.2	Optimal MGMT inhibition using lomeguatrib	76
4.3	Lomeguatrib does not affect cell proliferation and cell survival.....	77
4.4	High dose lomeguatrib decreases radiation-induced G2/M arrest.....	78
4.5	Lomeguatrib enhances radioresistance at high lomeguatrib doses.....	80
4.6	Radiation-induced DNA damage is not affected by lomeguatrib	82
4.7	Lomeguatrib does not affect radiation-induced apoptosis	83
4.8	Migration is suppressed upon high dose lomeguatrib and irradiation	85
4.9	Lomeguatrib does not affect tumor growth <i>in vivo</i>	87
5.	Conclusion and Outlook.....	90
6.	References	92
	List of Figures.....	106
	List of Tables	108
	Appendix	109
	Publications	111
	Acknowledgments	112

Abstract

Glioblastoma multiforme is a devastating diagnosis resulting in death within 15 months. Treatment resistance, recurrence, and relapse remain critical challenges yet to be overcome. Therefore, identifying molecular markers and understanding the underlying mechanisms of chemo- and radioresistance is crucial to improve therapy and treatment outcome. Promoter methylation status of the O⁶-methylguanine-DNA-methyltransferase (MGMT) is an established biomarker to predict chemotherapy treatment outcome. While patients with a methylated promoter benefit from chemotherapy, those with an unmethylated promoter fail chemotherapy. Since studies investigating the effect of MGMT on radiotherapy are limited this study aimed to improve glioblastoma radiotherapy by inhibiting MGMT to enhance radioresponse. The findings of this study demonstrate a strong dose-dependent effect of lomeguatrib in combination with ionizing radiation. While low concentrations increased radiosensitivity, high concentrations increased radioresistance, reduced the radiation-induced G2/M arrest, and decreased migration. Tumor growth was not affected by lomeguatrib upon a single dose of 20 mg kg⁻¹. In conclusion, this work provides the first insight into the effects of the MGMT inhibitor lomeguatrib and lays the foundation for further investigations to identify the underlying role of MGMT during radiotherapy to eventually improve a personalized therapy regime in the future.

Zusammenfassung

Glioblastoma multiforme ist noch immer eine verheerende Diagnose, welche innerhalb von 15 Monaten nach der Diagnose zum Tod führt. Therapieresistenz und Rezidive sind nach wie vor kritische Hürden, die es zu bewältigen gilt. Die Identifizierung molekularer Marker und das Verständnis zugrundeliegender Mechanismen der Chemo- und Radioresistenz sind entscheidend für die Verbesserung der Therapie und der Behandlungsergebnisse. Der Methylierungsstatus der Promoterregion der O⁶-Methylguanin-DNA-Methyltransferase (MGMT) ist ein etablierter Biomarker zur Vorhersage des Behandlungserfolgs bei Chemotherapie. Patienten mit einem methylierten Promoter profitieren von der Chemotherapie, während Patienten mit einem nicht methylierten Promoter keine Verbesserung durch Chemotherapie haben. Da es nur wenige Studien gibt, die sich mit den Auswirkungen von MGMT auf die Strahlentherapie befassen, war das Ziel dieser Arbeit, die Strahlentherapie des Glioblastoms durch Inhibierung des MGMTs zu verbessern und das Ansprechen auf die Strahlentherapie zu erhöhen. Die Ergebnisse dieser Studie deuten auf eine starke Dosisabhängigkeit von Lomeguatrib in Kombination mit Bestrahlung hin. Während niedrige Konzentrationen die Strahlenempfindlichkeit erhöhten, steigerten hohe Konzentrationen die Strahlenresistenz, reduzierten den strahleninduzierten G2/M Arrest und verringerten das Migrationsverhalten. Das Tumorwachstum wurde durch eine Einzeldosis von 20 mg kg⁻¹ nicht beeinflusst. Zusammenfassend lässt sich sagen, dass diese Arbeit einen ersten Einblick in die Wirkung des MGMT-Inhibitors Lomeguatrib bietet. Dies ist die Grundlage für weitere Untersuchungen zur Identifizierung der Rolle von MGMT während der Strahlentherapie, um ein personalisiertes Therapiesystem anbieten zu können.

List of Abbreviations

AIC	5-amino-imidazole-4-carboxamide
APS	Ammonium persulfate
BSA	Bovine serum albumin
CCNU	1-(2-chloroethyl)-3-cyclohexyl-1-nitrosourea, Lomustine
CFA	Colony forming assay
CNS	Central nervous system
CT	Computer tomography
DNA	Deoxyribonucleic acid
DNA-PKcs	DNA-dependent protein kinase catalytic subunit
DSB	Double-strand break
dTTP	Deoxythymidine triphosphate
ECM	Extracellular matrix
EGFR	Epithelial growth factor receptor
EOR	Extent of resection
FACS	Fluorescence-activated cell sorting
FCS	Fetal calf serum
FDA	Food and Drug Administration
GBM	Glioblastoma multiforme
Gy	Gray
HR	Homologous recombination
IDH	Isocitrate dehydrogenase
i.p.	intraperitoneally
J	Joule
KPS	Karnofsky Performance Status
LET	Linear energy transfer

List of Abbreviations

LM	Lomeguatrib
LOH	Loss of heterozygosity
LQM	Linear quadratic model
MGMT	O ⁶ -methylguanine DNA-methyltransferase
MMP	Matrix Metalloproteinase
MMR	Mismatch Repair Pathway
MRI	Magnetic resonance imaging
MTIC	3-methyl-(triazen-1-yl) imidazole-4-carboximide
NaCl	Sodium chloride
NCCN	National Comprehensive Cancer Network
NHEJ	Non-homologous end-joining
NOS	not otherwise specified
PE	Plating efficiency
PTEN	Phosphatase and tensin homolog
qPCR	Quantitative polymerase-chain-reaction
RB	Retinoblastoma
RNA	Ribonucleic acid
ROS	Reactive oxygen species
RT	Radiotherapy
SAM	<i>S</i> -adenosylmethionine
SBRT	Stereotactic radiosurgery
s.c.	Subcutaneous
SDS	Sodium dodecyl sulfate
SF	Survival fraction
SSB	DNA single-strand break
TBS-T	Tris-buffered saline with Tween-20
TGF- β	Transforming growth factor- β

List of Abbreviations

TMZ	Temozolomide
TTF	Tumor treating fields
O ⁶ -BG	O ⁶ -benzylguanine
O ⁶ -MG	O ⁶ -methylguanine
PET	Positron emission tomography
WHO	World Health Organization

1. Introduction

Cancer is one of the leading causes of death worldwide with 14 million cases diagnosed and 8.2 million people dying each year [1]. Tumors of the central nervous system (CNS) account for 2 % of all diagnosed cancers with 256,000 new cases per year and are the 17th most common cancer [2]. The yearly incidence rate of 4 – 8 cases per 100,000 worldwide is relatively low, however, mortality rates are significantly high making it the 12th most cause of cancer-related deaths. The most common and most aggressive malignancy of the CNS is Glioblastoma multiforme (GBM) [1].

1.1 Glioblastoma multiforme

The World Health Organization (WHO) published a classification of tumors of the central nervous system in 2007 [3] and an updated version in 2016 [4]. The updated version is not only based on microscopic analyses of hematoxylin and eosin-stained sections, immunohistochemistry of lineage-associated proteins, and characterization of ultrastructures but also includes molecular markers to define a more detailed classification [4]. GBM is classified as a grade IV diffuse astrocytic tumor of the CNS presenting diffuse infiltration into surrounding tissues with great destructive potential, uncontrolled cellular proliferation, genomic instability, as well as intense resistance to chemo- and radiotherapy [5]. Important characteristics of GBM include nuclear atypia, high mitotic activity, vascularization, necrosis, pleomorphism, and microvascular atypia [4].

The more recently published version of the WHO classification now includes a more detailed differentiation towards a different origin of primary and secondary

GBM: GBM is subdivided into isocitrate dehydrogenase (IDH)-wildtype, IDH-mutant and not otherwise specified (NOS) [4].

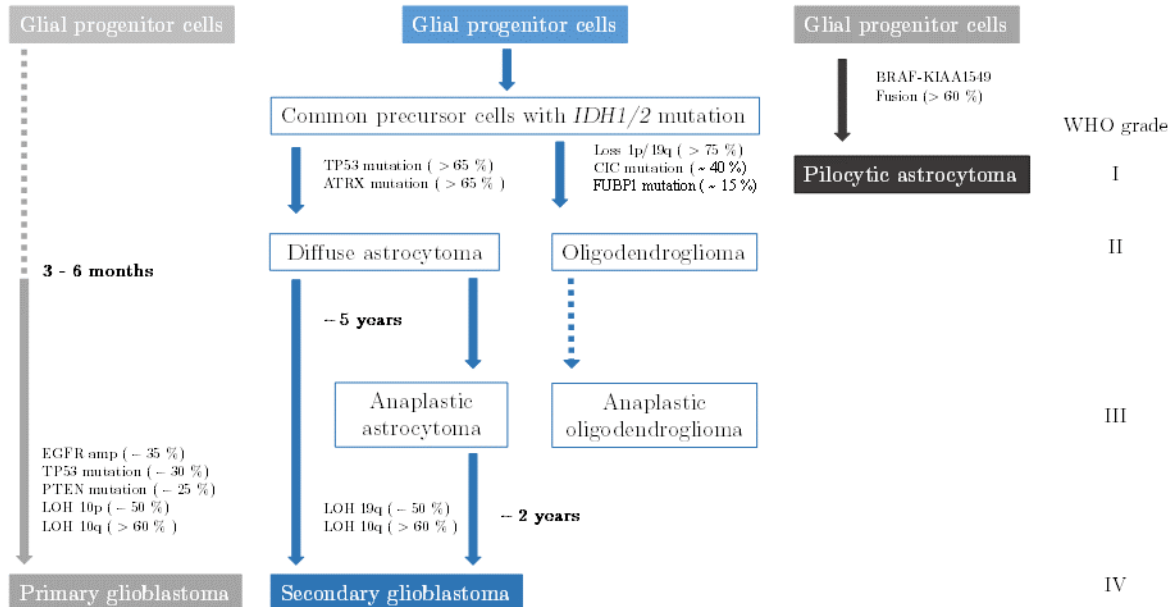


Figure 1.1: Development of GBM.

Shown is the course to primary and secondary glioblastoma with its characteristic mutations. Figure adapted from [1].

IDH-wildtype or primary GBM account for 90 % of all glioblastoma, which rapidly develops from glial progenitor cells within three to six months (Figure 1.1). The median overall-survival is 15 months with a median age at diagnosis of 62 years [4; 6; 7]. The unique mutation pattern includes EGFR amplification [8], PTEN mutation [7; 9; 10], and loss of chromosome 10 [7-9]. In contrast, IDH-mutated or secondary glioblastoma only accounts for less than 10 % of all GBM but develops from low-grade astrocytomas (WHO grade II) and anaplastic astrocytomas (WHO grade III) over several years (Figure 1.1) [10; 11]. The median overall-survival is 31 months with a median age at diagnosis of 44 years [4; 6; 7; 11]. Characteristic mutations include TP53 mutation [1; 7; 8], loss of heterozygosity (LOH) on chromosomes 10q and 19q [1; 7-9; 12], deletion of p16 [7; 13], and RB inactivation [7; 13; 14]. NOS glioblastoma is either primary or secondary GBM but due to the patient's age, a full evaluation of

the IDH status cannot be performed or gives inconclusive results [4]. Furthermore, GBM presents intratumoral heterogeneity, which includes epigenetic lesions as well as a putative stem cell subpopulation [2]. Although CD133 is not fully accepted as the ultimate GBM stem cell marker, a significantly higher expression has been found in primary, compared to secondary GBM [15] contributing to the extensive resistance to chemo- and radiotherapy of primary GBM.

1.1.1 Treatment of GBM

Treatment of GBM always includes an interdisciplinary approach. The first tool to diagnose an alleged GBM makes use of imaging modalities, such as magnetic resonance imaging (MRI), computer tomography (CT), or positron emission tomography (PET) [16]. MRI is the imaging gold standard giving the necessary details concerning the tumor location as well as adjacent anatomical landmarks, such as sensory and motor cortices to precisely plan surgical resection of the gross tumor volume. However, grade of malignancy, exact tumor delineation, and differentiation between recurrent tumors and necrotic tissues present limitations of this imaging modality [17]. PET, in contrast, gives more insight on the heterogeneity, grade of malignancy as well as correct delineation of the tumor. It allows a more differential and noninvasive diagnosis due to the administration of a radioactive tracer [17]. The most commonly used radiotracer is 18F-2-fluoro-2-deoxy-D-glucose (18F-FDG) [17], which is taken up by glucose-consuming tissues. Since high-grade tumor cells are characterized by a high glucose metabolism due to their increased proliferation rate, 18F-FDG accumulates in tumors and can be visualized by a PET scanner. Low-grade tumors in contrast are often hypometabolic lesions and can be differentiated from high-grade tumors due to low glucose uptake [17]. Since normal brain tissue also has a high glucose metabolism imaging of cerebral gliomas has its limitations. Therefore,

alternative amino acid PET tracers have been developed such as ^{11}C -methylmethionine (^{11}C -MET), O-(2-[^{18}F]-fluoroethyl)-L-tyrosine (^{18}F -FET), and 3,4-dihydroxy-6-[^{18}F]-fluoro-L-phenylalanine (^{18}F -FDOPA) [17]. These tracers are characterized by low uptake in the normal grey matter as well as in inflammatory tissues allowing for a more precise surgery planning and exact radiation treatment planning after surgery. Follow-up imaging using PET enables differentiation between pseudoproggression – due to chemoradiation, recurrence, and progression. Despite all advantages, PET is not yet included in the standard treatment of care for GBM but due to rapid development of new radiotracers PET is expected to be included into the routine of GBM diagnosis in the near future.

After the diagnosis of GBM surgical resection will follow. The ultimate goal of surgical resection is the maximal safe resection to relieve symptoms including headaches, vomiting, visual impairments, nausea, and somnolence [18]. However, complete resection is almost impossible due to the high invasive characteristic and extensive vascularization of GBM into the surrounding healthy brain tissue and makes recurrence highly possible [5]. Consequently, the extent of resection (EOR) will determine treatment outcome as a higher EOR is associated with prolonged survival without postoperative neurological morbidities [19]. Post-operative MRI is usually performed within 72 hours after surgery to determine the EOR. Further, a pathological examination confirms the diagnosis of GBM and allows an investigation of molecular markers such as the methylation status of the promoter region of the O6-methylguanine DNA-methyltransferase (MGMT) and IDH status, which are decisive for the further treatment course.

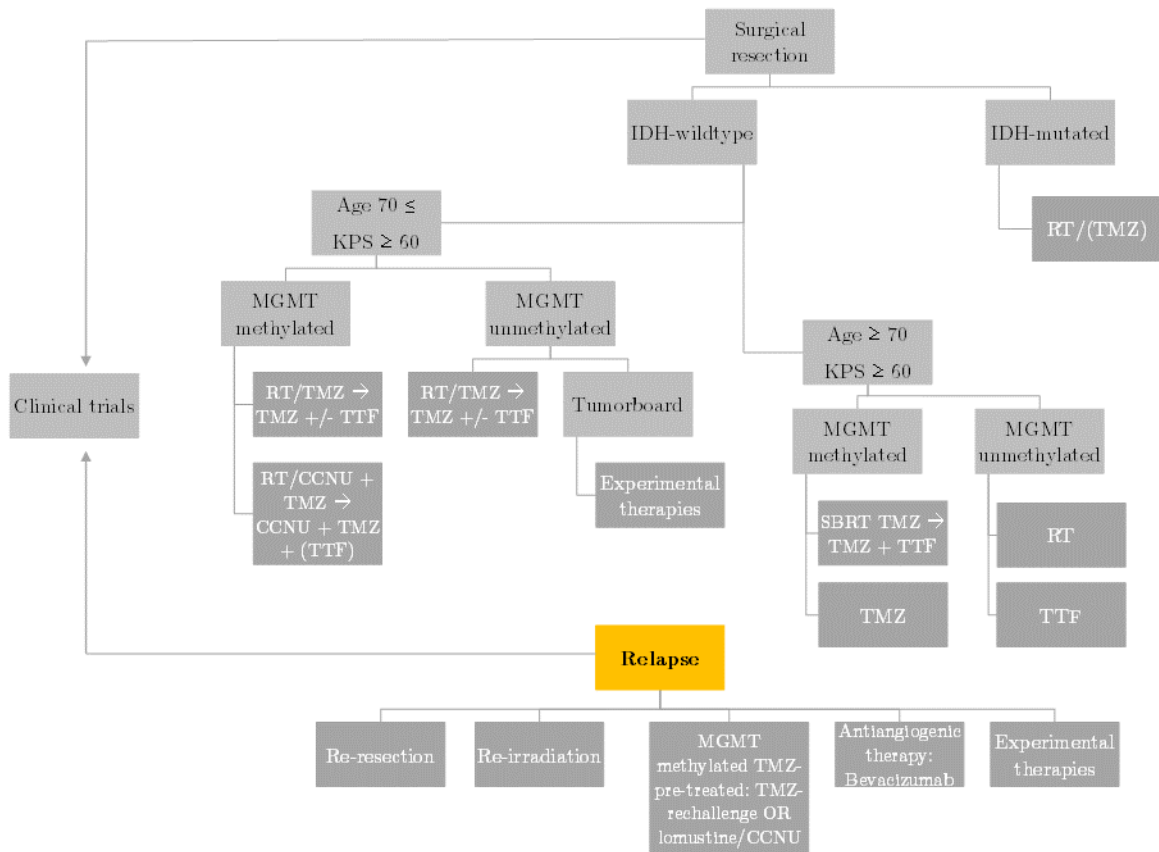


Figure 1.2: Treatment scheme for Glioblastoma multiforme.

Shown is the standard therapy of newly diagnosed GBM. IDH: isocitrate dehydrogenase; KPS: Karnofsky Performance Status; SBRT: stereotactic radiosurgery; MGMT: O6-methylguanine-DNA-methyltransferase; RT: radiotherapy; TMZ: temozolomide; TTF: tumor-treating fields; CCNU: Lomustine. Figure adapted from [20].

In dependence on the IDH and MGMT status, the Karnofsky Performance Status (KPS) as well as the age of the patient, alternative treatment options may be considered. Figure 1.2 gives an overview of possible alternative treatment options. For patients with an IDH wildtype and a methylated MGMT status standard treatment continues with radiotherapy concomitant with temozolomide (TMZ). In contrast, IDH mutated and MGMT unmethylated patients receive radiotherapy only and TMZ cycles can be omitted. Further, MGMT unmethylated patients may be offered experimental therapies as well as participation in clinical trials.

In 2011 the Food and Drug Administration (FDA) approved the first tumor treating fields (TTF) device and was also added to the National Comprehensive

Cancer Network (NCCN) guidelines for the treatment of glioblastoma [21]. TTF devices deliver low-intensity, intermediate-frequency (100 – 300 kHz) alternating electric fields to the patient's scalp via transducer arrays [21; 22]. These electric fields target dividing glioblastoma cells and cause apoptosis and mitotic arrest [22]. In a randomized phase III clinical trial from 2009 – 2014 TTFs showed beneficial effects in terms of progression-free survival and overall survival after standard radiochemotherapy [22].

Relapse and recurrence are highly possible during the first 6 months after treatment completion [20]. For these patients re-resection, re-irradiation, and further cycles of chemotherapy might be considered. Alternative blood-brain-barrier crossing chemotherapeutic agents such as lomustine (CCNU) or carmustine can be administered but also TMZ rechallenge is possible [20]. However, mostly MGMT methylated patients benefit from additional chemotherapy cycles.

1.1.1.1 TMZ and MGMT

Since 2005 the chemotherapeutic agent temozolomide (TMZ) is given simultaneously to radiotherapy in daily oral doses. During radiotherapy patients receive 75 mg cm⁻² per day for six weeks and after four weeks the dose is increased to 150 mg cm⁻² given in cycles for five days every 28 days. Every two to three cycles MRI is performed to follow up on possible relapses and to monitor changes in the resection cavity respectively in the surrounding brain tissue [4].

Temozolomide is a derivative from an imidazotetrazine. As a prodrug, it is stable at acidic pH and therefore is suitable for oral administration since it survives the gastric acid [23]. At neutral to basic pH found e.g. in brain tumors, it rapidly hydrolyzes [23]. Spontaneous ring-opening leads to the formation of the active alkylating metabolite 3-methyl-(triazene-1-yl) imidazole-4-carboximide (MTIC).

However, MTIC is unstable at a pH below 7 but stable in alkaline environments [24]. Therefore, MTIC is hydrolyzed to form 5-amino-imidazole-4-carboxamide (AIC) and methyl diazonium ions that produce methyl adducts via the reaction of nucleophilic sites on the DNA [23]. These nucleophilic sites include the N7 and O6 position of the base guanine as well as the N3 position of the base adenine [23; 25]. In regards to the importance of MGMT in GBM, only the O6 position of the base guanine as a target for DNA methylation by TMZ is the most important site for its anti-cancer activity [24; 26].

Figure 1.3 illustrates the mode of action of TMZ in the absence of MGMT.

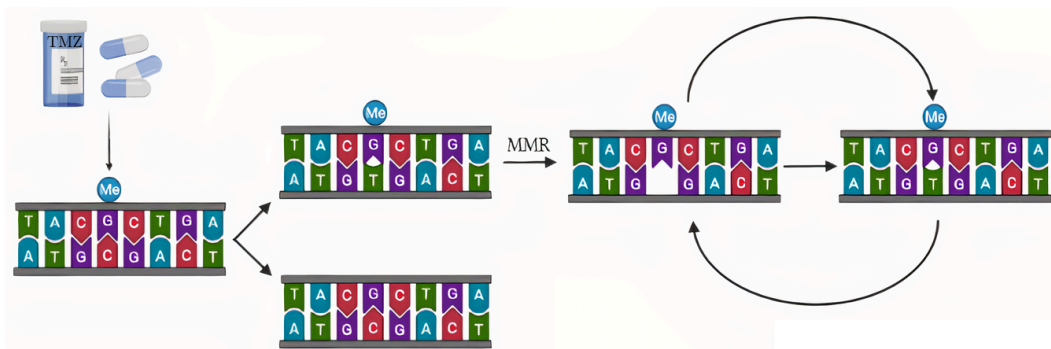


Figure 1.3: Temozolomide mode of action.

Shown is the mode of action of temozolomide in the absence of MGMT. Created with BioRender.com.

The methyl adducts are added to 5 % to the O6 position of guanine [24]. During the completion of DNA replication the methylated base guanine, O6-methylguanine (O6-MG), mismatches with thymine creating a wobble base pair. The DNA mismatch repair (MMR) pathway recognizes this mismatch via mismatch recognition complexes [27]. Accessibility to the wobble base pair is created by single-stranded DNA nicks. The mismatched base thymine is then digested by the 5'-3' exonuclease I and the gap is filled by the DNA polymerase δ , however, with another thymine [27]. Due to continuous cycles of thymine deletion and insertion depletion of deoxythymidine triphosphate (dTTP) eventually leads to a lack in DNA synthesis and subsequent cell death due to DNA double-strand breaks [27].

In Figure 1.4 the mode of action of temozolomide in the presence of MGMT is shown.

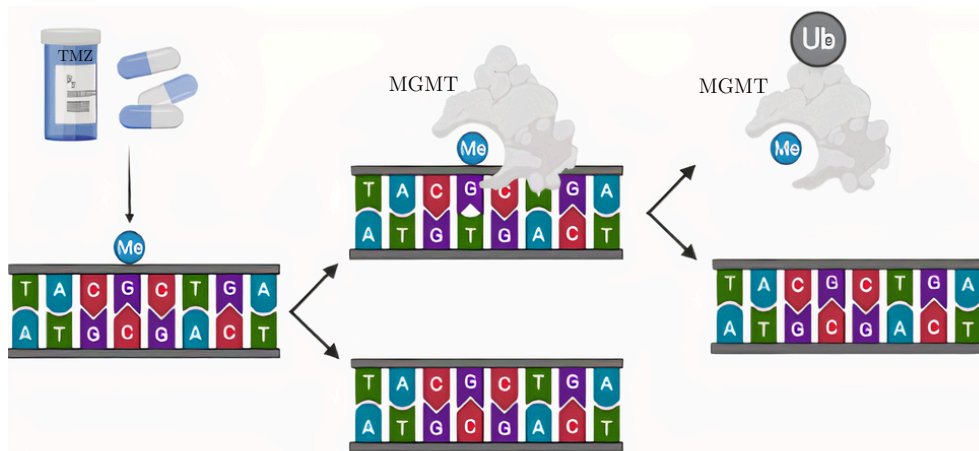


Figure 1.4: Mode of action of temozolomide in the presence of MGMT. Shown is the mechanism of MGMT counteracting TMZ efficacy. Created with BioRender.com.

MGMT is a protein involved in the mismatch repair pathway protecting cells from cell death due to the aforementioned thymine deletion and insertion circles due to the addition of aberrant methyl adducts. MGMT specifically removes methyl groups from the O6 position at the base guanine and transfers it to a cysteine residue (Cys145) in its active site [28]. This leads to a conformational change ultimately leading to its degradation, since the cysteine site cannot be regenerated [29]. As one MGMT protein can remove only one methyl group the number of methyl groups that can be removed is closely correlated to the number of MGMT proteins present in the cell. This reaction is a suicide reaction and therefore MGMT is a protein and not an enzyme [28]. In the scenario shown in Figure 1.4, the aberrant methyl group that is removed by MGMT was added by TMZ on purpose; hence, MGMT counteracts the therapeutic efficacy of TMZ promoting treatment failure.

Hegi et al. published in 2005 that the MGMT promoter methylation status is an important prognostic marker to determine TMZ treatment outcome [30]. Those patients receiving radiotherapy concomitant to temozolomide and having a methylated MGMT promoter showed a significantly increased overall survival

compared to the MGMT unmethylated patients [30]. Ever since the MGMT promoter methylation status is routinely investigated in every patient as unmethylated patients have no or only little benefit from TMZ treatment.

Current research now focuses on finding new treatment options to deplete MGMT. The very promising substance O6-benzylguanine (O6-BG), which has antineoplastic activity is a guanine analog inactivating MGMT [31; 32]. O6-BG reacts with the cysteine residue Cys145 of the MGMT active site and transfers its benzyl moiety irreversibly to the cysteine thiol [33]. The resulting S-benzyl derivative prevents the reaction with an O6-alkylated guanine residue in the DNA ultimately leading to unrepaired DNA lesions [33]. In vitro experiments showed enhanced cytotoxicity to alkylating agents in the presence of O6-BG and further depletion of MGMT [34]. Dolan et al. further showed in vivo that low doses of O6-BG completely depleted MGMT, but higher doses are required for long-lasting effects increased acute toxicities particularly to the hematopoietic system [34]

O6-BG was further involved in phase I [35] and phase II [36] clinical trials. Despite an MGMT depletion in blood samples of the patients after O6-BG administration [35], no TMZ sensitization was observed [36]. Further, severe myelosuppression was commonly identified in patients with recurrent, TMZ-resistant GBM and was therefore never included in the standard therapy for GBM [35; 36].

1.2 Lomeguatrib

O(6)-(4-bromophenyl)guanine, also known as PaTrin-2 or lomeguatrib is a potent and specific MGMT inhibitor first synthesized by McElhinney et al. in 1998 [33]. In their study they aimed to synthesize O6-benzylguanine analogs, as they generated several guanine derivatives by reacting purine quaternary salts with alkoxides, to substitute basic rings with heterocyclic moieties at the O6 position of guanine [33].

Four candidates – O6-thenylguanine, O6-thiazole, 5-bromothenyl, and 2-chloro – initially proved to be highly valuable substitutes for O6-BG in clinical applications. Further in vivo experiments, using the 4-bromothenyl variant were conducted by Middleton et al. [37].

After a single dose of 20 mg kg⁻¹ lomeguatrib administration intra peritoneally (i.p.) MGMT depletion was observed in a subcutaneous melanoma tumor and also in normal tissues (liver, kidneys, lung, brain, and the bone marrow). Normal activity was restored to 50 % after 24 hours [37] indicating the need for cycling. First clinical trials suggest effective MGMT depletion in prostate, primary CNS, and colorectal cancers after a single dose of lomeguatrib [38].

However, lomeguatrib was not yet tested in GBM cell lines or GBM mouse tumor models or in combination with radiation.

1.3 Radiation

Since the discovery of x-rays by Wilhelm Conrad Röntgen in 1895 and the first medical application reported in 1896 the clinical use of x-rays has spread and developed rapidly throughout the world [39]. One year later, Antoine Henry Becquerel detected radioactivity from a uranium compound he kept in his vest pocket after he developed skin erythema and ulceration [39]. At this hour the study of radiobiology and ionizing radiation was born.

Ionization describes the process of energy absorption by orbital electron ejection from a molecule or an atom upon radiation. Ionizing radiation is subdivided into electromagnetic and particulate radiation [39]. X-rays and γ -rays are examples of electromagnetic radiations, while electrons, protons, α -particles, neutrons, and heavy charged ions are particulate radiations [39]. The process of energy absorption is either directly or indirectly ionizing: directly ionizing means a straightforward interaction of

a charged particle with the material it passes through to cause chemical and biological changes by disrupting atomic structures [39]. Indirectly ionizing radiations such as x- and γ -rays involve the absorbance into the material with subsequent production of fast electrons without causing chemical or biological damages themselves [39]. Depending on the material as well as the energy of the photon absorbance occurs according to different processes. The Compton process is the dominant process for high energies e.g. at linear accelerators used in radiotherapy (Figure 1.5).

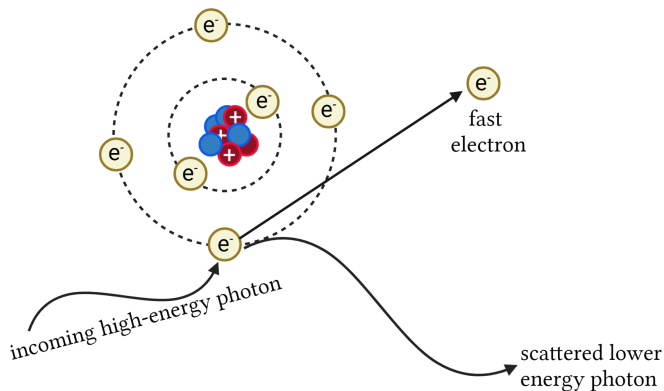


Figure 1.5: Compton process.

Shown is the scattering of a photon upon interaction with a high-energy photon. Figure adapted from [39] created with BioRender.com.

The incoming high-energy photon interacts with a free electron on the outer shell transferring parts of its energy as kinetic energy to the electron. During this process, a fast electron is produced, which in turn ionizes other atoms to exhibit its chemical and biological damage [39]. As a by-product, a scattered photon is produced, which is now lower in energy.

The photoelectric process is the dominant process at lower energies (Figure 1.6).

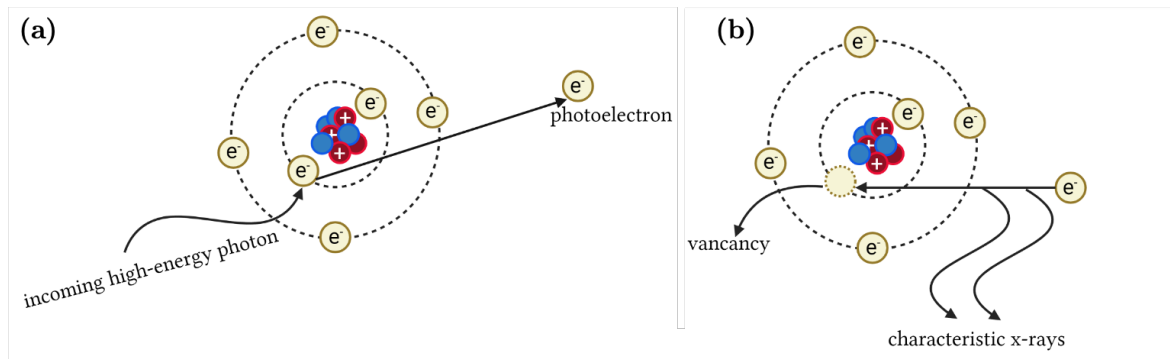


Figure 1.6: Photoelectric process and characteristic x-ray production.

Shown is (a) the interaction of an incoming high-energy photon with a bound electron and the subsequent photoelectron production. (b) shows the production of characteristic x-rays. Figure adapted from [39] created with BioRender.com.

The incoming high-energy photon interacts with a bound electron on the inner shells and transfers all its energy to the electron (Figure 1.6a). Parts of that energy is used to release it from the orbit, while the remaining energy is used as kinetic energy for motion [39]. The resulting vacancy in the atom orbit (Figure 1.6b) is either filled by a free electron from outside the orbit or by an electron from an outer orbit. In the latter case, energy levels are changed to a decreased potential energy which is compensated by the emission of a photon as characteristic x-rays [39].

The linear energy transfer (LET) describes the energy deposited in kiloelectron volt per unit track length ($\text{keV } \mu\text{m}^{-1}$). It can be subdivided into low LET (protons, x- and γ -rays) and high LET (α -particles, neutrons, and heavy-ions) and is decisive for the effectiveness of radiation on its most critical target – the Deoxyribonucleic acid (DNA).

1.4 Radiation Biology

Damages to the DNA are the biological effects of radiation and are either direct or indirect (Figure 1.7).

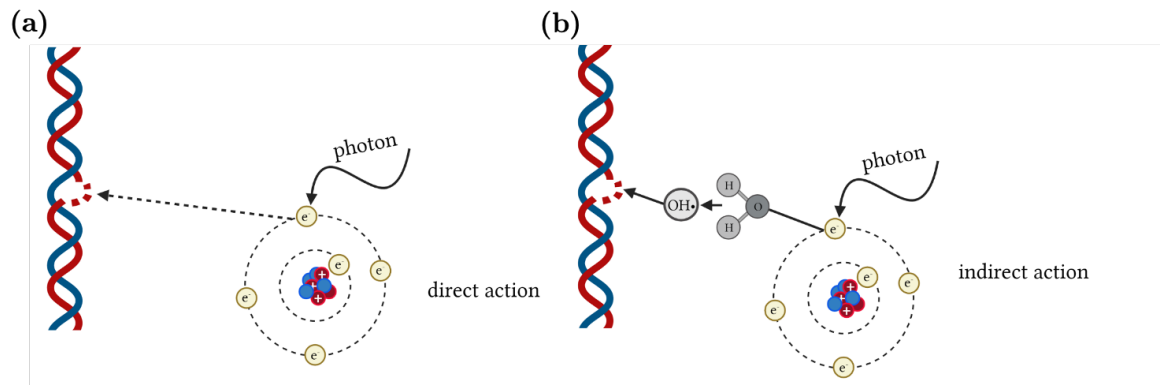


Figure 1.7: Direct and indirect effects of radiation.

During direct action, a photon gets absorbed to produce a secondary electron that directly damages the DNA. During indirect action, the secondary electron encounters a water molecule and transfers its energy to the water molecule to produce a hydroxyl radical. Figure adapted from [39] created with BioRender.com.

The interaction of the secondary electron resulting from the absorption of an incoming photon directly with the DNA (Figure 1.7a) is called direct action and is characteristic for high LET [39]. During indirect action (Figure 1.7b) the secondary electron interacts with other molecules such as water to produce free radicals, such as reactive oxygen species (ROS) that in turn damage the DNA [39] and is characteristic for low LET.

The unit to describe the absorbed dose is called Gray (Gy) and is defined as the absorption of one joule of energy per one kilogram of mass [40]. 1 Gy will produce approximately 105 ionizations, around 1,000 DNA base damages, around 1,000 DNA single-strand breaks (SSB), and 20 – 40 DSB [40]. The critical lesions of DSBs are repaired by either non-homologous end-joining (NHEJ) or homologous recombination (HR). While HR is error-free and the mechanism of choice during late S/G2 phase, NHEJ occurs in the G1 phase of the cell cycle and is more prone to errors [39].

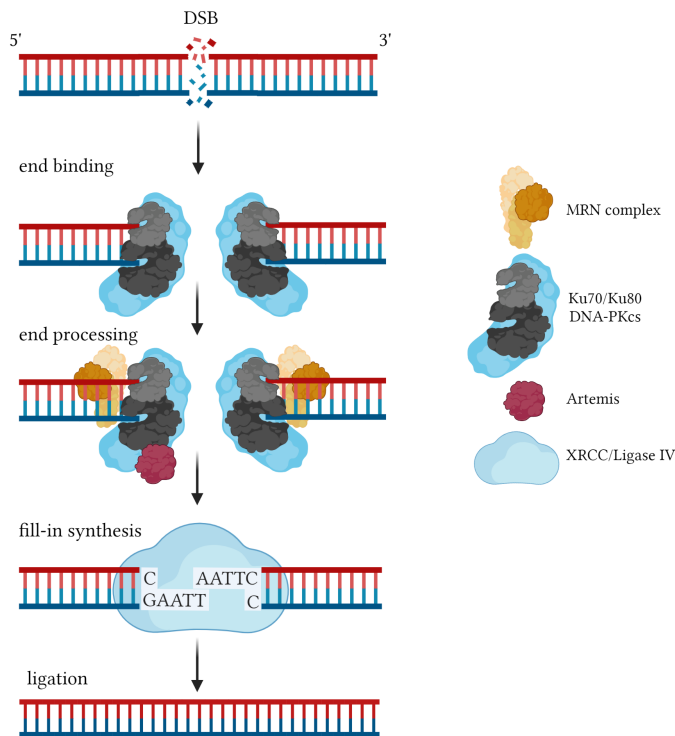


Figure 1.8: Non-homologous end-joining.

Shown is the repair of a DSB by NHEJ. Figure adapted from [39; 40] created with BioRender.com.

Figure 1.8 shows the process of DSB repair via NHEJ. After the DSB has occurred a Ku-heterodimer consisting of Ku70 and Ku80 subunits binds to the DNA ends [39]. It protects the ends from degrading via exonucleases and recruits the DNA-dependent protein kinase catalytic subunit (DNA-PKcs) [40]. Since the DSBs usually create incompatible ends, end processing is required. The MRN complex consisting of MRE11, RAD50, and NBS1 creates compatible ends. Further nuclease activity may be required and Artemis is recruited. Artemis binds to the DNA-PKcs which in turn phosphorylates Artemis to activate its endonuclease activity [41]. Artemis can trim both 5' and 3' overhangs; while 5' overhangs are trimmed to create blunt ends, 3' overhangs are trimmed to leave four to five nucleotide single-stranded overhangs [41]. After successful end processing, the gaps are filled by XRCC5, and ends are ligated by DNA ligase IV [39].

The other important mechanism in DSB repair is homologous recombination (Figure 1.9).

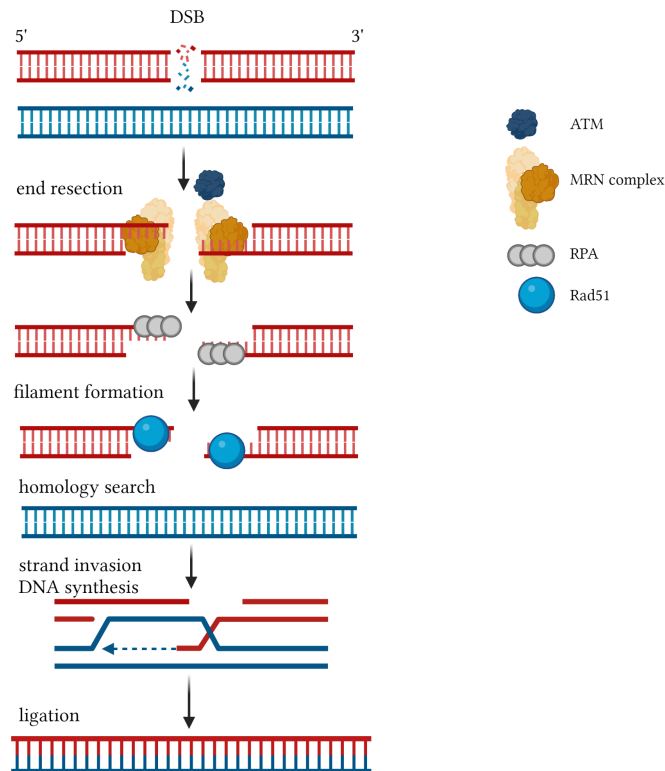


Figure 1.9: Homologous recombination.

Shown is the process of DSB repair via HR. Figure adapted from [39; 40; 42] created with BioRender.com.

During late S/G2 phase, DSBs are repaired via HR as it requires a sister chromatid as a template. Ataxia-telangiectasia mutated (ATM) and ataxia-telangiectasia and Rad3 related (ATR) are sensors for DSBs and are recruited to the site of the DSB [39]. ATM and ATR phosphorylate the histone subunit H2AX to γ H2AX that in turn recruits the tumor suppressor breast cancer type 1 susceptibility protein (BRCA1) to regulate the MRN complex [42]. End resection by the MRN complex immediately results in covering of the single-stranded ends by the replication protein A (RPA) but gets further displaced by RAD51 [42]. Upon RAD51 binding, which is called filament formation, the search for a homologous sequence is initiated. After a match was successful 3' strand invasion leads to a displacement loop (D-loop) formation also

called a Holliday junction. The invaded 3' strand now uses the complementary strand as a template to fill the gaps using DNA polymerase δ . Final ligation restores the DNA double-strand break.

Damages to the DNA and most importantly the dysfunctions or failure to repair DSB will ultimately result in cell death which is the goal of radiotherapy. Low doses of radiation are sufficient to cause DSBs but cells might undergo several rounds of cell division accumulating chromosome aberrations and mutations before they die eventually [40]. These effects are not only observed in cancer tissues but also in normal tissues. In order to observe short- as well as long-term effects of radiation in normal tissue and also in cancerous tissue it is necessary to eliminate stem cells and their progenitor cells [40]. Only upon stem cell-killing, radiation damage becomes noticeable from early effects such as breakdown of the skin to late reactions including fibrosis to second tumors [40]. However, it is not possible to only kill cancer (stem) cells and spare normal (stem) cells. Therefore, the right timing, dosage, fractionation, and treatment planning are required to limit normal tissue damage to a minimum and achieve tumor control at the same time.

In the brain, this is particularly difficult due to severe side effects such as neurocognitive dysfunction, endocrine dysfunction, and neurosensory impairment caused by irradiation of the hippocampus and cerebral cortex, hypothalamus, and pituitary gland, as well as the optic nerve and optic chiasm [43].

Knowledge of physics, chemistry, and biology of radiation is of great importance to apply and also to develop new treatment options and improve radiotherapy of GBM.

1.5 Aim

The aim of this study was to determine the role of MGMT during radiotherapy in human glioblastoma multiforme cell lines *in vitro* and *in vivo*. Since MGMT promoter unmethylated patients have a worse treatment outcome upon alkylating chemotherapy agents, new treatment options need to be developed in order to inactivate MGMT. Three human MGMT unmethylated glioblastoma cell lines were chosen and treated with the MGMT inhibitor lomeguatrib to reduce MGMT protein levels. Changes in radiosensitivity were determined via the colony formation assay, as well as effects in cell cycle, apoptosis, and DNA repair was analyzed. Finally, the inhibitor was tested *in vivo* to determine tumor growth delay upon MGMT protein inhibition.

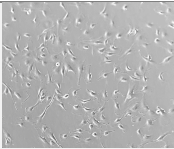
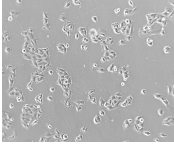
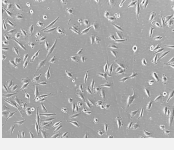
2. Materials and Methods

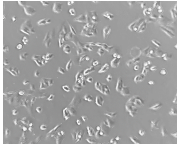
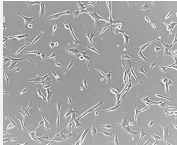
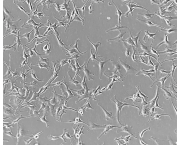
2.1 In vitro

2.1.1 Cell Culture

Established human glioblastoma multiforme cell lines were obtained from the University Hospital of Heidelberg (LN18, LN229) and the Institute of Radiobiology, Helmholtz Zentrum München (A172). T98G and U118 were purchased from the American Type Culture Collection (ATCC) and U251 from Cell Lines Service GmbH (CLS). Cell line authentication was done by Eurofins Genomics. All cell cultures were incubated in a humidified atmosphere of 5 % CO₂ at 37°C. LN18, LN229, U118, and U251 were grown in high glucose DMEM (D6429, Sigma-Aldrich, St. Louis, MO, USA) and T98G in low glucose DMEM (D6046, Sigma-Aldrich, St. Louis, MO, USA) supplemented with 10 % Fetal calf serum (FCS) (F7524, Sigma-Aldrich, St. Louis, MO, USA), 100 U mL⁻¹ penicillin and 100 U mL⁻¹ streptomycin (P0781, Sigma-Aldrich, St. Louis, MO, USA). Cell culturing was done under sterile conditions in a safety cabinet and the absence of mycoplasma was regularly checked.

Table 2.1: Characteristics of established human glioblastoma multiforme cell lines.

	<i>Organism</i>	<i>Tissue</i>	<i>p53</i>	<i>PTEN</i>	<i>MGMT</i>	<i>Image</i>
<i>A172</i>	<i>Homo sapiens</i>	brain	wt	mut	m	
<i>LN18</i>	<i>Homo sapiens</i>	brain, frontal right	wt	wt	um	
<i>LN229</i>	<i>Homo sapiens</i>	brain, right frontal parieto-occipital cortex	mut	wt	m	

<i>T98G</i>	<i>Homo sapiens</i>	brain	mut	mut	um	
<i>U118</i>	<i>Homo sapiens</i>	brain	mut	mut	um	
<i>U251</i>	<i>Homo sapiens</i>	brain	mut	mut	m	

Mut: mutated, wt: wild-type, m: methylated, um: unmethylated

2.1.2 Cell irradiation

X-ray irradiation was performed at an RS225A irradiation device (Gulmay, XStrahl, Camberley, UK) at a dose rate of 0.9 Gy min^{-1} at 15 mA and 200 kV with a 0.5 mm copper filter and a distance to the x-ray tube of 15 cm.

2.1.3 Lomeguatrib treatment

Lomeguatrib was purchased from MedChemExpress LLC (Princeton, NJ, USA) and dissolved in DMSO (Sigma-Aldrich, St. Louis, MO, USA). The stock solution of 6.13 mM was stored in 100 μl aliquots at -80°C for up to six months. Immediately before use, the stock solution was diluted at 1:10 or 1:100 in medium. The final DMSO concentration in the medium did not exceed 0.3 % and was without cytotoxic effects. Cells were seeded at a density of 4×10^5 to 6×10^5 and lomeguatrib was added 24 hours before x-ray irradiation.

2.1.4 Doubling time calculation

Doubling times of the six different cell lines were determined using the alamarBlue proliferation assay.

The experiment was done in a 96-well plate format for all six cell lines. Every 24 hours for three consecutive days, 10 % alamarBlue was added to the samples and after an incubation period of four hours, the absorption was measured at a wavelength of 595 nm and 630 nm. Doubling times were calculated using the following formula:

$$\text{Doubling Time}(h) = \frac{\text{duration} * \log(2)}{\log(\text{final absorption}) - \log(\text{initial absorption})}$$

2.1.5 Colony-forming assay (CFA)

CFAs are used to determine radiosensitivity of different cell lines. 48 hours before irradiation appropriate numbers of cells per dose were pre-plated into 12-well plates and 24 hours before irradiation treated with 1 μ M or 20 μ M lomeguatrib. Plates were irradiated with 0 Gy, 1 Gy, 2 Gy, 4 Gy, 6 Gy, and 8 Gy. After a 12-day (LN18) or 7-day (T98G, and U118) incubation period the medium was removed, and plates were washed with PBS. Colonies were fixed with 100 % -20°C cold methanol and stained using 0.1 % crystal violet. Colonies of at least 50 cells were manually counted as one colony using a GelCount™ (Oxford Optronix Ltd., Oxford, UK) colony counting device. Plating efficiencies, as well as the survival fractions, were calculated using the following formulas:

$$\text{Plating efficiency (PE)} = \frac{\text{number of colonies counted}}{\text{number of cells seeded}} * 100$$

$$\text{Survival fraction (SF)} = \frac{\text{number of colonies}}{(\text{number of cells seeded} * PE)} * 100$$

Survival curves were plotted in GraphPad Prism (GraphPad Software Inc., San Diego, USA) and fitted to the linear-quadratic model:

$$SF = e^{-\alpha D - \beta D^2}$$

α and β values were derived from the linear-quadratic model and D_{50} values were calculated using the following formula:

$$D_{50} = \frac{-\alpha + \sqrt{\alpha^2 - 4\beta \ln(0.5)}}{2\beta}$$

2.1.6 Cell cycle flow cytometry

48 hours prior to irradiation with 0 Gy and 8 Gy 600,000 cells were seeded per T25 flask. 24 hours before irradiation cells were treated with 1 μ M or 20 μ M lomeguatrib. 24 hours after irradiation cells were trypsinized and resuspended in cold PBS. The cell suspension was then slowly dropped to -20°C cold 70 % ethanol and stored at -20°C for at least two hours. After centrifugation at 500 g for 5 minutes remaining ethanol was removed and cells were incubated with propidium iodide (PI) staining solution (0.02 mg/ml PI (P3566, Thermo Fisher, Waltham, MA, USA), Triton X-100 (T8787, Sigma-Aldrich, St. Louis, MO, USA) and 0.2 mg/ml DNase-free RNase A (R4875, Sigma-Aldrich, St. Louis, MO, USA) in PBS) for 30 minutes at room temperature in the dark. FACS analysis was performed in the FACSCalibur. Cell cycle distribution was analyzed in the ModFit LT™ software (Verity Software House Inc., Topsham, ME, USA).

2.1.7 γ H2AX foci

Cells were seeded in chamber slides 24 hours prior to lomeguatrib and 48 hours before irradiation at 0 Gy and 8 Gy. 30 minutes, as well as 24 hours after irradiation cells, were washed with 1 x PBS and fixed with 2 % paraformaldehyde (PFA) for 30 minutes. After three washing steps with PBS cells were permeabilized three times in PBS + 0.15 % Triton X-100 for 5 minutes each. In order to prevent unspecific bindings blocking was done three times for 10 minutes in PBS supplemented with 0.15 % Glycine and 1 % Bovine Serum Albumin (BSA). Afterward, the cells were incubated with the primary antibody H2AX clone JBW301 (05636, Merck Millipore, Burlington, USA) diluted 1:500 in blocking buffer overnight at 4°C in a humidified chamber. After a wash step with PBS for 5 minutes incubation for 20 minutes in PBS and 0.15 %, Triton X-100 was performed prior to another wash step with PBS and blocked for 7 minutes. The secondary antibody Alexa Fluor 488 goat-anti mouse (A323723, Invitrogen, Carlsberg, USA) was diluted 1:1000 in blocking buffer and incubated for 1 hour in a humidified chamber in the dark. Cells were washed with PBS and 0.15 % Triton X-100 for 10 minutes and two times with PBS for 5 minutes each. Nuclei were stained using 1.5 $\mu\text{g ml}^{-1}$ Hoechst (Hoechst 33342, Trihydrochloride, Trihydrate, H1399, Invitrogen, Carlsberg, USA) for 5 minutes. Five wash steps using PBS were performed to completely remove the remaining Hoechst. Fresh PBS was added and slides were kept at 4°C in a humidified chamber until slides were analyzed. Scanning was performed using the MetaSystems (Altlussheim, Germany) Metafer slide scanning platform assembled on an inversed ZEISS Axio Observer (Jena, Germany) coupled to a CoolCube4 camera (MetaSystems, Altlussheim, Germany). At least 10,000 nuclei were scored automatically for γ H2AX foci using the Metafer 5 software (Version 4.2.133) with a self-developed classifier for γ H2AX. Pictures were acquired at 20 x magnification.

2.1.8 Caspase 3/7 flow cytometry

Detection of apoptotic cells was performed using the CellEvent™ Caspase-3/7 Green Flow Cytometry Assay Kit (C10427, Thermo Fisher, Waltham, MA, USA). 48 hours before 0 Gy and 8 Gy x-ray irradiation, 600,000 cells were seeded per T25 flask. 24 hours before irradiation cells were treated with 1 μ M or 20 μ M lomeguatrib and incubated for 48 hours at 37°C and 5 % CO₂. Cells were trypsinized and centrifuged at 500 g for 5 minutes at room temperature. Cell pellets were resuspended in 1 ml PBS and 1 μ l of the CellEvent™ Caspase-3/7 Green Detection Reagent was added. Incubation was done for 25 minutes at 37°C followed by the addition of 1 μ l of the 1 mM SYTOX® AADvanced™ dead cell stain solution. After a 5-minute incubation step at 37°C FACS analysis was performed immediately at the FACSCalibur.

2.1.9 Migration

Investigation of the migratory behavior was tested via the wound healing assay using ibidi 2-well μ -dish inserts (81776, ibidi, Martinsried, Germany). Cells were seeded into both chambers of the ibidi dish and treated with 0 μ M, 1 μ M, or 20 μ M lomeguatrib 24 hours after seeding. 24 hours after lomeguatrib treatment cells were exposed to 0 Gy or 8 Gy and immediately afterward the silicon inserts were removed, cells washed with 1 x PBS and medium was replaced by 0.1 % FCS containing medium to avoid proliferation. Initial pictures (0 h) were taken immediately as well as after 6 h, 24 h, 30 h, and 48 h. The area covered by the cells was analyzed using the MRI Wound Healing Tool plug-in in ImageJ (https://github.com/MontpellierRessourcesImagerie/imagej_macros_and_scripts/wiki/Wound-Healing-Tool).

2.2 Molecular biology

2.2.1 MethyQESD

For the determination of the MGMT promoter methylation status a methylation-quantification of endonuclease-resistant DNA (MethyQESD) was performed according to Bettstetter [44]. Here, DNA was digested by a methylation-specific restriction enzyme and the amount of undigested DNA is quantified by qPCR.

DNA was isolated using the AllPrep DNA/RNA Mini Kit (802048, Qiagen, Hilden, Germany) according to the manufacturer’s instructions. For the quantification digestion (Q) 1 µg DNA was digested with 40 U HinP1 restriction enzyme (NEB, Ipswich, MA, USA). In the calibration digestion (K) 1 µg DNA was digested with 20 U XbaI and 20 U DraI (NEB, Ipswich, MA, USA) restriction enzymes. The reactions were incubated at 37°C overnight and then heat-inactivated at 70°C for 20 minutes the next day. Afterward, the restriction digestions were transferred to ice immediately. 3 µl of each restriction digestion reaction was added per 20 µl reaction with 0.5 µM of the forward and reverse primers shown in Table 2.2.

Table 2.2: Primer for MethyQESD.

<i>Gene symbol</i>	<i>Sequence</i>	<i>Company</i>
<i>MGMT Msdig F1</i>	CCCGCATATGCTGGGACAG	Eurofins Genomics
<i>MGMT Msdig R1</i>	CCCAGACACTCACCAAGTCG	Eurofins Genomics

Quantification of the methylated DNA was performed in the Roche LightCycler480 in a 96-well format using the QuantiNova SYBR Green PCR Master Mix Kit (208152, Qiagen, Hilden, Germany) using the settings in Table 2.3.

Table 2.3: Settings for qPCR.

<i>Cycles</i>	<i>temperature</i>	<i>time</i>	<i>note</i>
<i>Stage 1</i>	95°C	15 min	initial denaturation
	94°C	10 sec	
<i>Stage 2</i>	60°C	17 sec	45 cycles
	72°C	10 sec	
<i>Stage 3</i>	according to instrument settings		Melting Curve

Calculation of the percentage of MGMT promoter methylation was done using the following formulas:

$$\Delta C_t = Q_{C_t} - K_{C_t}$$

$$\% \text{ methylation} = E^{\Delta C_t} * 100$$

with E being the efficiency of the qPCR.

2.2.1.1 qPCR efficiency

The efficiency of the qPCR was determined by performing a geometric efficiency assessment. Therefore, an untreated sample from the calibration restriction digestion was used to prepare the following dilutions: 1:4, 1:16, 1:64, 1:256, 1:1,024, 1:4,096 and 1:16,384. 3 μ l of the dilution was mixed with 0.5 μ M of the forward and reverse primer seen in Table 2.2, as well as the QuantiNova SYBR Green PCR Master Mix. The qPCR was run according to the program as seen in Table 2.3. Amplification and standard curves were derived from the LightCycler480 software (Figure 2.1).

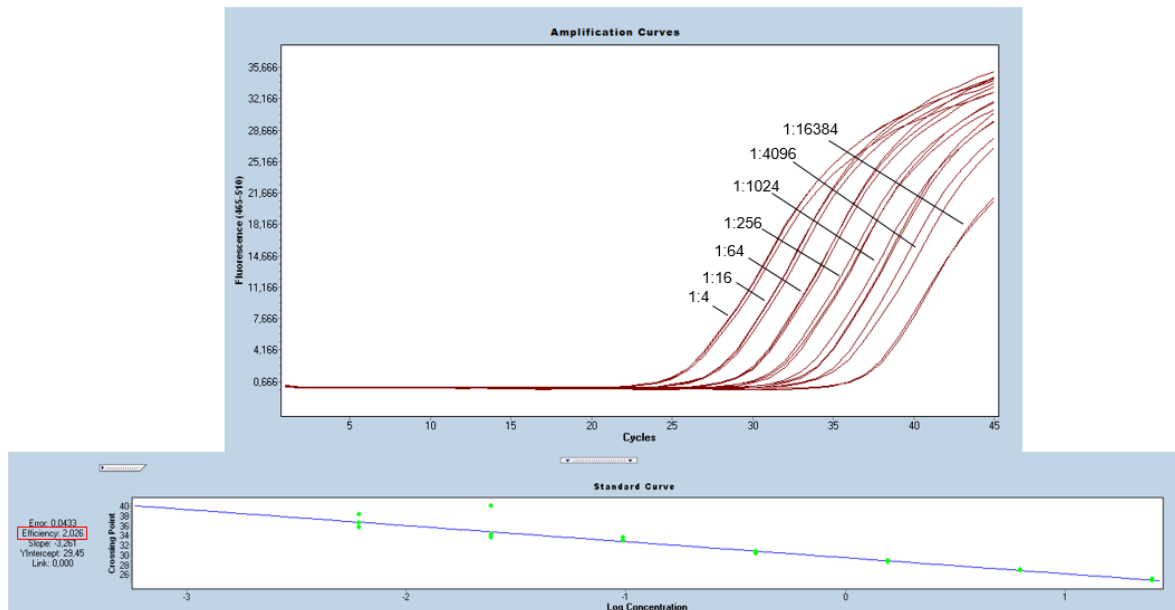


Figure 2.1: PCR amplification curve. Shown is the standard curve of the diluted standards in duplicates and the qPCR efficiency.

The experiment was repeated twice giving a PCR efficiency value of 2.054 ± 0.028 .

2.3 Protein techniques

2.3.1 Harvesting of protein samples

In order to determine MGMT inhibition upon lomeguatrib treatment, 600,000 cells were seeded in T25 flasks and incubated at 37°C and 5 % CO₂ overnight. Cells were then exposed to different lomeguatrib concentrations and harvested after 4 – 48 hours by trypsinization. For the detection of autophagy, cells were treated with 1 μM or 20 μM lomeguatrib, and positive control cells were treated with 300 nM rapamycin for 24 hours followed by 0 Gy and 8 Gy irradiation. 24 hours after irradiation cells were harvested and centrifuged at 12,000 g for 15 minutes and 4°C. Isolation of the proteins was done in radioimmunoprecipitation assay buffer (RIPA; 150 mM NaCl, 50 mM Tris, 0.1 % SDS, 1% Triton X-100, 0.5 % sodium deoxycholate, 10x phosphatase-inhibitor, 25x protease inhibitor, 1 mM phenylmethylsulfonyl fluoride (PMSF)) for 30 minutes on ice with vortexing every few minutes. After another

centrifugation step at 15,000 g for 10 minutes and 4°C, the supernatant containing the proteins was transferred to new 1.5 mL Eppendorf tubes and stored at -80°C until further use.

2.3.2 Protein concentration determination

For the determination of the protein concentration, the Pierce™ BCA™ Protein-Assay (23225, Thermo Fisher Scientific, Waltham, MA, USA) was used. Therefore, a BSA standard dilution series was prepared according to Table 2.4 below. 1:10 diluted samples, as well as the standards in duplicates, were incubated with the supplied working reagent for 30 minutes at 37°C in the dark, and measurement was done at 550 nm in the Varioskan LUX™ microplate reader (Thermo Fisher Scientific, Waltham, MA, USA).

Table 2.4: Preparation of BSA standard dilution series.

	<i>concentration</i> [$\mu\text{g}/\text{ml}$]	<i>RIPA</i> [μl]	<i>stock</i> [μl]
<i>A</i>	2000	0	300
<i>B</i>	1500	125	375
<i>C</i>	1000	325	325
<i>D</i>	750	175	175 of B
<i>E</i>	500	325	325 of C
<i>F</i>	250	325	325 of E
<i>G</i>	125	325	325 of F
<i>H</i>	25	400	100 of G
<i>I</i>	0	400	-

2.3.3 SDS-PAGE

Electrophoretic separation of the proteins was performed using a NuPAGE™ 4 – 12 % Bis-Tris Gel (NP0336, Thermo Fisher Scientific, Waltham, MA, USA). 10 µg of protein was mixed with 1 x Laemmli buffer and denatured by heating for 10 minutes at 96°C. Immediately afterward the samples were loaded onto the gel together with a Precision Plus Protein™ Standard Dual Color Standard marker (1610374, Bio-Rad Laboratories Inc., Hercules, USA) diluted 1:1 in 4 x Laemmli Buffer. The protein separation in 1 x NuPAGE™ MES SDS Running Buffer (NP0002, Thermo Fisher Scientific, Waltham, MA, USA) was started for 10 minutes at 100 V and then increased to 130 V for 75 minutes.

2.3.4 Transfer

For the transfer of the proteins from the acrylamide gel to a membrane, the Trans-Blot Turbo Mini 0.2 µm Nitrocellulose Transfer Pack (1704158, Bio-Rad, Laboratories Inc., Hercules, CA, USA) was used. The gel was equilibrated in 1 x TOWBIN Buffer (25 mM Tris, 192 mM Glycine, H₂O, and 20 % methanol) for 10 minutes to remove traces of SDS and then placed in-between the Transfer Pack. The electrical field was applied in a way that the proteins were able to migrate from the gel onto the membrane, from the cathode to the anode. Blotting was done in the Trans-Blot® Turbo Transfer-System (1704150, Bio-Rad, Laboratories Inc., Hercules, CA, USA) using the preset settings for low molecular weight proteins (1.3 A, 25 V, 5 min) as well as mixed molecular weight proteins (1.3 A, 25 V, 7 min).

2.3.5 Immunological detection

In order to prevent unspecific binding of antibodies to the membrane, the membrane was blocked in 1 x ROTI@block (A151.2, Carl Roth, Karlsruhe, Germany) for at least one hour. Afterward, the membrane was cut at appropriate positions to add the primary antibodies anti-MGMT (sc-56157 MT3.1, Santa-Cruz, Dallas, TX, USA) diluted 1:200 and anti- β -actin (ab5326, Sigma-Aldrich, St. Louis, MO, USA) diluted 1:100,000 and incubated overnight at 4°C in a rotor creating constant movement. The membrane was washed with 0.1 % TBST (10 x TBS, Tween® 20) the next day three times for ten minutes each and incubated with the secondary antibody anti-mouse IgG (H+L) AP conjugate (sc-2008, Santa Cruz, Dallas, TX, USA) diluted 1:10,000 for 2 hours at room temperature. After three washing steps with 0.1 % TBST, detection was done using the Novex™ AP Chromogenes Substrate (BCIP/NBT) (WP20001, Thermo Fisher Scientific, Waltham, MA, USA).

For quantification of the bands, ImageJ software was used. First, background subtraction was performed, sample bands were normalized to the loading control and finally normalized to untreated controls.

2.4 In vivo experiments

2.4.1 Animal Model

All animal experiments were approved by the ethics committee of the Government of Upper Bavaria (reference number 55.2-2532.Vet_02-20-104). 6 weeks old female Crl:NMRI-*Foxn1^{nu}* nude mice were obtained from Charles River Laboratories (Wilmington, MA, USA) and housed at the TranslaTUM, Technical University Munich. All animals were kept in special air-conditioned rooms at 20 – 24° C with a 45 – 65 % relative humidity and a 12-hour light-dark cycle. The mice were housed in

individually ventilated cages (IVC, Sealsafe Next Greenline cage, Type GM500 plus, Tecniplast Deutschland GmbH, Hohenpeißenberg, Germany) with a maximal occupancy of six mice per cage. Autoclaved water as well as autoclaved commercial laboratory animal maintenance diet (1324 SP – 10 mm pellets, Altromin Spezialfutter GmbH + Co. KG, Lage, Germany) was available *ad libitum*.

2.4.2 Whole-body irradiation

Prior to tumor cell injection whole body irradiation was performed with 4 Gy x-rays at 200 kV and a 0.5 mm copper filter in an RS225A irradiation device (Gulmay Ltd, XStrahl, Camberley, UK). Up to ten mice were irradiated at the same time in a Green Line cage allowing mice to fully move in two dimensions; a perforated Plexiglas plate constrained the mice to the bottom of the cage to ensure correct dosimetry. Immediately after whole-body irradiation mice received the antibiotic Convenia® (20 µl per 20 g mouse, Zoetis, Parsippany-Troy Hills Township, NJ, USA) subcutaneously.

2.4.3 Subcutaneous injection of tumor cells

Two days after the whole body irradiation mice were injected subcutaneously with human glioblastoma multiforme cells. Mice were anesthetized with 3 % isoflurane using oxygen as carrier gas. After the mice lost their righting response Bepanthen® eye ointment (Bayer AG, Leverkusen, Germany) was applied. 3×10^6 glioblastoma cells (LN18 or U118) in 50 µl Matrigel were injected into the right flank using a 1 ml syringe and a 27 G needle.

2.4.4 Tumor volume measurement

Twice per week mice were weighed and the tumor volume was determined via caliper and ultrasound using a Logiq-5 Ultrasound Machine with a 10 MHz linear transducer (General Electric, Boston, MA, USA). For the caliper, two diameter measurements were taken and the tumor volume was calculated using the following formula:

$$tumor\ volume\ [mm^3] = length\ [mm] * width^2[mm] * \frac{\pi}{6}$$

Ultrasound allows a more precise measurement and with the following formula, tumor volume was calculated:

$$tumor\ volume\ [mm^3] = length\ [mm] * width\ [mm] * depth[mm] * \frac{\pi}{6}$$

2.4.5 Lomeguatrib administration and radiation therapy

When tumors reached a volume of 60 – 100 mm³, lomeguatrib or sodium chloride as a control substance was administered followed by local radiation therapy using a Small Animal Radiation Research Platform (SARRP, XStrahl Ltd, Camberley, UK). 24 hours prior to radiation therapy mice received 20 mg kg⁻¹ lomeguatrib intraperitoneally, control mice received the corresponding volume of sodium chloride. Afterward, mice were anesthetized with 3 % isoflurane and oxygen as carrier gas. After Bepanthen[®] eye ointment was applied mice were placed onto the mouse bed within the SARRP and the tumor-bearing flank was exactly positioned. Anesthetic maintenance with 1 – 2 % isoflurane was ensured during the whole procedure and mice were monitored with an in-built camera. Mice were randomly assigned to either

the sham, 5 Gy or 15 Gy group, where the dose was precisely delivered to the tumor. Mice from the sham group underwent the same procedure without delivering any dose. A cone-beam computer tomography (CBCT) was acquired at 60 kV and 0.8 mA from each mouse. Muriplan preclinical treatment planning software (XStrahl) was used to calculate the dose distribution and arrange the beams precisely to the tumor. The dose was delivered at 220 kV and 13 mA using a 10 x 10 mm³ collimator and an anterior to posterior and posterior to anterior (AP-PA) arrangement of two beams. AP-PA is an irradiation technique also used for breast cancer patients to deliver a uniform dose within the tumor and avoid radiation toxicities to the surrounding healthy tissue and the skin. Immediately after irradiation mice were closely monitored for one hour. Tumor volume measurement was followed up until tumors reached the fourfold output volume or a termination criterion was reached.

2.4.5.1 Radiation therapy at Gulmay irradiation device

During the irradiation of the mouse study, the SARRP machine produced an error and could no longer be used. Unfortunately, some of the mice were not irradiated at this time point but tumors were already implanted. From an ethical point of view as well as to retain the three R principles – Replacement, Reduction, and Refinement – it was decided to irradiate the tumors of the remaining mice in the Gulmay RS225 irradiation cabinet (Gulmay, XStrahl, Camberley, UK) at a dose rate of 0.9 Gy min⁻¹ at 15 mA and 200 kV with a 0.5 mm copper filter and a distance to the x-ray tube of 15 cm. Mice were anesthetized using 1 mg ml⁻¹ Medetomidin, 5 mg ml⁻¹ Midazolam, and 0.05 mg ml⁻¹ Fentanyl (MMF) and fixed on Plexiglas plates using Leukofix with the tumor-bearing flank stretched out. Lead plates of 8 mm were used to cover the body of the mice to deliver the dose only to the stretched flank with a safety margin of 1 mm. Small lead shields were used to cover the foot of the mice. The tumor-bearing

flank was positioned at the isocenter of the Gulmay and the dose of either 5 Gy or 15 Gy was delivered with a single beam.

2.5 Statistics

Mean values were calculated and are presented as \pm standard error of the mean (SEM). Student's t-test was used to calculate differences in mean values between groups. Differences between pre- and post-plating as well as the 0 μM , 1 μM , and 20 μM lomeguatrib treated cells were calculated by applying Two-Way ANOVA in GraphPad Prism. Probability values of $p < 0.05$ were regarded as statistically significant. In order to ensure reproducibility of the results, each experiment was repeated at least three times.

3. Results

3.1 Comparison of pre- vs. post-plating in clonogenic survival

During the preparation of this thesis, the experimental setup of the colony-forming assay had to be changed due to the change from using MGMT knockdown cell lines to MGMT inhibition using the inhibitor lomeguatrib. Therefore, CFAs with post-plating and pre-plating were performed and their survival curves are presented in Figure 3.1.

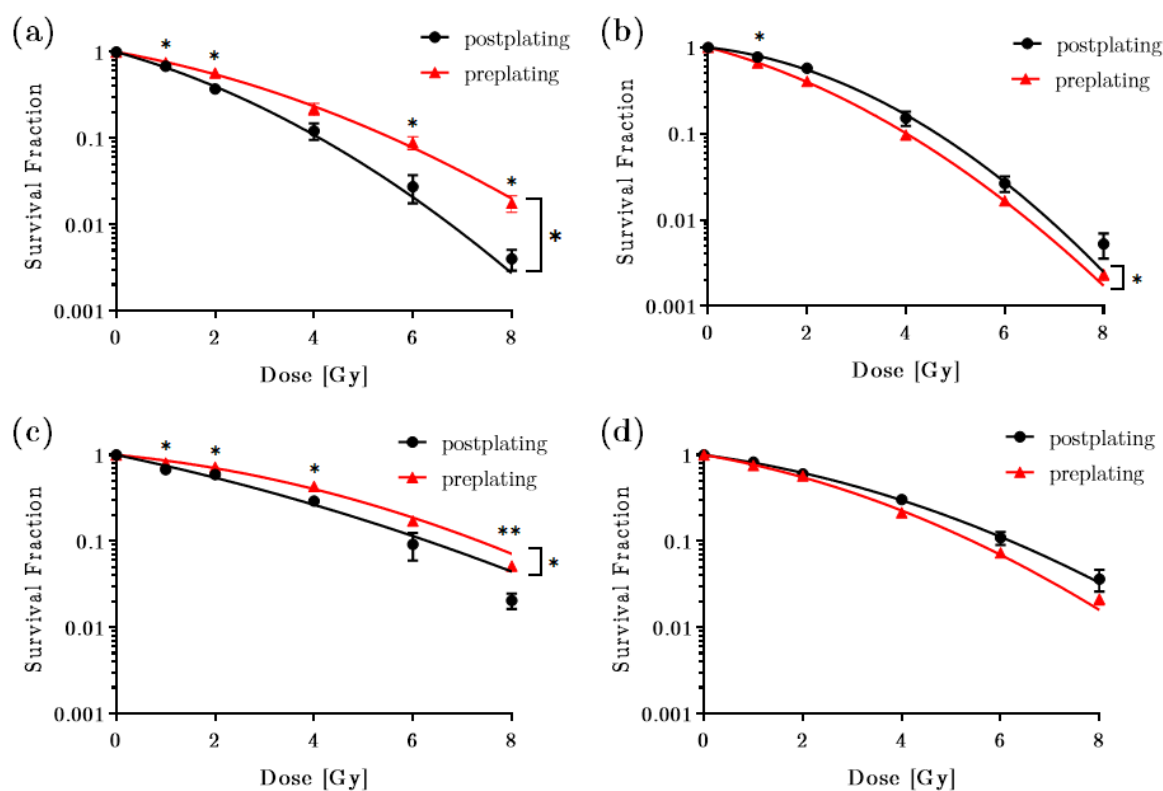


Figure 3.1: Colony-forming assay (CFA) to compare survival fractions after pre- and post-plating. Shown are (a) LN18, (b) LN229, (c) T98G, and (d) U251 cell lines seeded in 12-well plates before (pre-plating) or after (post-plating) x-ray irradiation. Experiments were performed at least three times and error bars present the SEM. Two-Way ANOVA was used to calculate differences between post- and pre-plating, Student's T-test was applied to compare single doses. (* $p \leq 0.05$, ** $p \leq 0.01$).

The plating efficiency for LN18 post-plating was $47.7 \% \pm 6.5 \%$, and $30.2 \% \pm 7.6 \%$ for the pre-plating setup. Significant differences in the survival curves were observed at 1 Gy ($p = 0.041$), 2 Gy ($p = 0.029$), 6 Gy ($p = 0.017$), and 8 Gy ($p =$

0.011). For LN229 the post-plating PE was $71.4 \% \pm 5.58 \%$ and was therefore very similar to the pre-plating PE of $71.5 \% \pm 10.6 \%$. Differences were detected at 1 Gy ($p = 0.047$) only. The PE for T98G post-plating was $30.2 \% \pm 4.5 \%$ and $10.4 \% \pm 0.9 \%$ for pre-plating. Significant differences in the survival curves were observed at 1 Gy ($p = 0.020$), 2 Gy ($p = 0.027$), 4 Gy ($p = 0.016$), and 8 Gy ($p = 0.004$). In the U251 cell line PE were also different with $50.4 \% \pm 4.5 \%$ for post-plating and $65.3 \% \pm 5.3 \%$. However, statistical analysis did not reveal significant differences between post- and pre-plating.

Table 3.1: D50 values. Shown are the D50 values of LN18, LN229, T98G, and U251 cell lines after pre- and post-plating. Dose in Gy required to reduce survival to 50 % of the cells.

Cell line	method	D ₅₀ [Gy]	p-value	
LN18	pre-plating	2.27 ± 0.24	0.033	*
	post-plating	1.59 ± 0.10		
LN229	pre-plating	1.58 ± 0.04	0.070	ns
	post-plating	2.19 ± 0.22		
T98G	pre-plating	3.29 ± 0.14	0.010	*
	post-plating	2.25 ± 0.19		
U251	pre-plating	2.25 ± 0.14	0.302	ns
	post-plating	2.62 ± 0.25		

Table 3.1 shows the dose required to reduce survival to 50 %. Significant differences between pre- and post-plating were detected for LN18 ($p = 0.033$) and T98G ($p = 0.010$).

3.2 Radiosensitivity of different GBM cell lines

Radiosensitivity of six established human glioblastoma multiforme cell lines was determined using the colony-forming assay (CFA). Cells were pre-plated into 12-well plates followed by exposure to 0 Gy, 1 Gy, 2 Gy, 4 Gy, 6 Gy, and 8 Gy ionizing radiation. Figure 3.2 shows the survival curves of the six investigated cell lines.

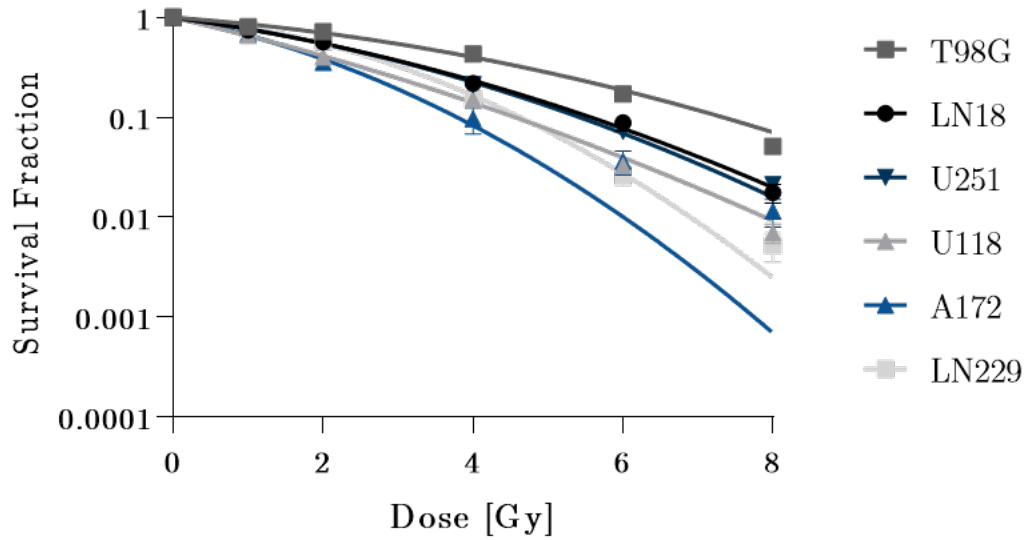


Figure 3.2: Colony-forming assay (CFA) of six established human glioblastoma cell lines. Shown are the survival curves of A172, LN18, LN229, T98G, U118, and U251 fitted to the linear-quadratic model. Experiments were repeated at least four times and error bars present the standard error of the mean.

A172 was the most radiosensitive cell line with a D_{50} of 1.55 ± 0.03 Gy, followed by U118 with a D_{50} of 1.62 ± 0.14 Gy, while T98G was the most radioresistant cell line with a D_{50} of 3.29 ± 0.22 Gy. LN18, LN229, and U251 were comparable intermediate radiosensitive with D_{50} values of 2.27 ± 0.24 Gy, 2.19 ± 0.22 Gy, and 2.25 ± 0.14 Gy.

Table 3.2: Radiobiological parameters of the established human glioblastoma cell lines.

Cell line	D_{50} [Gy] ^a	D_{10} [Gy] ^b	α [Gy ⁻¹] ^c	β [Gy ⁻²] ^c
A172	1.55 ± 0.03	3.88 ± 0.31	0.5195 ± 0.2598	0.0093 ± 0.0046
LN18	2.27 ± 0.24	5.52 ± 0.33	0.2353 ± 0.1358	0.0333 ± 0.0192
LN229	2.19 ± 0.22	4.59 ± 0.26	0.1526 ± 0.0881	0.0773 ± 0.0447
T98G	3.29 ± 0.14	7.34 ± 0.03	0.1264 ± 0.0632	0.0255 ± 0.0127
U118	1.62 ± 0.14	4.53 ± 0.21	0.3912 ± 0.2259	0.0264 ± 0.0153
U251	2.25 ± 0.14	5.42 ± 0.03	0.2276 ± 0.1314	0.0363 ± 0.0210

a: D_{10} dose [Gy] required to reduce cell survival to 10%.

b: D_{50} dose [Gy] required to reduce cell survival to 50%.

c: α and β values calculated from the linear-quadratic equation: $\ln SF = -\alpha \times D - \beta \times D^2$.

3.3 MGMT promoter methylation and MGMT protein expression

In order to verify the MGMT methylation status of the six human glioblastoma cell lines, MethyQESD was established according to Bettstetter *et al.* [44]. Two cell lines were unmethylated (LN18 and U118), two cell lines were methylated (A172 and LN229), and two cell lines were hemi-methylated (T98G and U251). The methylation of the MGMT promoter region in % is presented in Table 3.3.

Table 3.3: MGMT promoter methylation.

Cell line	Methylation [%]	Status
A172	116.50 ± 17.99	M
LN18	0.82 ± 0.32	UM
LN229	176.87 ± 21.92	M
T98G	50.01 ± 4.10	UM/M
U118	13.75 ± 5.97	UM
U251	29.72 ± 2.42	UM/M

M: methylated; UM: unmethylated; UM/M: hemi-methylated

Since the methylation status alone is not directly associated with MGMT protein expression Western Blot analysis was performed in order to verify MethyQESD results and determine cell lines with high MGMT protein expression.

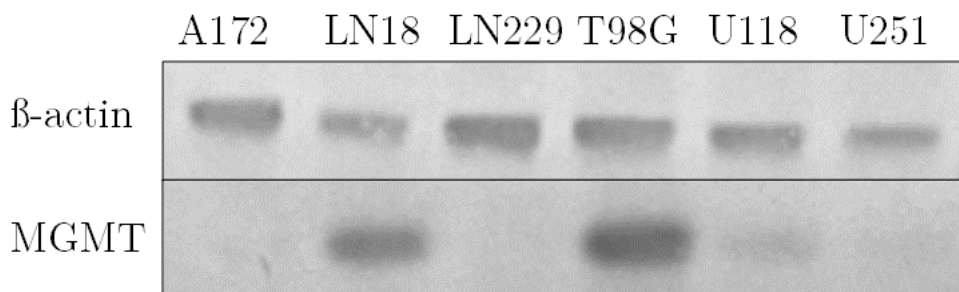


Figure 3.3: Western Blot analysis of all parental cell lines. Parental cell lines were analyzed regarding MGMT protein expression. Shown is the representative blot for the expression of MGMT and the housekeeper β -actin.

In line with the MethyQESD results LN18, T98G, and U118 are MGMT expressing cell lines, while A172 and LN229 do not express MGMT. The hemi-methylated U251 cell line shows low MGMT expression.

3.4 MGMT protein inhibition using Lomeguatrib

Since LN18, T98G, and U118 cells revealed the highest MGMT protein expression among the six tested cell lines, these three cell lines were subject to all further investigations.

In order to determine optimal conditions for MGMT inhibition, Western Blot was performed testing different concentrations of lomeguatrib for different time points. The representative blots are presented in Figure 3.4 and the quantification of MGMT relative to the β -actin expression is shown in Figure 3.5.

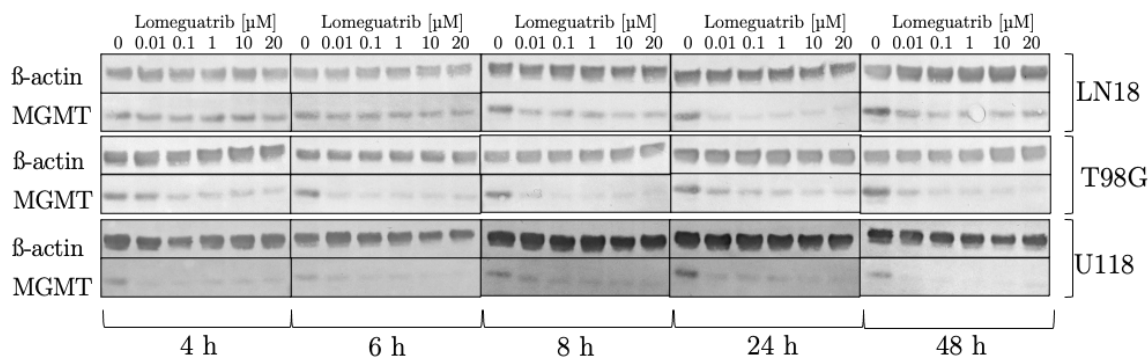


Figure 3.4: Western Blot analysis of LN18, T98G, and U118 cell lines. Increasing concentrations of lomeguatrib were added for 4 h, 6 h, 8 h, 24 hours, and 48 h prior to lysate preparation. Shown are the representative blots for the expression of MGMT and the housekeeper β -actin. Figure reprint from [45].

Significant MGMT inhibition was observed in LN18 cells only from the 6-hour time point on, while in T98G cells lomeguatrib significantly decreased MGMT protein expression already after 4 hours in all tested concentrations. U118 cells show significant MGMT inhibition at the 4-hour time point as well, however, after 8 hours and 48 hours MGMT inhibition was only significantly altered at 20 μ M respectively 0.01 μ M lomeguatrib.

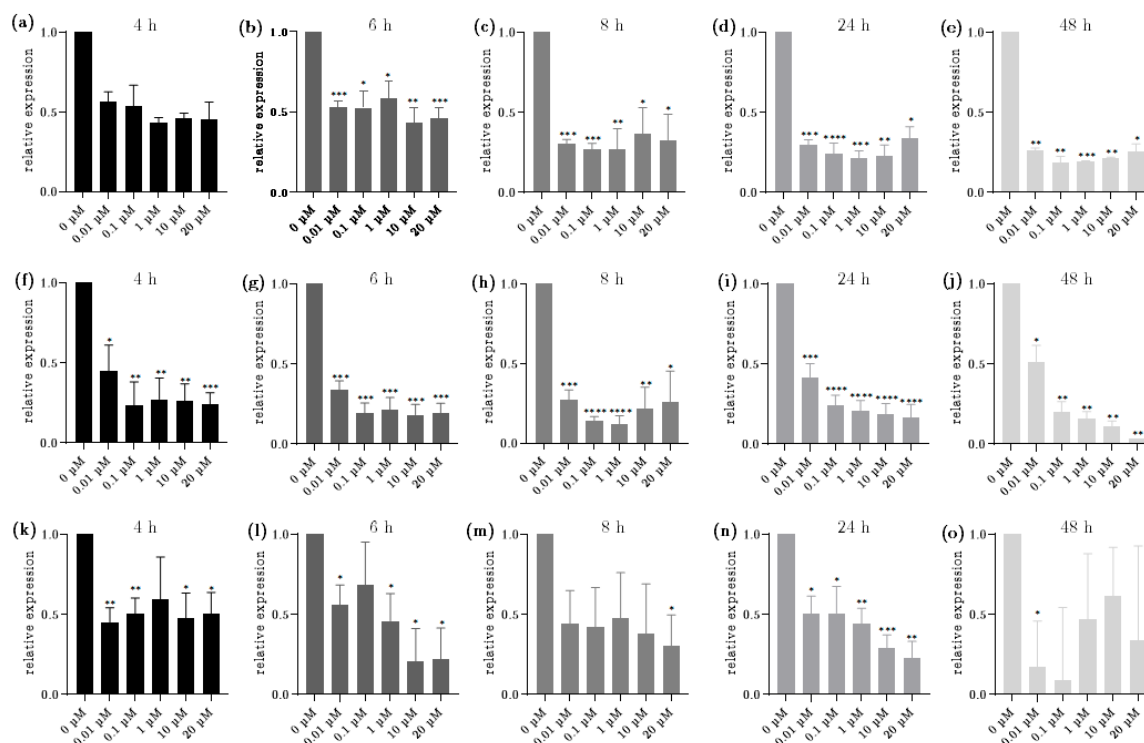


Figure 3.5: Western Blot quantification of LN18, T98G, and U118 cell lines. Quantification of at least three independent replicates with increasing concentrations of lomeguatrib for 4 h, 6 h, 8 h, 24 hours, and 48 h prior to lysate preparation. Error bars present the SEM of three replicates. Shown are LN18 (a-e), T98G (f-j), and U118 (k-o). (* $p \leq 0.05$, ** $p \leq 0.01$, *** $p \leq 0.001$, **** $p \leq 0.0001$).

Since a significant reduction in MGMT protein levels after 24 hours of lomeguatrib treatment was observed in all cell lines this treatment time was chosen for all following experiments with a concentration of 1 μM and 20 μM .

3.5 Cell proliferation

In order to determine the effects of lomeguatrib on cell proliferation, the alamarBlue proliferation assay was performed. 1 μM and 20 μM lomeguatrib were added for 24 hours and proliferation was measured every 24 hours for 72 hours.

LN18 and T98G were fast proliferating cell lines with doubling times of $16.4 \text{ h} \pm 5.4 \text{ h}$, and $16.1 \text{ h} \pm 1.8 \text{ h}$ respectively. U118 was slower proliferating with a doubling

time of 20.1 ± 4.8 h (Table 3.4). Neither 1 μM lomeguatrib nor 20 μM lomeguatrib changed the doubling times of the tested cell line.

Table 3.4. Doubling times of glioblastoma cell lines. Combination with 0 μM , 1 μM , and 20 μM lomeguatrib for 24 hours. P-values were calculated using Student's t-test. Table reprint from [45].

Cell line	Lomeguatrib [μM]	Doubling time [h]	p-value
LN18	0	16.4 ± 5.4	
	1	16.1 ± 4.8	0.9541
	20	22.6 ± 5.3	0.3065
T98G	0	16.1 ± 1.8	
	1	25.2 ± 1.8	0.5238
	20	30.6 ± 4.2	0.5135
U118	0	20.1 ± 4.8	
	1	18.0 ± 7.3	0.7425
	20	21.4 ± 9.7	0.8757

3.6 Cell survival upon lomeguatrib treatment

GBM cell lines were exposed to increasing concentrations of lomeguatrib for 8 to 12 days in order to determine its effect on cell survival without irradiation. A significant reduction in cell survival was seen in all cell lines upon 50 μM lomeguatrib treatment (Figure 3.6). In the T98G cell line already 10 μM and 20 μM , lomeguatrib significantly decreased cell survival.

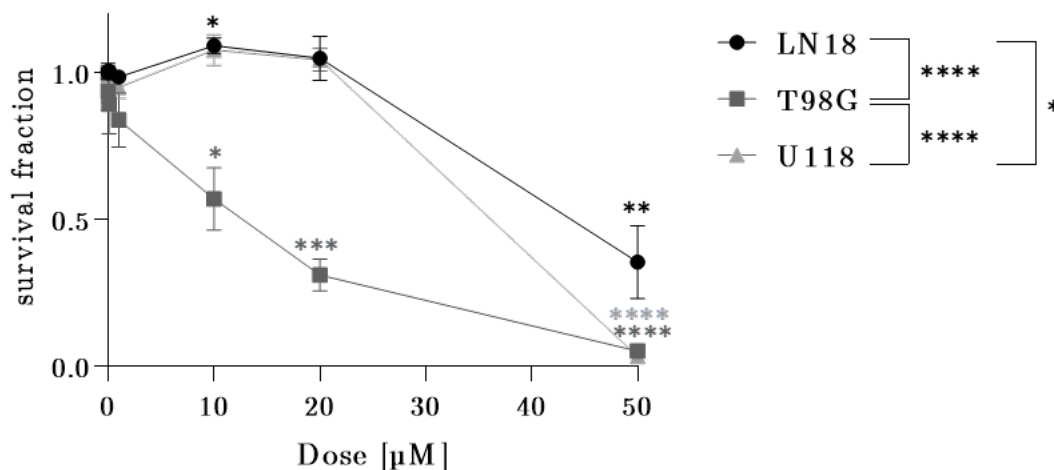


Figure 3.6: Cell survival after lomeguatrib treatment. Shown are the survival curves of LN18, T98G, and U118 exposed to increasing lomeguatrib concentrations for 8 to 12 days before colony fixation. Error bars present the SEM of three replicates. (* $p \leq 0.05$, ** $p \leq 0.01$, *** $p \leq 0.001$, **** $p \leq 0.0001$).

3.7 Lomeguatrib on cell cycle distribution

Cell cycle distribution was analyzed via FACS analysis 24 hours after treatment upon different lomeguatrib concentrations (Figure 3.7).

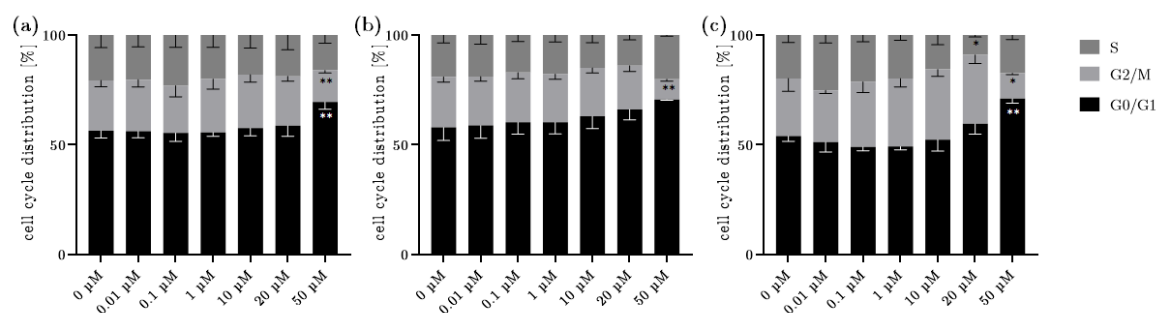


Figure 3.7: Cell cycle distribution after lomeguatrib treatment. (a) LN18, (b) T98G, and (c) U118 cells were treated with increasing concentrations of lomeguatrib for 24 hours prior to cell cycle FACS analysis. Significances were calculated in comparison to the untreated sample using Two-Way ANOVA. Error bars present the SEM of three replicates. Figure modified from [45]. (* $p \leq 0.05$, ** $p \leq 0.01$, *** $p \leq 0.001$).

Lomeguatrib doses from 0.01 µM to 20 µM did not change cell cycle distribution in the three tested cell lines. However, 20 µM lomeguatrib decreased U118 cells in S phase ($p = 0.0411$) compared to the untreated sample. Upon 50 µM lomeguatrib G1 phase distribution was increased in LN18 ($p = 0.0016$) and U118 ($p = 0.0059$) cells.

G2/M phase was decreased in all cell lines (LN18: $p = 0.0031$; T98G: $p = 0.0061$; U118: $p = 0.0686$).

3.8 MGMT expression, ionizing radiation, and lomeguatrib

As it is known that radiation decreases DNA methylation the effect of 8 Gy ionizing radiation alone as well as in combination with lomeguatrib was tested using Western Blot analysis. Figure 3.8 shows the representative blots for LN18, T98G, and U118 cell lines and the respective quantification of MGMT relative to β -actin expression.

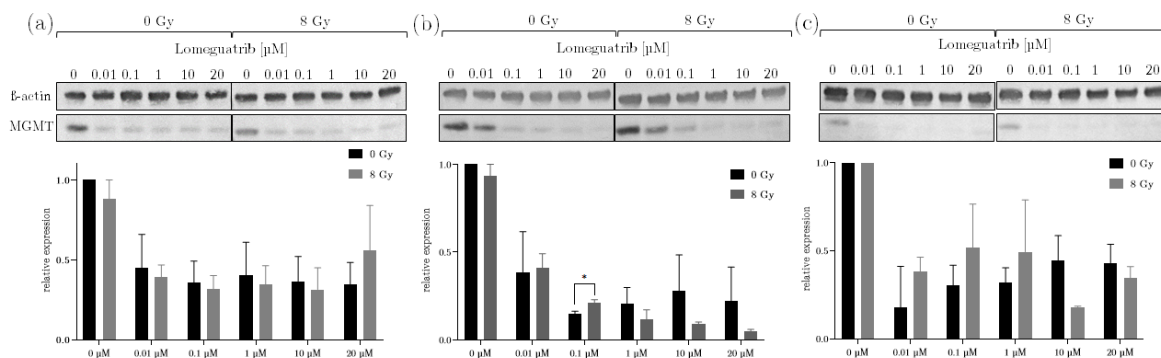


Figure 3.8: Western Blot analysis after combined irradiation and lomeguatrib treatment. Increasing concentrations of lomeguatrib were added for 24 hours before 0 Gy and 8 Gy irradiation. Lysates of (a) LN18, (b) T98G, and (c) U118 were prepared 24 hours after irradiation. Shown are the representative blots as well as the quantification of MGMT relative to β -actin expression. Error bars present the SEM of three replicates. Figure modified from [45]. (* $p \leq 0.05$).

Upon 8 Gy ionizing radiation alone no change in MGMT expression was observed in any cell line. The combination of lomeguatrib and irradiation did not change the expression of MGMT as well. Only in T98G upon 8 Gy ionizing radiation and 0.01 μ M lomeguatrib MGMT expression is higher compared to the sham irradiated sample.

3.9 Clonogenic cell survival upon combined lomeguatrib treatment

Lomeguatrib treatment of 1 μM and 20 μM for 24 hours prior to irradiation significantly changed the cell survival in all three tested MGMT unmethylated cell lines in a dose-dependent manner.

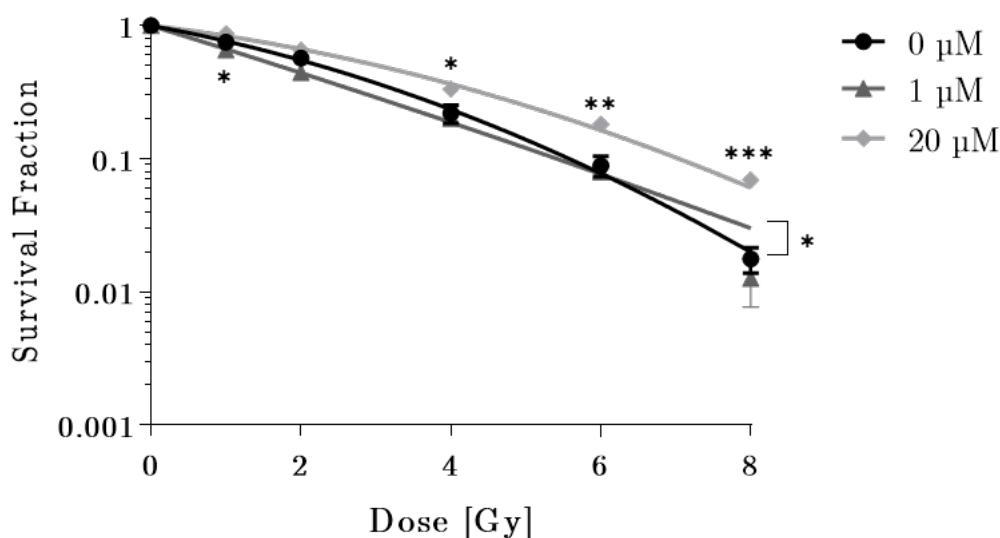


Figure 3.9: CFA of LN18 cells treated with 0 μM , 1 μM , and 20 μM lomeguatrib. Shown are the survival curves fitted to the linear-quadratic model. Significances between 0 μM and 1 μM are indicated below the curve, differences between 0 μM and 20 μM are shown above the curve, calculated applying Student's t-test. Error bars present the SEM of at least three replicate experiments. Figure reprint from [45]. (* $p \leq 0.05$, ** $p \leq 0.01$, *** $p \leq 0.001$).

24 hours of 1 μM or 20 μM lomeguatrib treatment significantly changed cell survival in LN18 cells (Figure 3.9). While 1 μM lomeguatrib shows an enhanced radiosensitizing effect ($p = 0.0126$), no effect was seen upon 20 μM lomeguatrib treatment. Significant differences between 0 μM and 1 μM were calculated only at 1 Gy ($p = 0.0074$ for 1 μM) applying Student's t-test. However, significant differences between 0 Gy and 20 μM were calculated at 4 Gy ($p = 0.0452$), 6 Gy ($p = 0.112$), and 8 Gy ($p = 0.0004$). The D_{50} value required to reduce cell survival to 50 % of 2.27

Gy in the untreated LN18 cell line increased to $3.05 \text{ Gy} \pm 0.04 \text{ Gy}$ upon $20 \text{ }\mu\text{M}$ lomeguatrib ($p = 0.0447$), and did not significantly change to $1.71 \text{ Gy} \pm 0.16 \text{ Gy}$ upon $1 \text{ }\mu\text{M}$ lomeguatrib treatment ($p = 0.1396$). The Sensitization Enhancement Ratio (SER) indicates the degree of the sensitizing agent with a value greater than 1 showing a radiosensitizing effect. Here, $1 \text{ }\mu\text{M}$ lomeguatrib shows a radiosensitizing effect with an SER of 1.36 ± 0.08 , while $20 \text{ }\mu\text{M}$ shows a decrease in SER to 0.76 ± 0.06 .

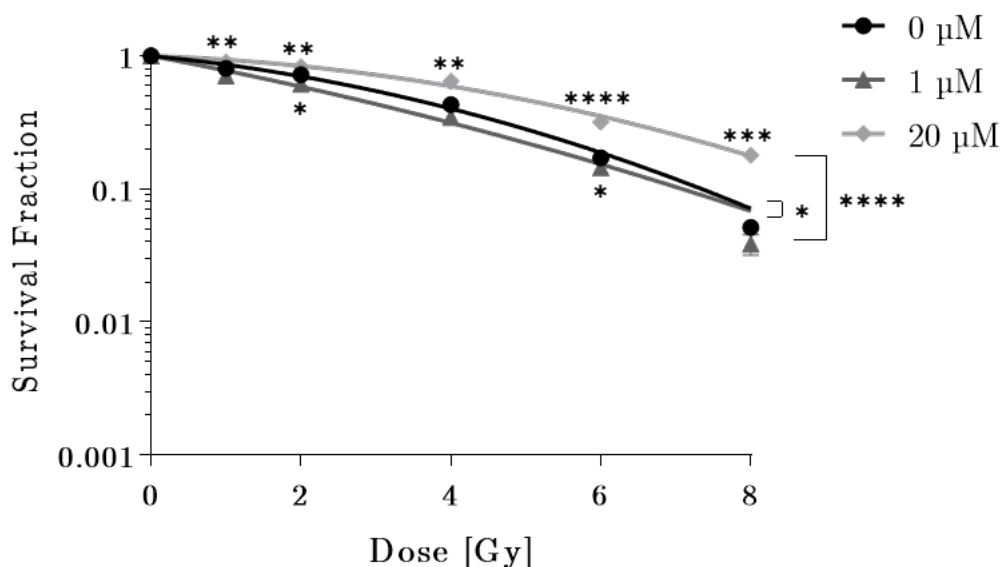


Figure 3.10: Colony-forming assay of T98G with $1 \text{ }\mu\text{M}$ or $20 \text{ }\mu\text{M}$ lomeguatrib. Shown are the survival curves fitted to the linear-quadratic model of T98G cells treated with $0 \text{ }\mu\text{M}$, $1 \text{ }\mu\text{M}$, and $20 \text{ }\mu\text{M}$ lomeguatrib for 24 hours before x-ray irradiation. Error bars present the SEM of three replicates. Significances between $0 \text{ }\mu\text{M}$ and $1 \text{ }\mu\text{M}$ are indicated below the curve, differences between $0 \text{ }\mu\text{M}$ and $20 \text{ }\mu\text{M}$ are shown above the curve. Error bars present the SEM of at least three replicate experiments. Figure reprint from [45]. (* $p \leq 0.05$, ** $p \leq 0.01$, *** $p \leq 0.001$, **** $p \leq 0.0001$).

Figure 3.10 shows the survival curves of T98G cells treated with $0 \text{ }\mu\text{M}$, $1 \text{ }\mu\text{M}$ or $20 \text{ }\mu\text{M}$ lomeguatrib. Here, $1 \text{ }\mu\text{M}$ lomeguatrib exhibits a radiosensitizing effect ($p = 0.0150$), while $20 \text{ }\mu\text{M}$ lomeguatrib increases radioresistance ($p < 0.0001$). Significant differences were calculated at all doses for the $20 \text{ }\mu\text{M}$ treatment ($p = 0.0075$ for 1 Gy , $p = 0.0093$ for 2 Gy , $p = 0.0023$ for 4 Gy , $p < 0.0001$ for 6 Gy , and $p = 0.0002$ for 8 Gy). The D_{50} of the untreated T98G cells is $3.29 \text{ Gy} \pm 0.12 \text{ Gy}$, indicating a higher

radioresistance than LN18 cells. Upon 1 μM lomeguatrib treatment the D_{50} reduces to $2.54 \text{ Gy} \pm 0.18 \text{ Gy}$ ($p = 0.0280$) and increases to $4.72 \text{ Gy} \pm 0.08 \text{ Gy}$ ($p = 0.0010$) after 20 μM lomeguatrib treatment. Accordingly, the SER for 1 μM lomeguatrib is 1.30 ± 0.05 , indicating a radiosensitizing effect, while the SER for 20 μM lomeguatrib treatment is 0.70 ± 0.01 indicating an enhanced radioresistance.

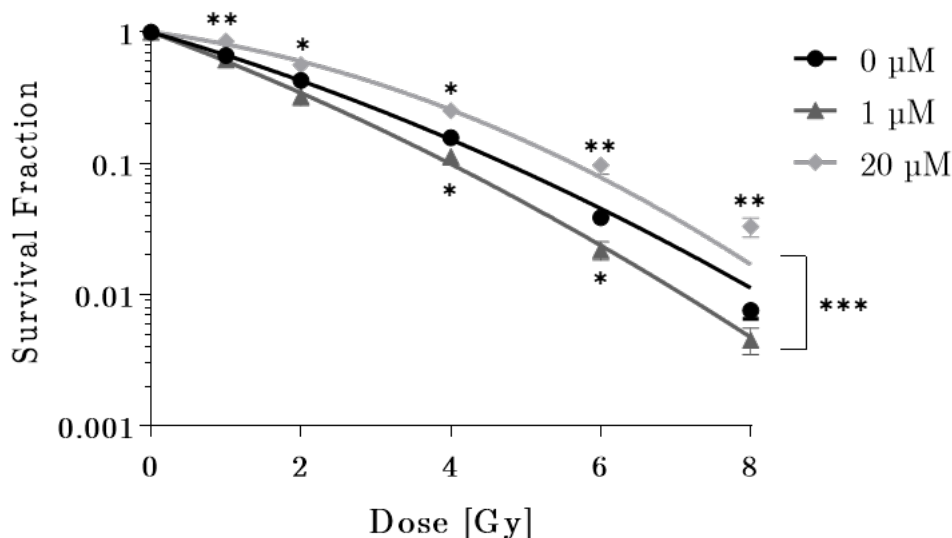


Figure 3.11: Colony-forming assay of U118 with 1 μM and 20 μM lomeguatrib. Shown are the survival curves fitted to the linear-quadratic model of U118 cells treated with 0 μM , 1 μM , and 20 μM lomeguatrib for 24 hours before x-ray irradiation. Significances between 0 μM and 1 μM are indicated below the curve, differences between 0 μM and 20 μM are shown above the curve. Error bars present the SEM of at least three replicate experiments. Figure reprint from [45]. (* $p \leq 0.05$, ** $p \leq 0.01$, *** $p \leq 0.001$, **** $p \leq 0.0001$).

The same results were found for the third cell line U118 (Figure 3.11), as well. Differences in the survival curves were only detected between 0 μM and 20 μM ($p = 0.0008$) applying Two-Way ANOVA. Upon 1 μM lomeguatrib the D_{50} changed to $1.36 \text{ Gy} \pm 0.09 \text{ Gy}$ compared to $1.67 \text{ Gy} \pm 0.11 \text{ Gy}$ of the untreated cells. 20 μM lomeguatrib significantly increased radioresistance with a D_{50} of $2.51 \text{ Gy} \pm 0.20 \text{ Gy}$ ($p = 0.0082$). Significant differences between the untreated cells and the 1 μM treated cells were determined at 4 Gy ($p = 0.0300$), and 6 Gy ($p = 0.0300$). Upon 20 μM lomeguatrib significant differences were determined at 1 Gy ($p = 0.0018$), 2 Gy ($p =$

0.0494), 4 Gy ($p = 0.0132$), 6 Gy ($p = 0.0032$), and 8 Gy ($p = 0.0014$). The SER shows a radiosensitizing effect of the lower lomeguatrib treatment with a value of 1.32 ± 0.12 and enhanced radioresistance at the higher concentration with an SER of 0.66 ± 0.08 .

Table 3.5 summarizes all D_{10} , D_{50} , and SER values.

Table 3.5: Linear-quadratic parameters. Shown are the biological parameters of LN18, T98G, and U118 cells with 0 μM , 1 μM , and 20 μM lomeguatrib treatment. Table modified from [45].

Cell line	LM	D_{10} [Gy] ^a	D_{50} [Gy] ^b	SER (50%) ^c	α [Gy ⁻¹] ^d	β [Gy ⁻²] ^d
LN18	0 μM	5.55 ± 0.30	2.27 ± 0.24	1	0.2353 ± 0.1358	0.0333 ± 0.0192
	1 μM	5.26 ± 0.18	1.71 ± 0.16	1.36 ± 0.08	0.3974 ± 0.1777	0.0065 ± 0.0029
	20 μM	7.28 ± 0.06	3.05 ± 0.04	0.76 ± 0.06	0.1517 ± 0.0876	0.0249 ± 0.0144
T98G	0 μM	7.05 ± 0.03	3.29 ± 0.12	1	0.1264 ± 0.0730	0.0255 ± 0.0147
	1 μM	6.66 ± 0.12	2.54 ± 0.18	1.30 ± 0.05	0.2439 ± 0.1408	0.0116 ± 0.0067
	20 μM	9.28 ± 0.08	4.72 ± 0.08	0.70 ± 0.01	0.0456 ± 0.0263	0.0214 ± 0.0123
U118	0 μM	4.63 ± 0.13	1.67 ± 0.11	1	0.3789 ± 0.1694	0.0246 ± 0.0110
	1 μM	4.14 ± 0.25	1.36 ± 0.09	1.32 ± 0.12	0.4360 ± 0.2517	0.0581 ± 0.0336
	20 μM	5.92 ± 0.26	2.51 ± 0.20	0.66 ± 0.08	0.1637 ± 0.0819	0.0474 ± 0.0237

a: D_{10} dose [Gy] required to reduce cell survival to 10%.

b: D_{50} dose [Gy] required to reduce cell survival to 50%.

c: SER (50%) Sensitization enhancement ratio calculated from $D_{50}(\text{untreated})/D_{50}(\text{treated})$

d: α and β values calculated from the linear-quadratic equation: $\ln \text{SF} = -\alpha \times D - \beta \times D^2$.

3.10 Cell cycle distribution after lomeguatrib and radiation

To further investigate the effects of lomeguatrib on cell cycle distribution, samples were irradiated 24 hours after lomeguatrib addition and subjected to cell cycle FACS analysis 24 hours afterward. Figure 3.12 shows the data for LN18 cells.

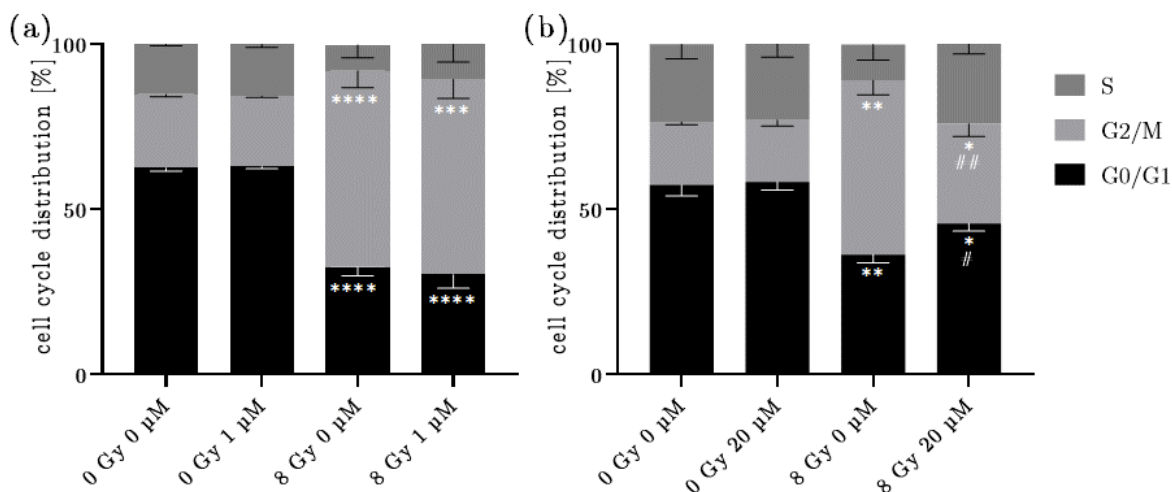


Figure 3.12: Cell cycle distribution in LN18 cells. (a) shows cell cycle distribution after 1 μM lomeguatrib and irradiation. (b) shows cell cycle distribution after 20 μM lomeguatrib and irradiation. Error bars present the SEM of three replicates. Asterisks indicate significances of the different treatments versus the 0 Gy 0 μM lomeguatrib sample of the respective cell cycle phase, while hash symbols represent significances between 0 Gy 0 μM to 0 Gy 1 μM or 20 μM and 8 Gy 0 μM to 8 Gy 1 μM or 20 μM . Figure reprint from [45]. (Student's t-test; * and # $p \leq 0.05$, ** and ## $p \leq 0.01$, *** $p \leq 0.001$, **** $p \leq 0.0001$).

8 Gy ionizing radiation enhanced the G2/M cell cycle fraction ($p < 0.0001$) and decreased G1 fraction ($p < 0.0001$). Neither 1 μM lomeguatrib nor 20 μM lomeguatrib alone did change cell cycle distribution nor did 1 μM lomeguatrib combined with 8 Gy irradiation compared to the sample that was irradiation only. However, the combination of 20 μM lomeguatrib with 8 Gy ionizing radiation decreased the fraction of cells in G2/M phase ($p = 0.0085$) and simultaneously increased G1 phase ($p = 0.0332$) but only a trend towards a decreased S phase ($p = 0.0687$) was observed compared to the sample that received 8 Gy irradiation only

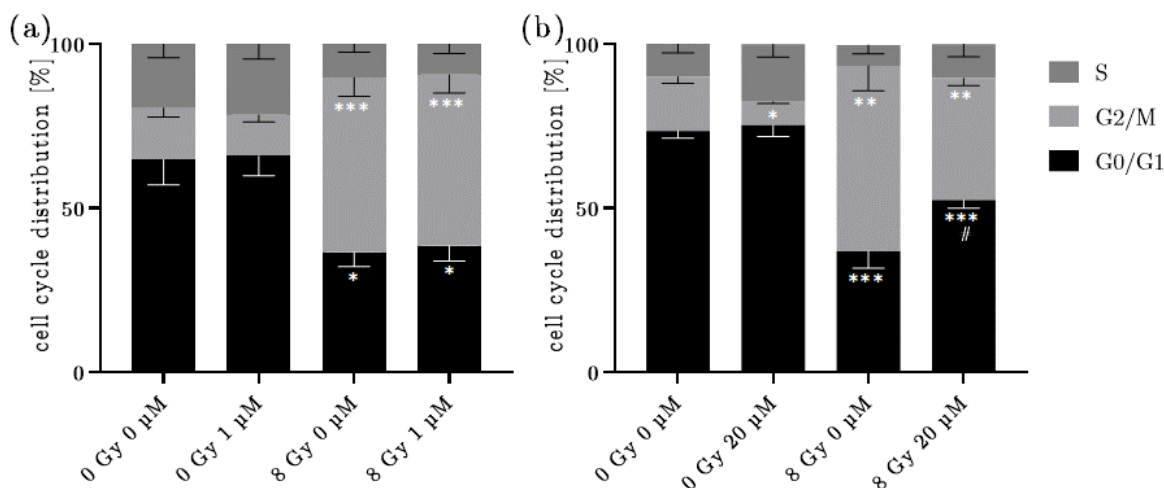


Figure 3.13: Cell cycle distribution after lomeguatrib and radiation treatment in T98G cells. (a) shows cell cycle distribution after 1 μM lomeguatrib and radiation treatment. (b) shows cell cycle distribution after 20 μM lomeguatrib and 8 Gy irradiation. Error bars present the SEM of three replicates. Asterisks indicate significances of the different treatments versus the 0 Gy 0 μM lomeguatrib sample of the respective cell cycle phase, while hash symbols represent significances between 0 Gy 0 μM to 0 Gy 1 μM or 20 μM and 8 Gy 0 μM to 8 Gy 1 μM or 20 μM . Figure reprint from [45]. (Student's t-test; * and # $p \leq 0.05$, ** $p \leq 0.01$, *** $p \leq 0.001$, **** $p \leq 0.0001$).

Similar results were obtained in the T98G cell line; G2/M fraction decreased after 8 Gy ionizing radiation ($p = 0.0003$), as well as 1 μM lomeguatrib alone, did not affect cell cycle distribution. 20 μM lomeguatrib in contrast decreased cells in G2/M phase ($p = 0.0140$). G1 phase increased ($p = 0.0342$) and a trend towards a decreased G2/M phase ($p = 0.0511$) was observed in the 8 Gy irradiated and 20 μM lomeguatrib treated samples, compared to the sample of 8 Gy irradiation only.

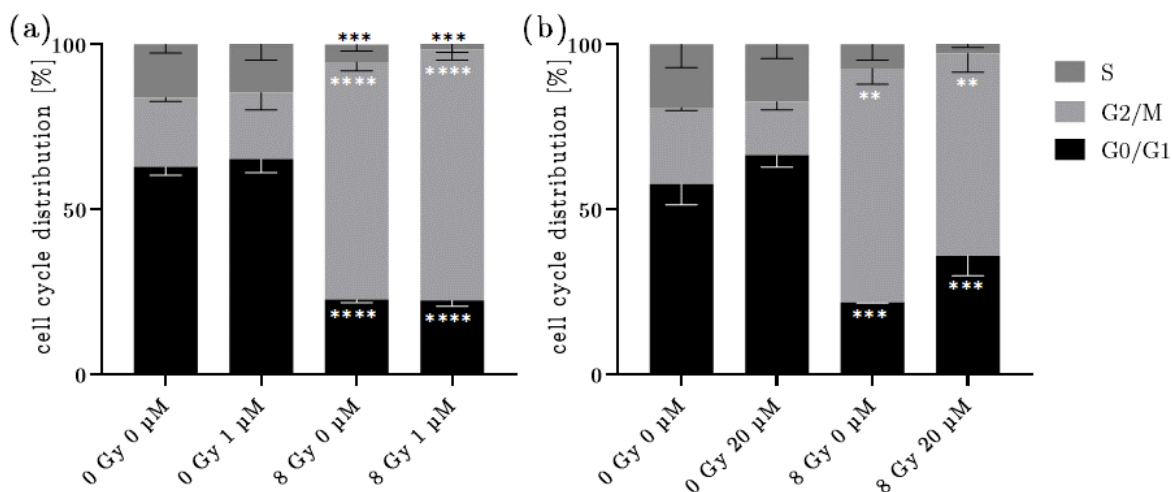


Figure 3.14: Cell cycle distribution after lomeguatrib and radiation treatment in U118 cells. (a) shows cell cycle distribution after 1 μM lomeguatrib and radiation treatment. (b) shows cell cycle distribution after 20 μM lomeguatrib and 8 Gy irradiation. Error bars present the SEM of three replicates. Asterisks indicate the significances of the different treatments versus the 0 Gy 0 μM lomeguatrib sample of the respective cell cycle phase. Figure reprint from [45]. (Student's t-test; * $p \leq 0.05$, ** $p \leq 0.01$, *** $p \leq 0.001$, **** $p \leq 0.0001$).

A G2/M arrest was observed in U118 cells after 8 Gy irradiation as well ($p < 0.0001$). Neither 1 μM lomeguatrib treatment alone nor 20 μM lomeguatrib did affect cell cycle distribution. Also, no significant differences were detected comparing the 8 Gy irradiated sample to the 8 Gy and 1 μM lomeguatrib or 8 Gy and 20 μM lomeguatrib treated sample. Only a trend towards a decreased G2/M ($p = 0.0941$) and S phase ($p = 0.0532$) was observed upon 1 μM lomeguatrib. Further, a trend towards an increase in G1 cells was observed ($p = 0.0809$) comparing the sample that received 8 Gy only to the sample that received 8 Gy and 20 μM lomeguatrib.

Taken together all these results, these data suggest that lomeguatrib counteracts the radiation-induced G2/M arrest. A detailed list of all p-values is presented in Appendix Table A.1.

3.11 DNA damage and DNA repair

In order to analyze DNA double-strand breaks upon lomeguatrib treatment or ionizing radiation treatment alone as well as in combination γ H2AX foci were analyzed 30 minutes as well as 24 hours after irradiation, i.e. 24 hours, respectively 48 hours after 0 μ M, 1 μ M or 20 μ M lomeguatrib addition. Figure 3.15 shows the foci per LN18 cell nucleus 30 minutes and 24 hours after irradiation.

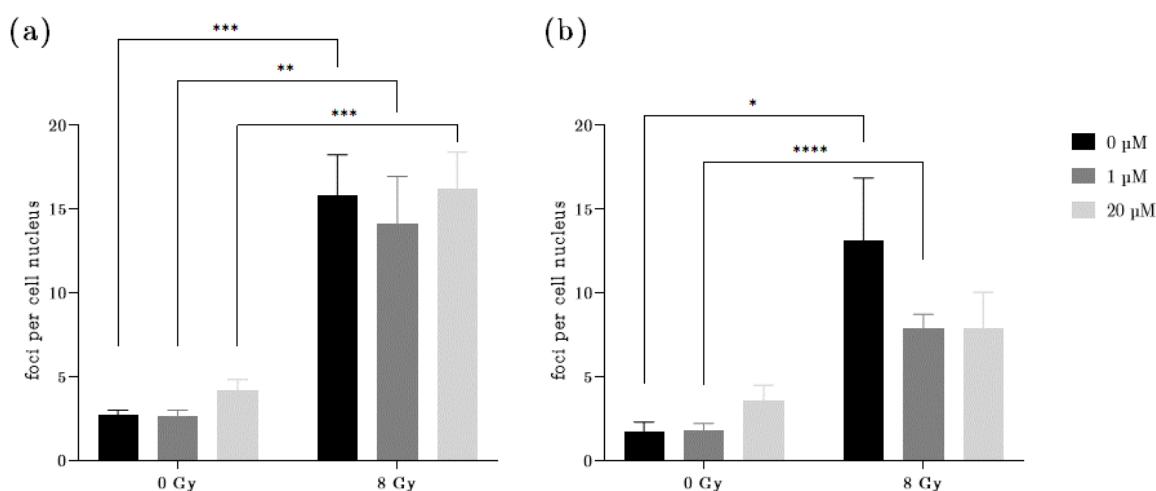


Figure 3.15: γ H2AX foci in LN18 cells. (a) shows the mean foci per cell 30 minutes after irradiation and (b) shows the mean residual foci after 24 hours. Error bars present the SEM of three replicates. (Student's t-test; * $p \leq 0.05$, ** $p \leq 0.01$, *** $p \leq 0.001$, **** $p \leq 0.0001$).

Mean γ H2AX foci per cell significantly increased 30 minutes after 8 Gy ionizing radiation with and without lomeguatrib. No differences were detected between the untreated and the 1 μ M or 20 μ M lomeguatrib treated samples with or without irradiation. 24 hours after 8 Gy irradiation mean γ H2AX foci reduced in all tested samples. No difference was detected between the lomeguatrib treatment groups.

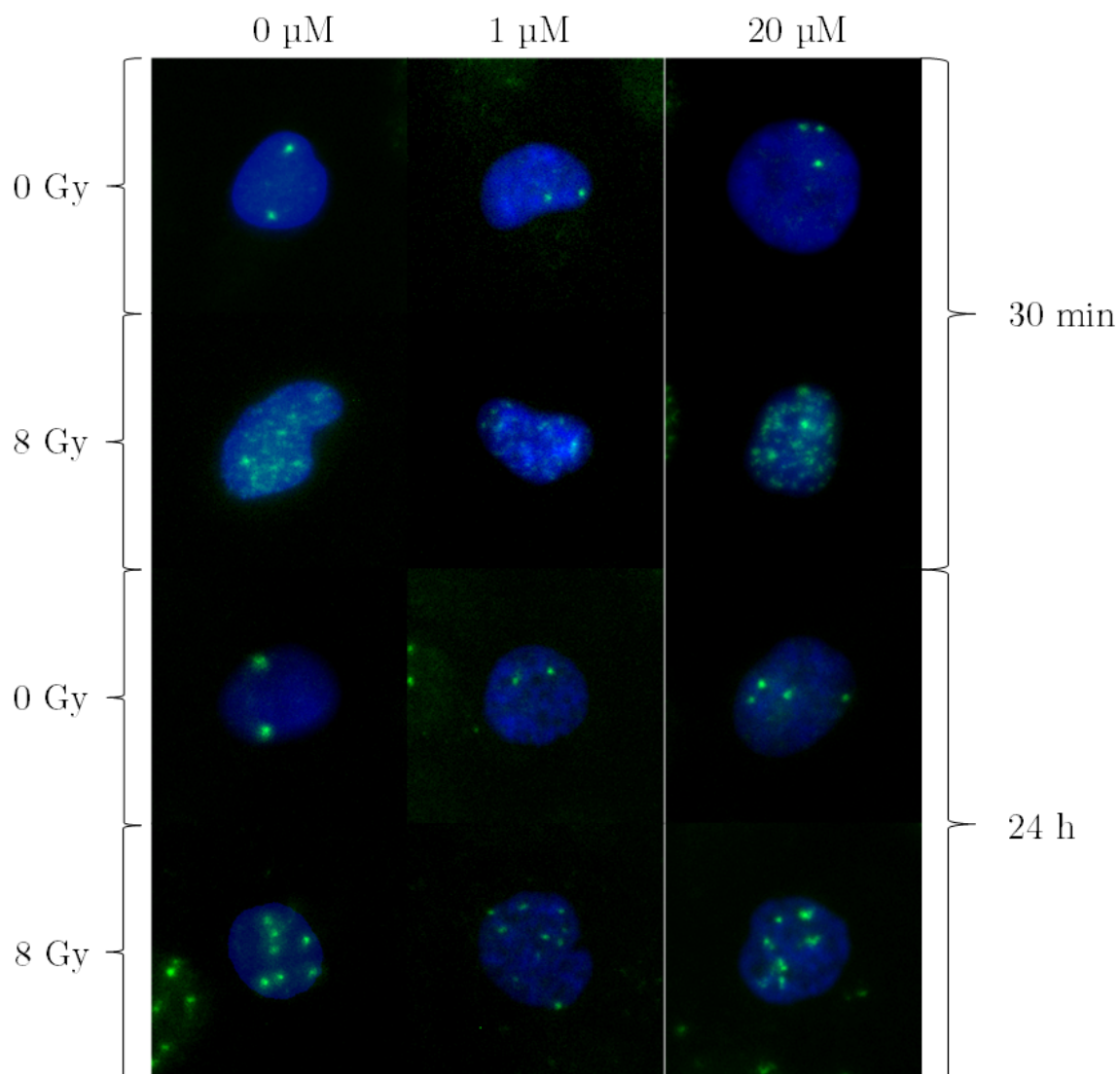


Figure 3.16: Exemplary figures of γ H2AX foci staining in LN18 cells. γ H2AX foci were stained 30 minutes, as well as 24 hours after 0 Gy and 8 Gy irradiation (green stain), and cell nuclei were stained using Hoechst (blue stain).

Figure 3.16 shows representative pictures of LN18 cell nuclei (blue stain) with γ H2AX foci (green stain).

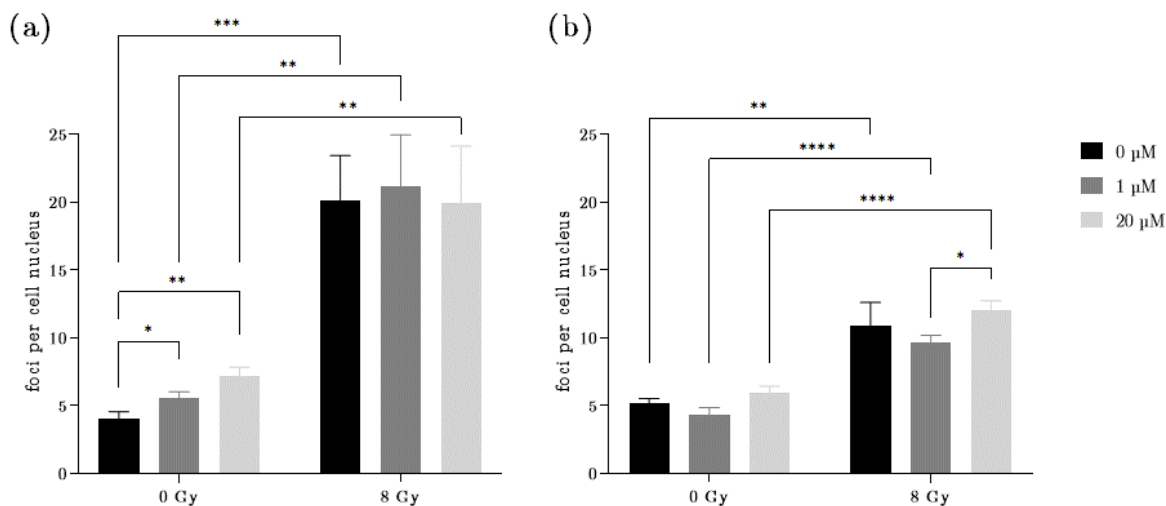


Figure 3.17: γ H2AX foci in T98G cells. (a) shows the mean foci per cell 30 minutes after irradiation and (b) shows the mean residual foci after 24 hours. Error bars present the SEM of three replicates. (Student's t-test; * $p \leq 0.05$, ** $p \leq 0.01$, *** $p \leq 0.001$, **** $p \leq 0.0001$).

Figure 3.17 shows the mean γ H2AX foci per cell nucleus in T98G cells. 30 minutes after 8 Gy irradiation the mean number of γ H2AX foci significantly increased in all lomeguatrib treatment groups. Significant differences were detected in the unirradiated samples between 0 μ M and 1 μ M lomeguatrib ($p = 0.0378$) and between 0 μ M and 20 μ M ($p = 0.0041$). 24 hours after irradiation the number of mean residual γ H2AX foci was still significantly increased compared to the unirradiated samples (0 μ M: $p = 0.0079$; 1 μ M $p < 0.0001$; 20 μ M: $p < 0.0001$). A significant difference between the lomeguatrib treatment groups was observed between 1 μ M and 20 μ M treated samples in combination with 8 Gy irradiation ($p = 0.0156$).

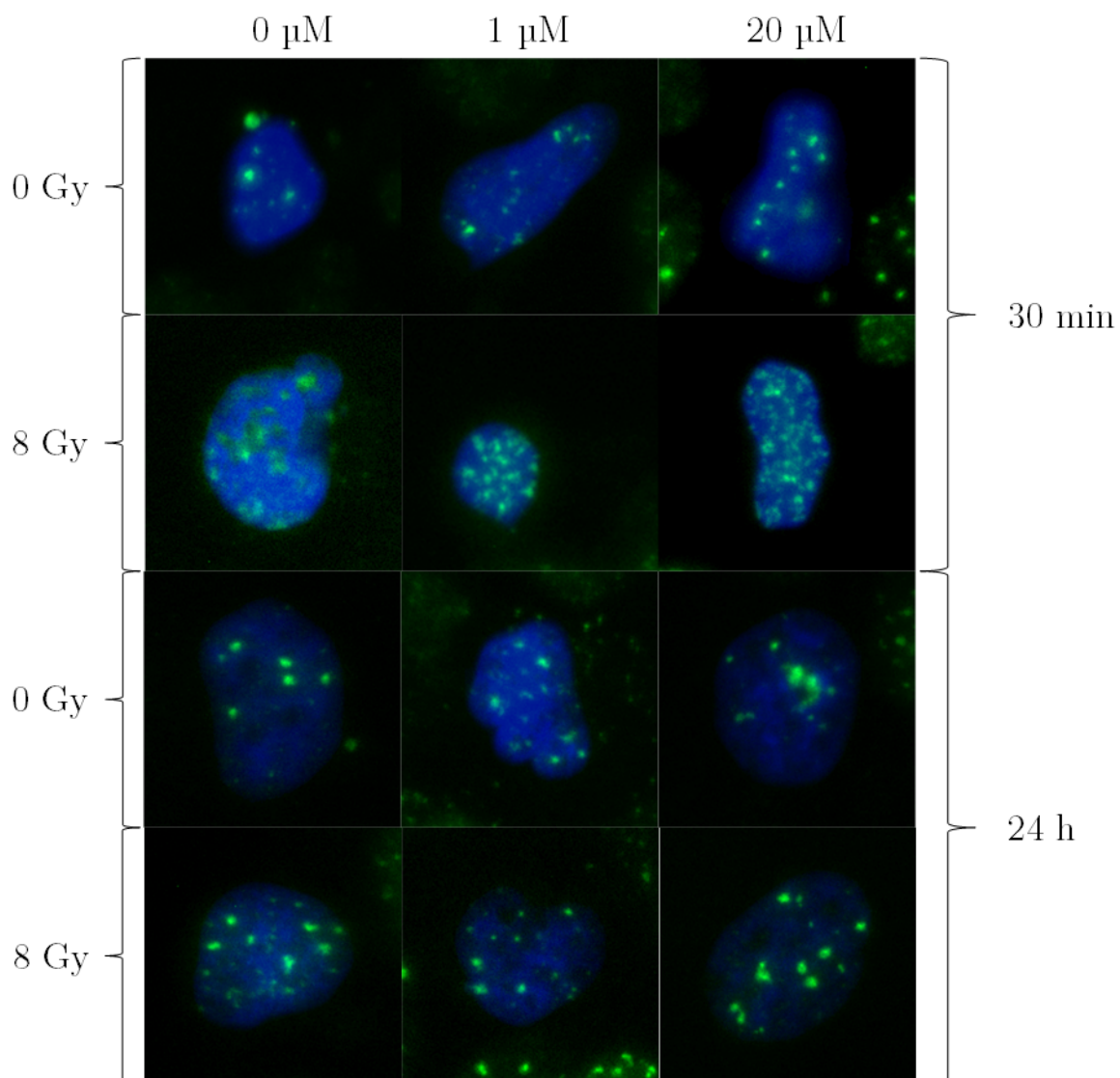


Figure 3.18: Exemplary figures of γH2AX foci staining in T98G cells. γH2AX foci were stained 30 minutes, as well as 24 hours after 0 Gy and 8 Gy irradiation (green stain), and cell nuclei were stained using Hoechst (blue stain).

Figure 3.18 shows representative pictures of T98G cell nuclei (blue stain) with γH2AX foci (green stain).

Figure 3.19 shows the foci per U118 cells after (a) 30 minutes and (b) 24 hours.

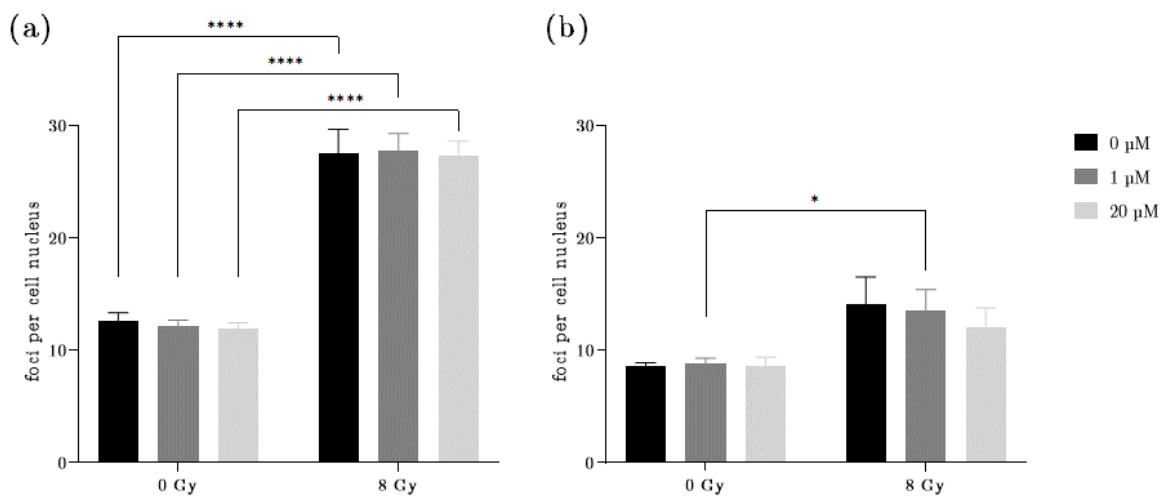


Figure 3.19: γ H2AX foci in U118 cells. (a) shows the mean foci per cell 30 minutes after irradiation and (b) shows the mean residual foci after 24 hours. Error bars present the SEM of three replicates. (Student's t-test; * $p \leq 0.05$, **** $p \leq 0.0001$).

A significant increase in γ H2AX foci 30 minutes after irradiation was observed for all lomeguatrib treatment groups ($p < 0.0001$). Significantly increased residual γ H2AX foci were observed after 24 hours only upon 1 μ M lomeguatrib treatment ($p = 0.0209$). However, no difference was observed upon lomeguatrib alone, or in combination with 8 Gy ionizing radiation, neither after 30 minutes nor after 24 hours.

In Figure 3.20 representative pictures of U118 cell nuclei (blue stain) with γ H2AX foci (green stain) are presented.

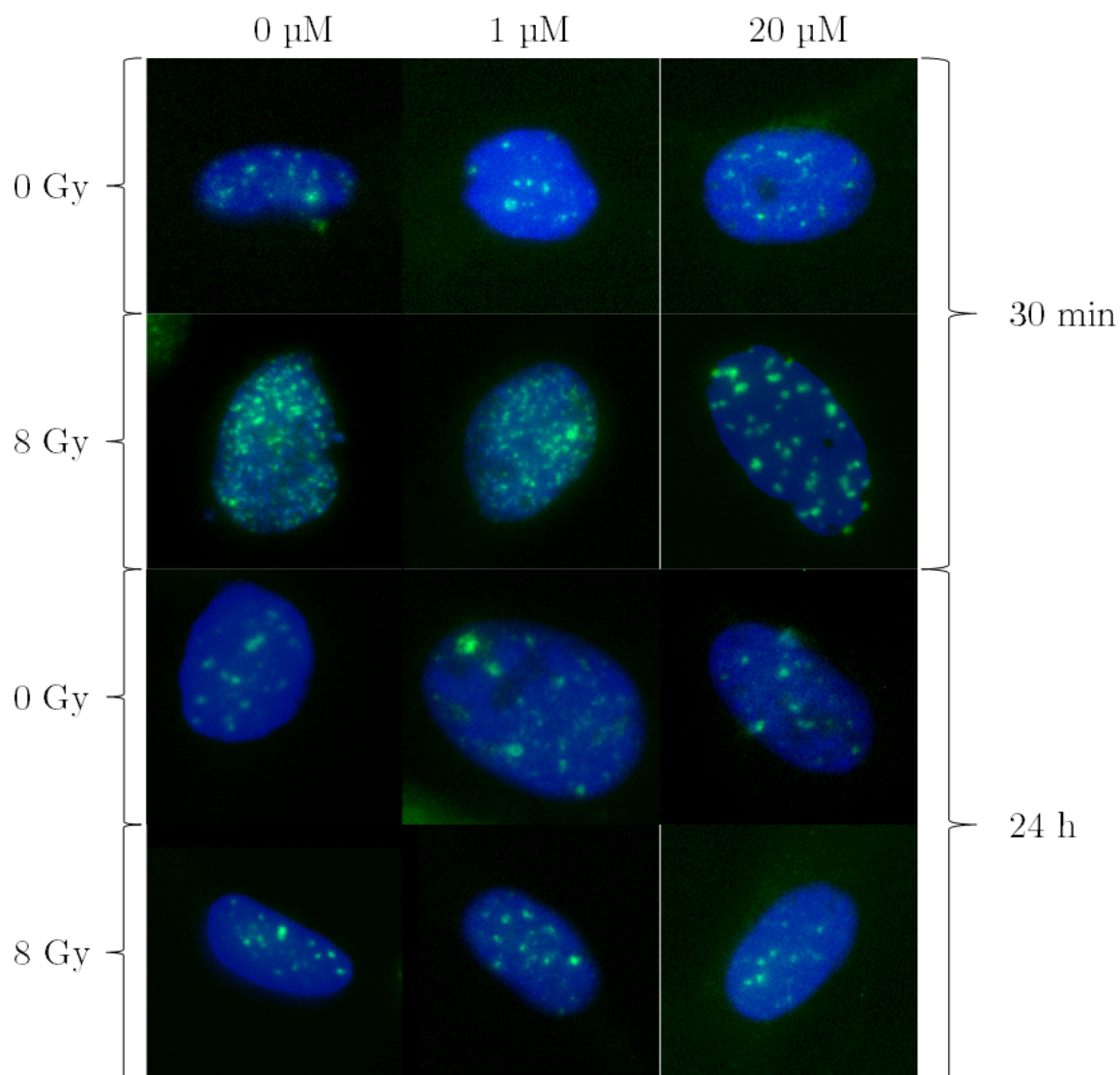


Figure 3.20: Exemplary figures of γ H2AX foci staining in U118 cells. γ H2AX foci were stained 30 minutes, as well as 24 hours after 0 Gy and 8 Gy irradiation (green stain), and cell nuclei were stained using Hoechst (blue stain).

In summary, lomeguatrib does not affect radiation-induced DNA damages.

3.12 Apoptosis

In order to investigate apoptosis induction upon lomeguatrib and the combination of lomeguatrib and radiation, caspase-3/-7 activation was analyzed by flow cytometry.

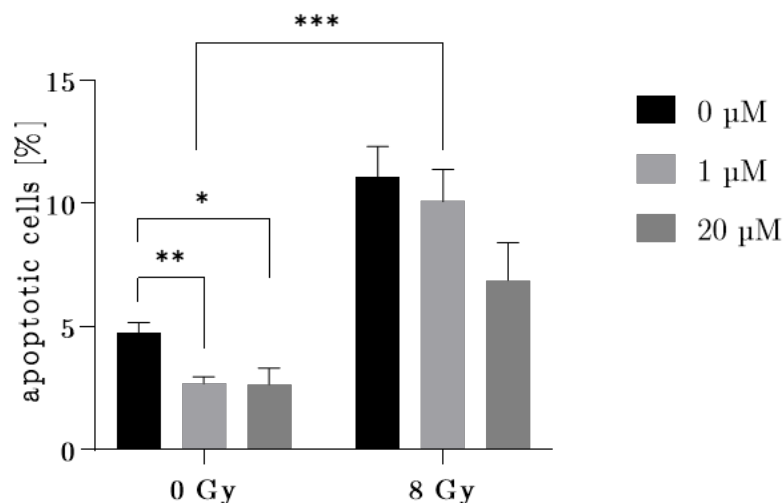


Figure 3.21: Apoptosis after lomeguatrib and radiation treatment in LN18 cells. Shown are the percentage of apoptotic cells 72 hours after 0 μM, 1 μM or 20 μM lomeguatrib treatment, and 48 hours after 0 Gy or 8 Gy ionizing radiation. Asterisks indicate significances between the treatment groups. Figure reprint from [45]. (Student's t-test; * $p \leq 0.05$, ** $p \leq 0.01$, *** $p \leq 0.001$).

Figure 3.21 shows the apoptotic cells 48 hours after irradiation, i.e. 72 hours after lomeguatrib treatment in LN18 cells. 1 μM as well as 20 μM lomeguatrib alone significantly decreased the number of apoptotic cells compared to the untreated sample. No effect was observed after combined radiation and lomeguatrib treatment. Radiation-induced apoptosis was observed after 8 Gy irradiation in combination with 1 μM lomeguatrib.

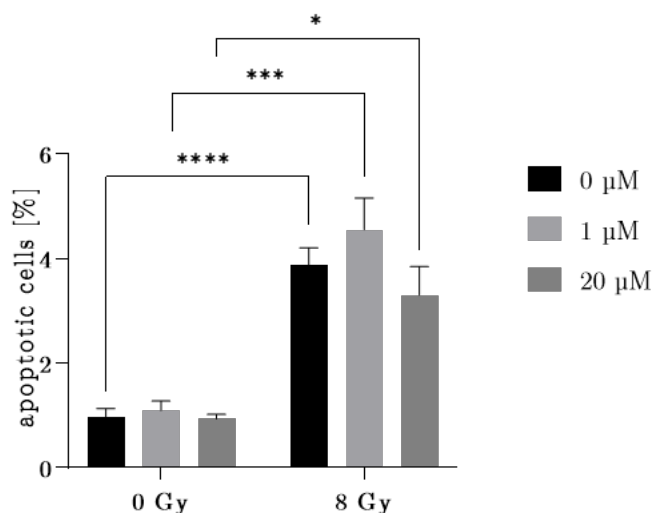


Figure 3.22: Apoptosis after lomeguatrib and radiation treatment in T98G cells. Shown are the percentage of apoptotic cells 72 hours after 0 μM, 1 μM or 20 μM lomeguatrib treatment, and 48 hours after 0 Gy or 8 Gy ionizing radiation. Asterisks indicate significances between the treatment groups. Figure reprint from [45]. (Student's t-test; * $p \leq 0.05$, *** $p \leq 0.001$, **** $p \leq 0.0001$).

Neither 1 μM nor 20 μM lomeguatrib alone or in combination with ionizing radiation affected apoptosis in T98G cells (Figure 3.22). 8 Gy ionizing radiation shows induction of apoptosis, as well as after 1 μM and 20 μM lomeguatrib compared to the respective untreated samples.

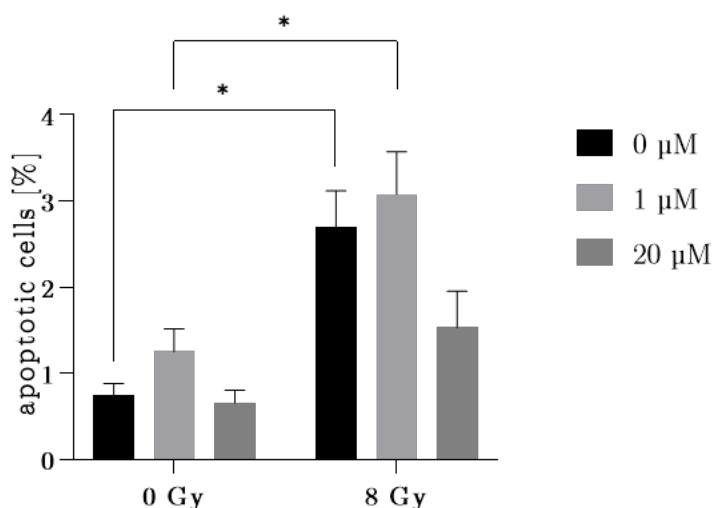


Figure 3.23: Apoptosis after lomeguatrib and radiation treatment in U118 cells. Shown are the percentage of apoptotic cells 72 hours after 0 μM, 1 μM or 20 μM lomeguatrib treatment, and 48 hours after 0 Gy or 8 Gy ionizing radiation. Asterisks indicate significances between the treatment groups. Figure reprint from [45]. (Student's t-test; * $p \leq 0.05$).

Radiation-induced apoptosis was observed in U118 cells as well (Figure 3.23). However, lomeguatrib alone nor in combination with ionizing radiation affected apoptosis.

In summary, these data suggest that lomeguatrib does not affect radiation-induced apoptosis.

3.13 Migration capacity of GBM cell lines

Since glioblastoma is characterized by intense migration, the migratory behavior was analyzed by the migration wound healing assay. Cells were exposed to 0 μM , 1 μM or 20 μM lomeguatrib for 24 hours before 0 Gy or 8 Gy irradiation followed by migration for 48 hours. Initial pictures were taken 24 hours after lomeguatrib treatment, i.e. immediately after irradiation, and denoted as 0 hours.

The basal migratory capacity of the LN18 cell line is presented in Figure 3.24 (a) without irradiation.

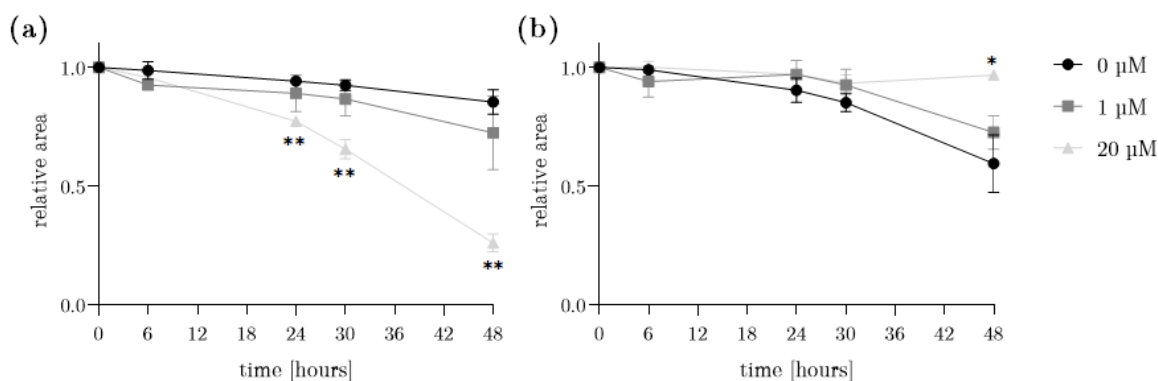


Figure 3.24: Relative wound closure LN18 cells. LN18 cells were exposed to 0 μM , 1 μM , or 20 μM lomeguatrib for 24 hours before (a) 0 Gy and (b) 8 Gy irradiation. Cells were allowed to migrate for 48 hours. Student's t-test was applied to calculate differences between 0 μM and 1 μM , and 0 μM and 20 μM indicated with asterisks. (* $p \leq 0.05$, * $p \leq 0.01$).

LN18 cells show significant basal migration behavior. Upon 20 μM lomeguatrib a significant increase in migration was observed after 24 hours ($p < 0.0001$), 30 hours ($p = 0.0015$), and 48 hours ($p = 0.0170$, Figure 3.24 a). After 8 Gy irradiation an increased migration behavior was detected after 24 hours ($p = 0.0167$) and after 48 hours ($p = 0.0288$, Figure 3.24 b) in the lomeguatrib untreated cells. 1 μM lomeguatrib only affected migration behavior in combination with irradiation after 48 hours ($p = 0.0177$). 20 μM lomeguatrib significantly decreased migration behavior 48 hours after 8 Gy irradiation compared to the 20 μM lomeguatrib unirradiated sample ($p = 0.0004$).

The basal migratory capacity of the T98G cell line is presented in Figure 3.25 (a) and in combination with 8 Gy ionizing radiation in Figure 3.25 (b).

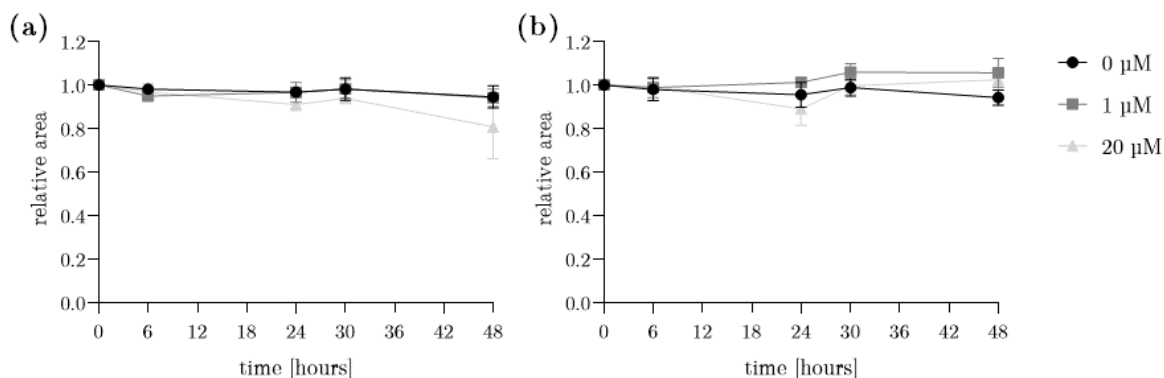


Figure 3.25: Relative wound closure T98G cells. T98G cells were exposed to 0 μM , 1 μM , or 20 μM lomeguatrib for 24 hours followed by 0 Gy (a) or 8 Gy (b) irradiation. Cells were allowed to migrate for 48 hours.

Student's t-test neither revealed differences between the untreated and the 1 μM or 20 μM lomeguatrib treated cells nor in combination with ionizing radiation at any time point.

The migration behavior of U118 is presented in Figure 3.26 (a) for 0 Gy and (b) for 8 Gy in addition to 0 μM , 1 μM , or 20 μM lomeguatrib.

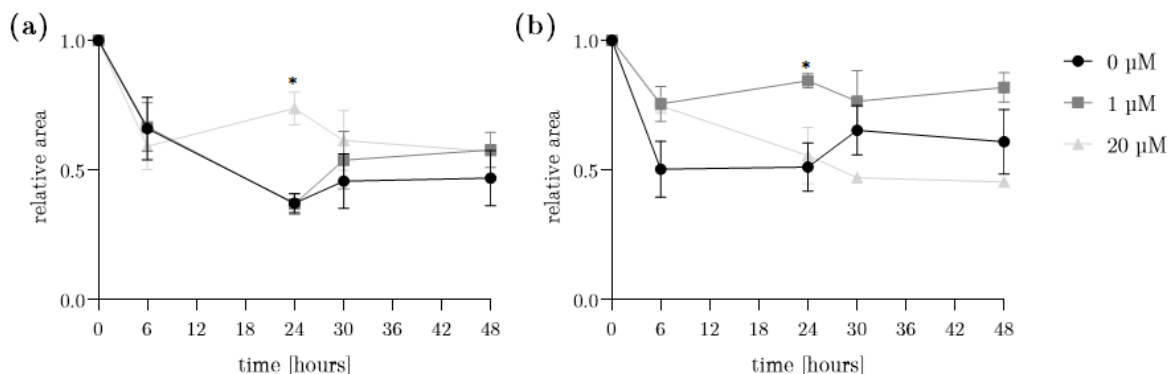


Figure 3.26: Relative wound closure U118 cells. U118 cells were exposed to 0 μM , 1 μM , or 20 μM lomeguatrib for 24 hours followed by 0 Gy (a) or 8 Gy (b) irradiation. Cells were allowed to migrate for 48 hours. Student's t-test was applied to calculate differences between 0 μM and 1 μM , and 0 μM and 20 μM indicated with asterisks. (* $p \leq 0.05$).

U118 cells show high basal migration behavior, which is not altered by lomeguatrib. No significant differences were detected between the lomeguatrib untreated and treated samples except after 24 hours a significant difference in the 20 μM lomeguatrib compared to the untreated cells was detected ($p = 0.0238$, Figure 3.26 a). 24 hours after 8 Gy irradiation migration was significantly decreased upon 1 μM lomeguatrib compared to the 0 μM lomeguatrib sample ($p = 0.0264$; Figure 3.26 b). Significantly altered migration behavior was observed 6 hours, 30 hours, 24 hours, and 48 hours upon 0 μM , 1 μM , and 20 μM lomeguatrib in the unirradiated cells, as well as upon irradiation only (see Table A.2 for p-values).

All p-values are presented in Table A.2 and A.3 in the Appendix.

3.14 Tumor growth delay

In order to investigate the effects of lomeguatrib on tumor growth *in vivo* LN18 and U118 cells were injected subcutaneously into the right flank in NMRI immunodeficient nude mice. Mice were randomly distributed into either lomeguatrib or control (NaCl) group and further divided into sham group (0 Gy), 5 Gy, or 15 Gy irradiation groups. Tumor size was measured twice per week using caliper and ultrasound.

During the experiment, the SARRP irradiation device broke in the course of mice irradiation, therefore a switch to the Gulmay irradiation cabinet was required. A total of 15 mice were irradiated at the SARRP and ten mice at the Gulmay; eleven mice were sham irradiated. Since the irradiation devices exhibit different dose rates comparison of the results is required first.

The duration in days to reach the 4-fold initial tumor volume after 5 Gy and 15 Gy irradiation are presented in Table 3.6.

Table 3.6: Tumor growth of LN18 tumors. Shown is the time in days for the tumors to reach the 4-fold initial volume comparing Gulmay and SARRP irradiation.

	Dose [Gy]	Gulmay		SARRP	
		NaCl	Lomeguatrib	NaCl	Lomeguatrib
Caliper	5	21.7 ± 3.5	21.9 ± 9.7	42.5 ± 13.1	58.0 ± 20.4
	15	18.8 ± 2.8	23.3 ± 8.8	37.5 ± 5.3	41.1 ± 20.8
Ultrasound	5	46.2 ± 19.9	37.5 ± 13.4	103.1 ± 25.9	70.1 ± 42.3
	15	38.8 ± 9.5	64.4 ± 49.0	81.0 ± 42.4	75.1 ± 11.7

Unirradiated tumors of the control group reached the 4-fold initial volume after 32.3 days ± 11.6 days (caliper) respectively 79.9 days ± 33.1 days (ultrasound), while the lomeguatrib group reached the 4-fold initial volume after 35.8 days ± 20.9 days according to the caliper measurement and 51.7 days ± 14.2 days according to the

ultrasound measurement. Tumors irradiated at the SARRP took longer to reach the 4-fold initial volume (see Table 3.6 and 3.7). The difference between Gulmay and SARRP irradiation is presented in Table 3.7. below.

Table 3.7: Difference in tumor growth of LN18 tumors irradiated at Gulmay or SARRP. Shown is the difference in days for the tumors to reach the 4-fold initial volume comparing Gulmay and SARRP irradiation as well as the p-values calculated from Student's t-test.

Measurement	Treatment	Dose [Gy]	Difference [d]	p-value
Caliper	NaCl	5	20.8 ± 9.0	0.1046
		15	18.7 ± 4.3	0.0027
	Lomeguatrib	5	36.1 ± 17.4	0.0505
		15	17.9 ± 16.6	0.3274
Ultrasound	NaCl	5	56.9 ± 29.8	0.0665
		15	42.2 ± 27.9	0.2586
	Lomeguatrib	5	32.5 ± 32.1	0.4730
		15	10.7 ± 40.5	0.6656

Great deviations were detected between the tumor quadrupling time upon irradiation at the Gulmay and SARRP, which was significant in the 15 Gy NaCl group ($p = 0.0027$).

Figure 3.27 presents the relative tumor growth of LN18 derived tumors measured via caliper. Two-Way ANOVA revealed significant differences between Gulmay and SARRP irradiation in the NaCl treated tumors ($p = 0.0027$) and in the lomeguatrib treated tumors ($p = 0.0305$).

Figure 3.28 presents the relative tumor growth of LN18 derived tumors measured via ultrasound. Two-Way ANOVA revealed a significant difference between Gulmay and SARRP irradiation in the NaCl treated tumors ($p = 0.0410$) but no difference in the lomeguatrib treated tumors ($p = 0.5083$).

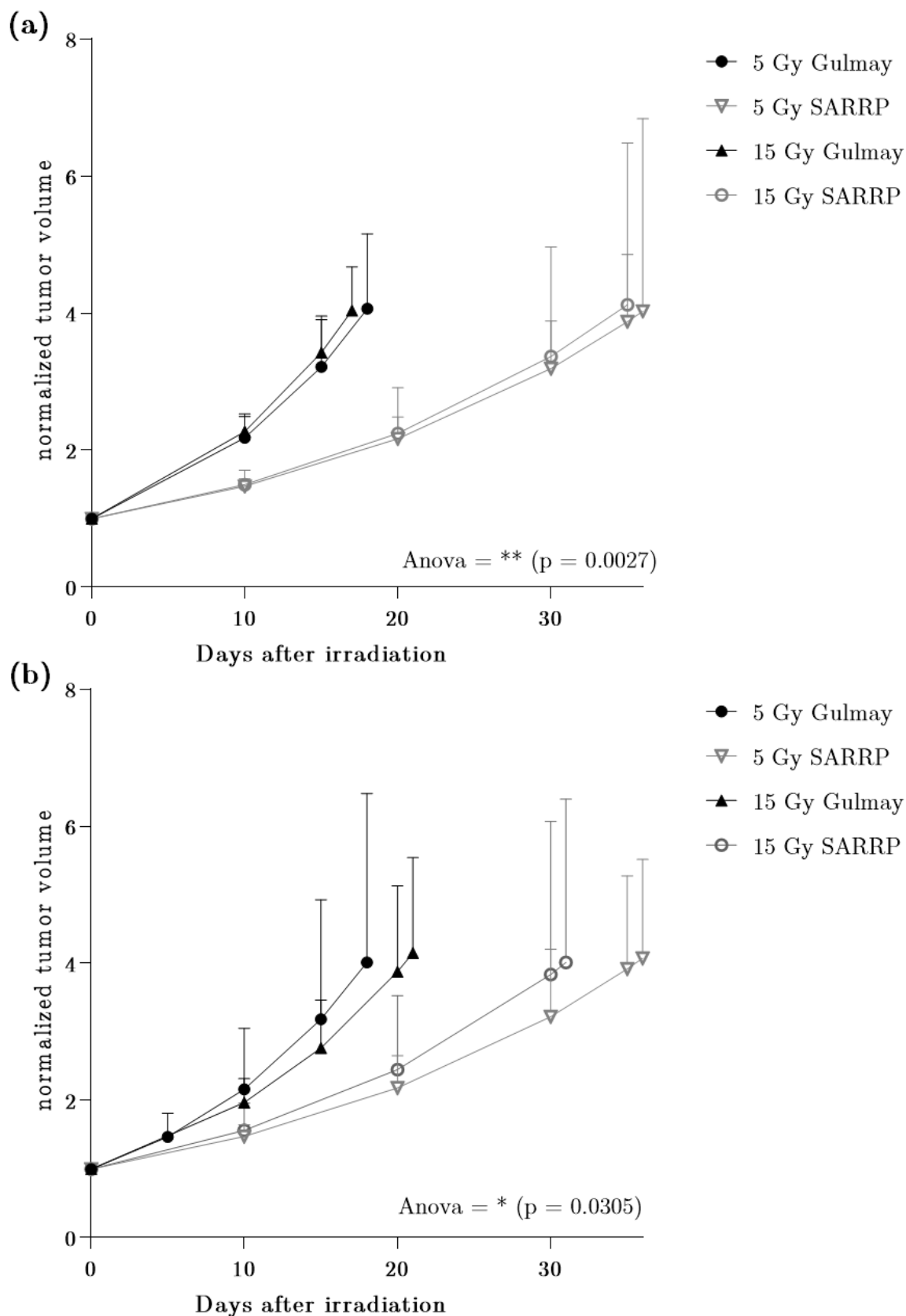


Figure 3.27: Relative tumor growth of LN18 tumors *in vivo* after irradiation and caliper measurement.

Tumors were treated with (a) NaCl and (b) LM.

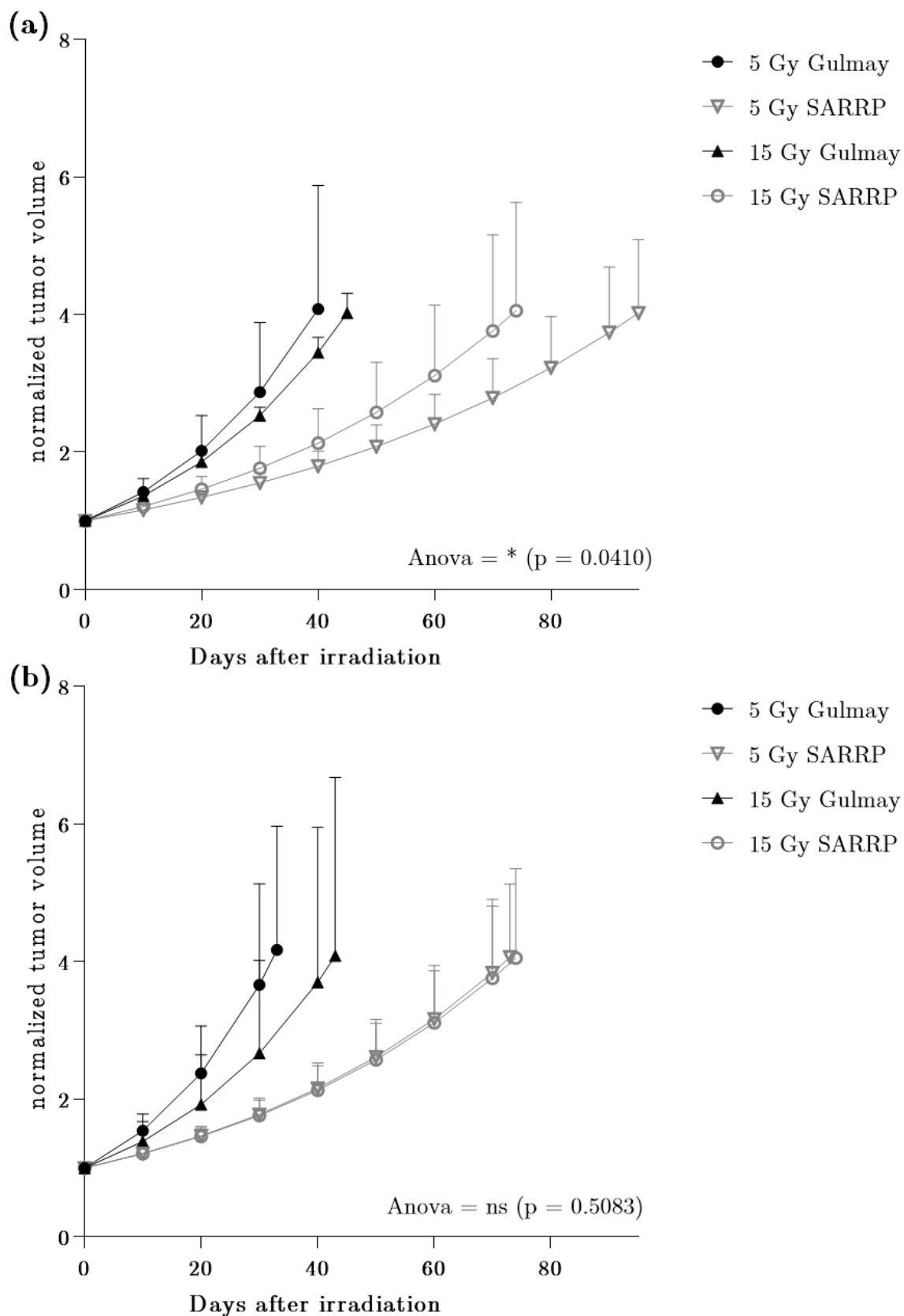


Figure 3.28: Relative tumor growth of LN18 tumors *in vivo* after irradiation and ultrasound measurement.

Tumors were treated with (a) NaCl and (b) LM.

Since significant differences between Gulmay and SARRP were detected and U118 implanted tumors were all irradiated at the SARRP, only the data from LN18 mice irradiated at the SARRP were used for further analysis.

Figure 3.29 presents the relative tumor growth of LN18 tumors. Two-Way ANOVA did not reveal any significant differences between the NaCl and the lomeguatrib treated mice. A significant increase in tumor quadrupling time was detected between the lomeguatrib 15 Gy irradiated tumors compared to the lomeguatrib unirradiated tumors upon ultrasound measurement ($p = 0.0332$).

However, significant differences were observed between the caliper and ultrasound measurements (see Table 3.8).

Table 3.8: Calculated p-values for caliper vs. ultrasound measurement. Shown are the p-values calculated using Student's t-test comparing the tumor quadrupling time of caliper to ultrasound.

Treatment	Dose [Gy]	p-value	
NaCl	0	0.0163	*
	5	0.0153	*
	15	0.0880	*
Lomeguatrib	0	0.1842	ns
	5	0.4784	ns
	15	0.0293	*

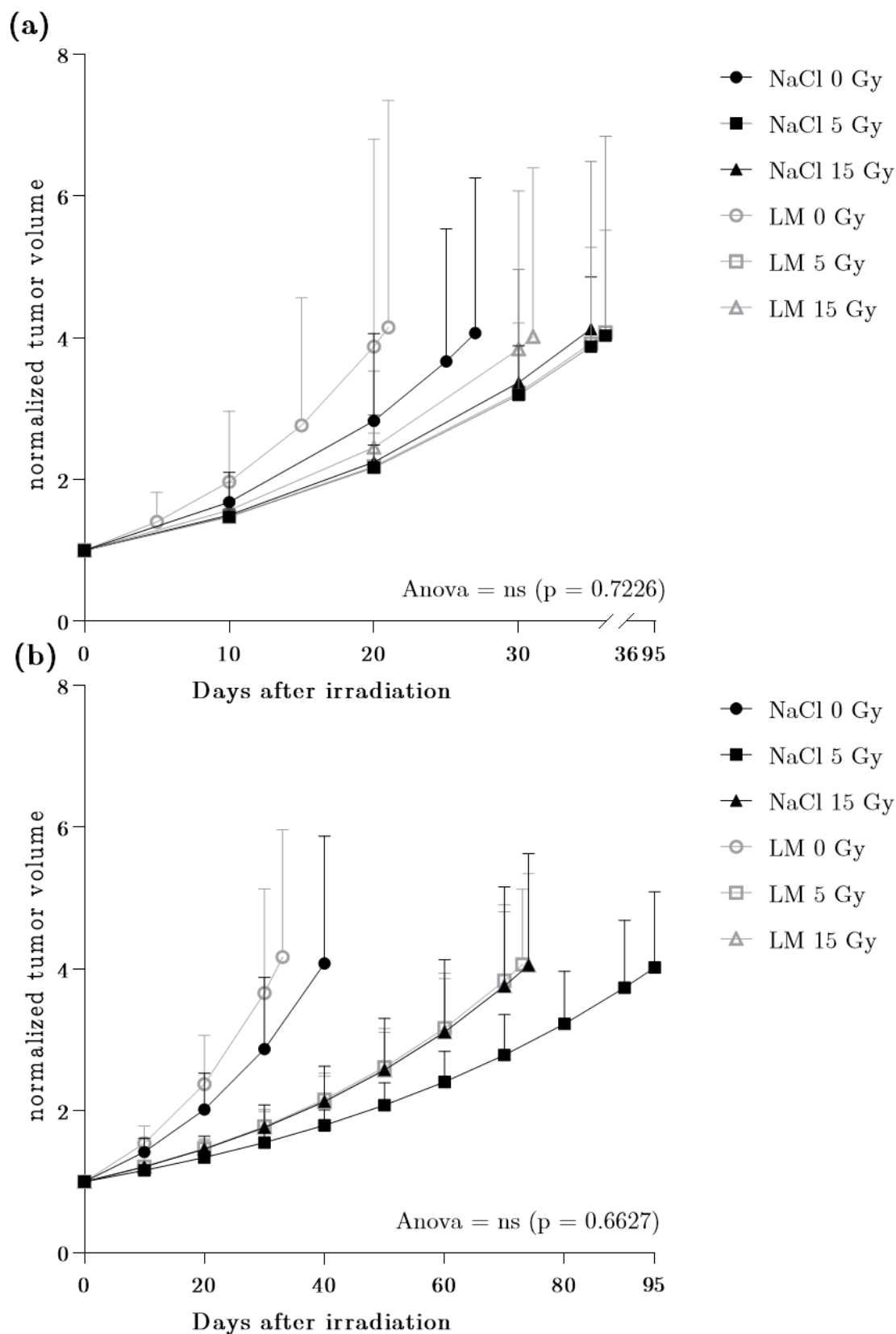


Figure 3.29: Relative tumor growth of LN18 tumors *in vivo* after irradiation.

Tumor volumes were measured by (a) caliper and (b) ultrasound and normalized to the volume of the day of irradiation.

Table 3.9 presents the tumor growth delay in days of LN18 cells. After 5 Gy irradiation, the tumor growth delay was greater compared to the 15 Gy irradiated tumors. There was no difference in growth delay between NaCl and lomeguatrib treatment.

Table 3.9: Tumor growth delay of LN18 tumors. Shown is the tumor growth delay upon 5 Gy and 15 Gy irradiation compared to the unirradiated tumors in days.

		Caliper		Ultrasound	
		NaCl [days]	LM [days]	NaCl [days]	LM [days]
0 Gy to 5 Gy	LN18	10.2 ± 11.7	22.2 ± 20.3	23.2 ± 33.1	18.4 ± 30.7
0 Gy to 15 Gy		5.2 ± 8.8	5.3 ± 18.9	1.1 ± 44.8	23.4 ± 12.2

LM: lomeguatrib

All U118 implanted tumors were irradiated at the SARRP. Table 3.10 summarizes the time in days of the U118 tumors to reach the 4-fold initial volume and Figure 3.30 presents the corresponding relative tumor growth of U118 cells *in vivo*.

Table 3.10: Tumor growth of U118 tumors. Shown are the days for the tumors to reach the 4-fold initial volume.

Measurement	Dose [Gy]	NaCl	Lomeguatrib
Caliper	0	65.5 ± 49.0	93.5 ± 51.2
	5	65.5 ± 20.6	73.5 ± 22.9
	15	80.1 ± 40.3	93.6 ± 28.4
Ultrasound	0	50.3 ± 11.5	57.8 ± 17.6
	5	64.1 ± 12.9	63.9 ± 6.4
	15	67.4 ± 13.4	73.7 ± 22.8

Student's t-test did not reveal any significant differences between lomeguatrib and NaCl treatment, or radiation treatment, or between the caliper and ultrasound measurements.

Table 3.11 summarizes the tumor growth delay in days for U118 implanted cell lines.

Table 3.11: Tumor growth delay of U118 tumors. Shown is the tumor growth delay upon 5 Gy and 15 Gy irradiation compared to the unirradiated tumors in days.

		Caliper		Ultrasound	
		NaCl [days]	LM [days]	NaCl [days]	LM [days]
0 Gy to 5 Gy	U118	0.0 ± 33.8	-20.0 ± 33.1	13.8 ± 12.2	6.1 ± 10.7
0 Gy to 15 Gy		14.6 ± 45.2	0.1 ± 35.6	17.0 ± 12.4	15.9 ± 18.1

LM: lomeguatrib

Tumor growth was delayed upon irradiation, with 15 Gy irradiation resulting in a greater tumor growth delay compared to the 5 Gy irradiated tumors. There was no difference in growth delay between NaCl and lomeguatrib treatment.

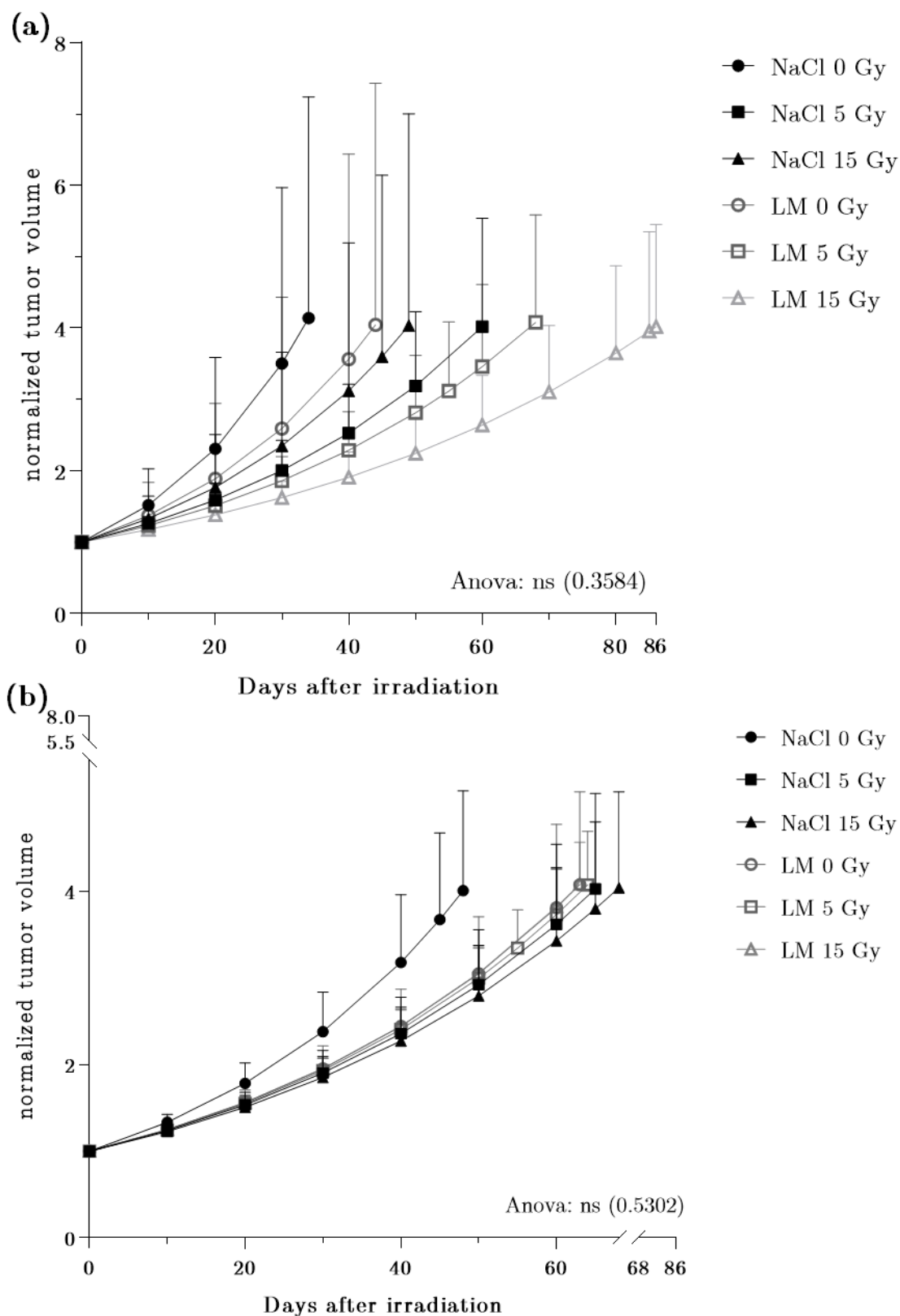


Figure 3.30: Relative tumor growth of U118 tumors *in vivo* after irradiation.

Tumor volumes were measured by (a) caliper and (b) ultrasound and normalized to the volume of the day of irradiation.

Two-Way ANOVA did not indicate significant differences for U118 implanted mice as well. Control NaCl mice and the lomeguatrib treated mice did not show any difference at any dose and also no differences between the irradiated and non-irradiation groups in either of the treatment groups were observed.

In order to determine a difference in the growth rate between the two cell lines *in vivo* Figure 3.31 shows the tumor growth curves measured via caliper and Figure 3.32 via ultrasound measurement for LN18 and U118 after irradiation and (a) NaCl treatment and (b) lomeguatrib treatment.

Significant differences between the two cell lines were found only after lomeguatrib treatment via caliper measurement between the unirradiated group ($p = 0.0461$), and the 15 Gy group ($p = 0.0251$).

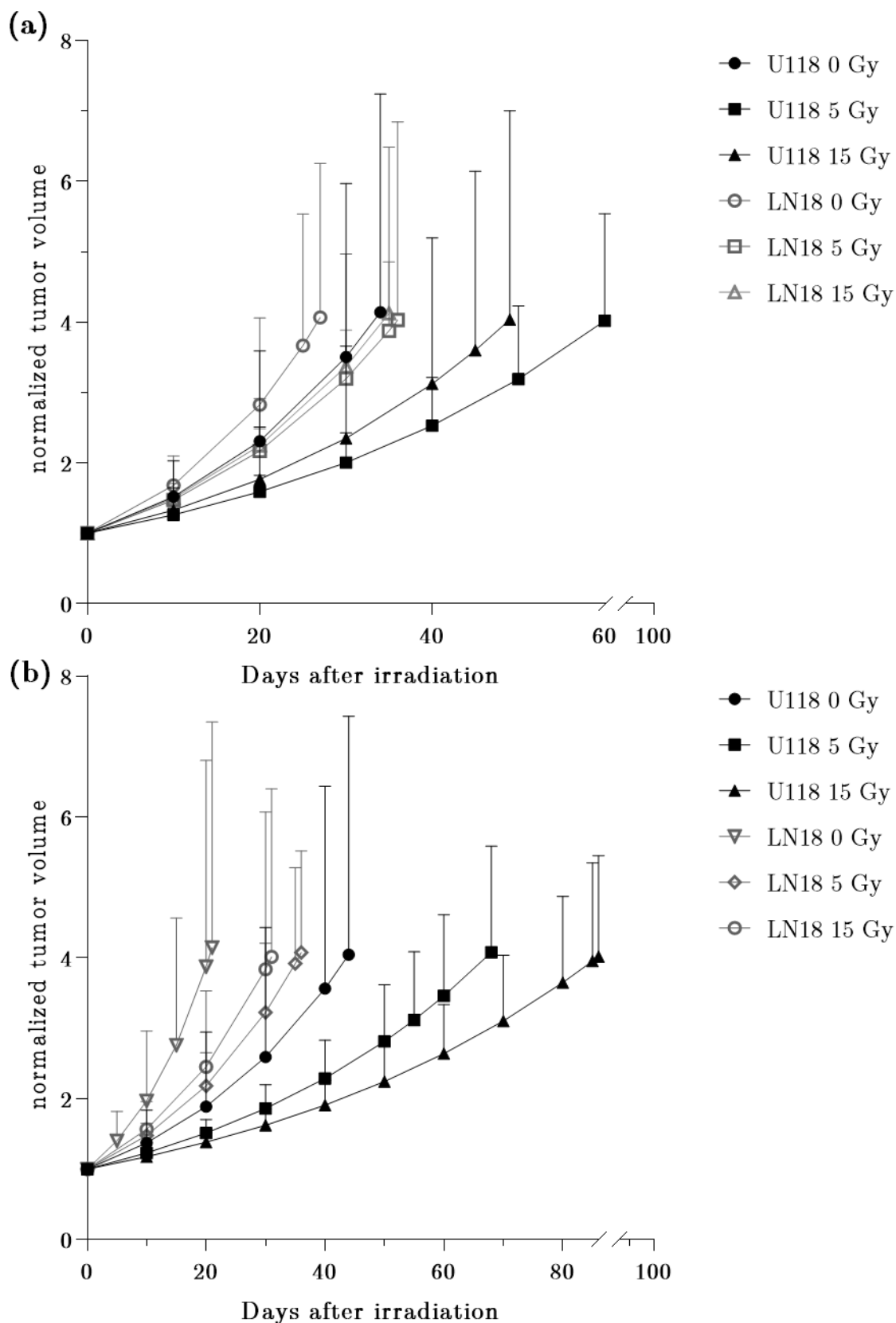


Figure 3.31: Relative tumor growth of LN18 and U118 tumors *in vivo*. Tumor volumes were measured by caliper after (a) NaCl and (b) Lomeguatrib treatment and normalized to the volume of the day of irradiation.

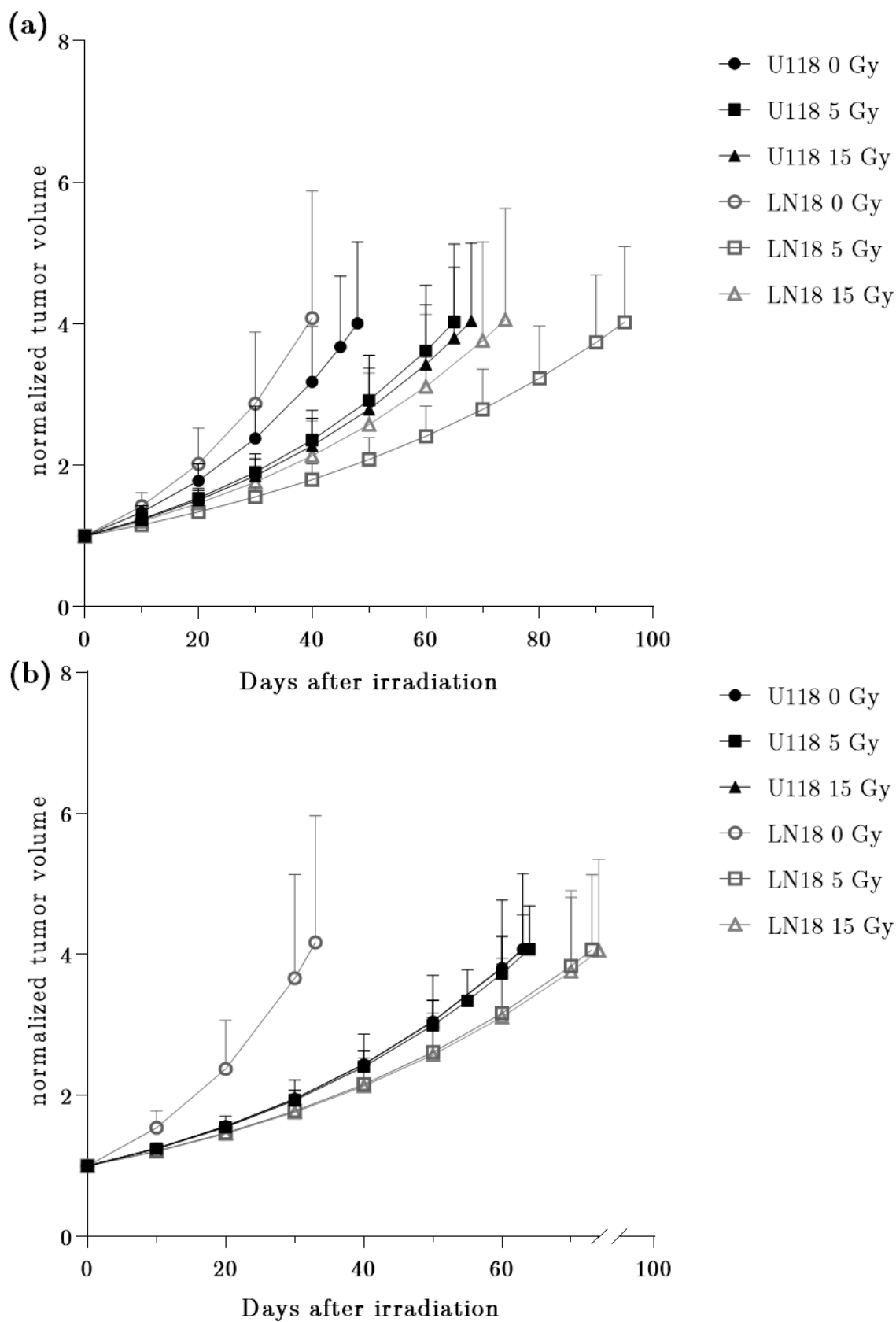


Figure 3.32: Relative tumor growth of LN18 and U118 tumors *in vivo*. Tumor volumes were measured by ultrasound after (a) NaCl and (b) Lomeguatrib treatment and normalized to the volume of the day of irradiation.

4. Discussion

Glioblastoma multiforme is still a deadly disease where most cases of death occur in the first 15 months after diagnosis. Despite extensive research in finding alternative treatment options as well as predictive biomarkers, such as MGMT promoter methylation status, the 5-year survival is still less than 3 % making GBM the deadliest of all cancers [46]. It is long known that MGMT promoter methylation is favorable during temozolomide therapy [30], however, advances and alternative treatment options for MGMT unmethylated patients have not yet proven beneficial. O6-benzylguanine [31; 35; 36], poly(ADP-ribose) polymerase (PARP) inhibitors [47-49] as well as micro RNAs (miRNAs) [50-52] present several approaches that have been or are currently tested in clinical trials for MGMT unmethylated patients; however, none of these approaches have been approved for daily GBM treatment. O6-benzylguanine was tested in phase I and phase II clinical trials but due to severe side effects was never included in standard GBM therapy [35; 36]. The PARP inhibitor veliparib inhibited cell proliferation in MGMT unmethylated cell lines in vitro as well as in vivo [48] but did not improve overall survival in a randomized phase I/II clinical trial [49]. Lastly, several miRNAs were found to regulate MGMT expression (summarized in [52]) but delivery to their target sites especially across the blood-brain-barrier is still a limiting factor.

In order to improve therapy for MGMT promoter unmethylated patients, the effects of lomeguatrib, a highly potent inhibitor of MGMT, in combination with ionizing radiation was investigated on MGMT unmethylated human glioblastoma multiforme cell lines.

4.1 Identification of MGMT expressing cell lines

The first step in this project was to identify MGMT promoter unmethylated cell lines with high MGMT protein expression. The MethyQESD results revealed an unmethylated promoter region in LN18 and U118 cells, while A172 and LN229 were promoter methylated. T98G and U251 were considered hemi-methylated. Western Blot analyses also showed high MGMT expression in LN18, T98G, and U118 cells, while no MGMT protein expression was detected in A172 and LN229 cells and only weak expression in U251 cells. These results are following the findings from Aasland et al. They analyzed the MGMT promoter methylation status via methylation-specific qPCR (MSP) and detected an unmethylated promoter region in LN18 and U118 cells as well and a methylated region in A172 and LN229 cells [53]. Only T98G and U251 were analyzed as unmethylated respectively methylated while in this work the promoter status was categorized as hemi-methylated in accordance to Yoshino et al [54]. Since the percentages of promoter methylation are not mentioned in the paper by Aasland et al. it is unknown how the cut-off values were defined. Aasland et al. further analyzed the correlation between promoter methylation, MGMT mRNA expression, MGMT protein expression, and MGMT activity and found differences among the cell lines but close correlations within each tested cell line [53]. This correlation was found by Yoshino et al. as well who also linked a correlation to TMZ resistance in MGMT expressing cell lines [54]. Also, Aasland et al. detected a negative effect after 6 Gy irradiation on MGMT promoter activity, but no difference in MGMT expression [53]. In this thesis, similar results were reported in the correlation between MGMT promoter methylation status and MGMT protein expression (Table 3.3 and Figure 3.3). Upon 8 Gy ionizing radiation no differences in MGMT protein expression were observed 24 hours after irradiation (Figure 3.8). These findings and other experiments led Aasland et al. to the conclusion that MGMT protein levels are mainly

regulated by the transcription factor SP1 and that miRNAs are not essential in regulating MGMT protein expression. Further, they concluded that MGMT is not transcriptionally regulated upon radiation or alkylating agent treatment and that epigenetic factors play a major role [53].

Since the findings from the literature concerning the correlation between MGMT promoter status and MGMT protein expression [53-55] support the data of this thesis the two MGMT promoter unmethylated cell lines LN18 and U118, as well as the hemimethylated cell line T98G were chosen for further investigations using lomeguatrib treatment. It was assumed that lomeguatrib only affects MGMT expression and that the promoter methylation status is not affected, which was also published by Ugur et al. [56].

4.2 Optimal MGMT inhibition using lomeguatrib

Different lomeguatrib concentrations ranging from 0.01 μM to 20 μM were tested for various durations from four hours to 48 hours. Assessment of MGMT protein inhibition was based on Western Blot analysis. The low concentration of 0.01 μM lomeguatrib reduced MGMT protein level by 60 % after six hours in all three cell lines (Figures 3.4 and 3.5). A comparable low IC₅₀ of 0.004 μM lomeguatrib was identified by Reinhard et al. in HeLa S3 cervix adenocarcinoma cells [57] as well as 0.006 μM after two hours of lomeguatrib treatment in MCF-7 breast adenocarcinoma cells by Clemons et al. [58]. A highly significant decrease in MGMT protein was observed 24 hours after 20 μM lomeguatrib treatment as it was also observed by St-Coeur et al. [59]. Taspinar et al. [60] and Ugur et al. [56] also tested higher concentrations up to 50 μM lomeguatrib in human GBM and anaplastic astrocytoma cells and demonstrated a decrease in MGMT protein expression. Therefore, lomeguatrib is a highly potent inhibitor of MGMT protein already at low concentrations.

Since highly significant MGMT protein inhibition was observed upon 1 μM lomeguatrib treatment in all three cell lines and other works demonstrated MGMT reduction after higher concentrations as well, 20 μM lomeguatrib treatment for 24 hours (Figures 3.4 and 3.5) was additionally included in this thesis for all further experiments.

4.3 Lomeguatrib does not affect cell proliferation and cell survival

Doubling times were determined for the three cell lines without lomeguatrib as well as in combination with 1 μM and 20 μM lomeguatrib. For LN18 a doubling time of 16.4 hours \pm 5.4 hours was determined, while Diserens et al., who established this cell line in 1981, determined a doubling time of 72 hours after 115 passages [61]. For T98G a doubling time of 16.1 hours \pm 1.8 hours was calculated and Oraiopoulou et al. identified 29.9 hours by generating a growth curve as well [62]. U118 cells were a slower proliferating cell line with a doubling time of 20.1 hours \pm 4.8 hours and Ying et al. even calculated 43.5 hours [63]. This deviation might be explained due to the fact that in this thesis the alamarBlue cell viability assay was used to calculate doubling times, which is based on cell metabolism while Diserens et al., Oraiopoulou et al., and Ying et al. generated growth curves from total cell numbers. Also, Diserens et al. passaged the cells up to passage 115, while in this work cells were passaged only up to passage 20.

Upon 1 μM or 20 μM lomeguatrib treatment the doubling times of the three cell lines did not change. This is in line with the results of Clemons et al. [58] who also did not observe a growth inhibitory effect after 0.006 μM lomeguatrib in MCF-7 cells.

Cell survival was significantly decreased upon 50 μM lomeguatrib in all cell lines (Figure 3.6). In T98G cells, lomeguatrib concentrations of 10 μM and 20 μM already

significantly reduced cell survival. Likewise, Signorell et al. [64] demonstrated no reduced cell viability in low concentrations ranging from 1.25 μM to 10 μM , but in higher concentrations of 20 μM and 40 μM lomeguatrib for 24 hours. Similar results were observed by Clemons et al., who observed reduced cell viability after 20 μM and 40 μM lomeguatrib as well [58]. St.-Coeur detected reduced cell viability to 72.5 % after 20 μM lomeguatrib in human GBM cell lines [59] and also Shi et al. reported reduced cell proliferation and cell survival in a pancreatic cancer cell line, but did not specify the administered lomeguatrib concentration [65]. Despite different entities, all published results reported reduced cell survival and cell proliferation after higher doses of lomeguatrib, which is well in line with the findings in this thesis.

4.4 High dose lomeguatrib decreases radiation-induced G2/M arrest

Cell cycle distribution was not significantly altered by low-dose lomeguatrib (Figure 3.7). Upon 20 μM lomeguatrib S phase significantly decreased in U118 cells and after 50 μM lomeguatrib G2/M phase decreased in all cell lines. In LN18 and U118 cells this result was complemented with an increase in G1 phase. These results are quite contrary to the results reported by Taspinar et al. and Ugur et al. [56; 60]. Both report no changes in cell cycle distribution after 50 μM lomeguatrib treatment. These deviations might occur due to the fact that they analyzed primary GBM cells respectively anaplastic astrocytoma cell lines.

Cell cycle plays a critical role during radiotherapy: while cells in S phase are least radiosensitive, cells in G2/M phase are most radiosensitive [66]. An inevitable G2/M arrest was observed 24 hours after 8 Gy ionizing radiation in all three cell lines (Figure 3.12 – 3.14). These results are confirmed in LN18 cells [67] and T98G cells [68]. It is long known that the cell cycle is arrested at the G2 checkpoint upon radiation damage

to the DNA [69] allowing the cells to repair the DNA before completing the cell cycle and therefore prevents mutations and chromosome aberrations.

At lower concentrations of 1 μM lomeguatrib did not affect cell cycle distribution in any of the tested cell lines, however, after 20 μM lomeguatrib treatment a reduced G2/M fraction was observed in T98G only (Figure 3.13). After the combination of 1 μM lomeguatrib and 8 Gy ionizing radiation a radiation-induced G2/M arrest was observed, but lomeguatrib did not have an additional effect (Figures 3.12 – 3.14). Only the combination of 20 μM lomeguatrib with 8 Gy radiation reduced the radiation-induced G2/M arrest and consequently increased G1 and S cell cycle fraction. A reasonable explanation for the reduced G2/M cell cycle fraction after irradiation might be a radioprotective property of high dose lomeguatrib.

This radioprotective property might be accounted for by the not yet identified interaction of lomeguatrib with key regulators of cell cycle checkpoints, such as the G2/M checkpoint. The G2/M checkpoint, also known as the DNA damage checkpoint, is regulated by CyclinB-Cdc2 complex activity. This complex is inactive upon phosphorylation and prevents cell cycle progression upon the G2/M checkpoint [70]. Only a positive feedback loop can activate Cdc25, a phosphatase, to dephosphorylate the inhibitors of the Cdc2-Cyclin B complex Wee1 and Myt1 [70]. However, a threshold needs to be passed since the accumulation of CyclinB-Cdc2 complex follows the all-or-nothing switch to enter mitosis [71]. Since there are limited papers published investigating lomeguatrib in GBM and none investigated lomeguatrib in combination with radiation, these findings are novel and need further investigation. One hypothesis explaining the decreased G2/M arrest only after the combination with ionizing radiation might be an inhibition of cyclin B or Cdc2 by lomeguatrib preventing their accumulation to initiate cell cycle progression beyond G2/M. A step further might also involve an upstream overexpression of Wee1 and Myt1, which are the direct inhibitors of the essential CyclinD-Cdc2 complex.

The second most important cell cycle checkpoint is the G1/S checkpoint which is responsible to check for sufficient growth factors in the environment. Upon deprived growth factors or other growth-inhibitory signals in the early-to-mid G1 phase withdrawal from cell cycle progression occurs [72]. This checkpoint admits cells for DNA replication and cell division and is mainly regulated by pRb (retinoblastoma protein) and E2F (transcription factor). pRb in its active form binds E2F so that E2F is unable to bind to the promoter regions of genes coding for necessary S phase transition proteins [73]. Inactivation of pRb via phosphorylation by the cyclin E:CDK2 and cyclin D:CDK4/6 complexes allows for cell cycle progression beyond G1 [73]. Since pRb is dysfunctional in many cancer types it is regarded as a tumor suppressor [72]. GBM is amongst the cancer types with a dysfunctional pRb signaling pathway and a CDK4/6 amplification [74] leading to a defective G1 to S cell cycle transition. As in this work, a growth inhibitory effect was observed in higher lomeguatrib concentrations as well as a G1 arrest, it can be hypothesized that lomeguatrib is also an inhibitor of CDK4/6. This may result in a lack of cyclin D:CDK4/6 complex unable to phosphorylate pRb leaving it always active with no cell cycle progression upon G1 phase.

In order to investigate the underlying mechanisms upon the decreased radiation-induced G2/M arrest upon 20 μ M lomeguatrib, it was hypothesized that lomeguatrib also enhances radioresistance in the clonogenic survival assay.

4.5 Lomeguatrib enhances radioresistance at high lomeguatrib doses

The clonogenic survival assay is the gold standard in radiation biology to determine the radiosensitivity of cell lines. Only cells that have survived a given dose of radiation and in addition have retained their reproductive integrity can divide

indefinitely and grow into colonies; these are called clonogenic cells [39]. The degree of radiosensitivity is an important tool to predict treatment outcomes and also to test new radiation modalities or drugs and inhibitors. By applying the linear-quadratic model to the survival data dose-survival curves are obtained which describe the loss of reproductive integrity in relation to the dose applied.

Since the different GBM cell lines are derived from different patients of different ethnicities, ages, and gender as well as from different regions within the brain it is not surprising that these cell lines differ in their radioresistance. Therefore, A172 and U118 are the most radiosensitive cell lines while T98G is the most radioresistant cell line. LN18, LN229, and U251 show comparable intermediate radioresistance. Wank et al. could also show that LN18 and LN229 are comparable radioresistant [75]. For the combined treatment of lomeguatrib and radiation, only the MGMT unmethylated cell lines were chosen including one of the most radiosensitive (U118), the most radioresistant (T98G), and one of the intermediates (LN18) cell lines. Concluding from these results there is no correlation between the MGMT status and the radiosensitivity of the cell lines.

As hypothesized, after combined 20 μM of lomeguatrib and ionizing radiation treatment all cell lines became more radioresistant compared to the cells that received radiation only (Figures 3.9 – 3.11). This is explained by the increased G1 and S cell cycle population upon high dose lomeguatrib and radiation, which are the radioresistant phases of the cell cycle. Interestingly, a radiosensitizing effect was detected after combined 1 μM low dose lomeguatrib and radiation treatment. These data are not explained by the cell cycle data presented earlier since in low doses of lomeguatrib no change in cell cycle was observed.

4.6 Radiation-induced DNA damage is not affected by lomeguatrib

In order to investigate the reason for the reduced G2/M arrest after combined high dose lomeguatrib and radiation DNA damage was analyzed by staining for γ H2AX DSB repair foci 30 minutes and 24 hours after radiation.

The predominant direct target of ionizing radiation is the DNA, making DNA double-strands breaks responsible for the therapeutic efficacy of radiotherapy. Upon DNA damages e.g. caused by ionizing radiation, cells can either die or survive. As mentioned earlier ATM, ATR, and DNA-PKcs are sensors for DSBs and phosphorylate the histone H2AX to γ H2AX at the site of the DSB to induce DNA repair via HR or NHEJ. Quantification of the phosphorylated form γ H2AX provides direct insight into the amount of DNA DSBs, as well as into the cell's capacity to repair these breaks over time since γ H2AX foci remain until the DSBs are repaired [76; 77]. As expected, a significant increase in γ H2AX foci was observed 30 minutes after 8 Gy ionizing radiation in all tested cell lines. A decrease in γ H2AX foci, i.e. repaired DNA DSBs, was observed in all cell lines 24 hours after irradiation due to the activated DNA DSB repair mechanisms. This is in accordance with the cell cycle results where a G2/M arrest was observed 24 hours after irradiation since the cells still show remaining DSB repair foci which are repaired during G2/M arrest.

Lomeguatrib alone or in combination with irradiation did not affect DNA repair in LN18 and U118 cells, since no significant differences were observed between untreated samples and samples treated with 1 μ M or 20 μ M lomeguatrib. However, in T98G 1 μ M as well as 20 μ M lomeguatrib exposure without irradiation significantly increased the number of γ H2AX foci per cell nucleus (Figure 3.17).

Taspinar et al. investigated DNA damages using the COMET assay upon 50 μ M lomeguatrib and observed a significant increase in DNA fragmentation in U118 and T98G cells [60]. These findings are contrary to our findings since we were not able to

detect significant differences in DNA double-strand breaks upon lomeguatrib treatment. These differences are explained by the fact that Taspinar et al. did not specify the duration of lomeguatrib treatment, used a higher concentration, and investigated DNA fragmentation, which includes DNA double- as well as single-strand breaks. In this thesis, only DNA double-strand breaks were analyzed, but it still might be possible to detect an increased γ H2AX foci upon 50 μ M lomeguatrib as well.

4.7 Lomeguatrib does not affect radiation-induced apoptosis

Since DSB induction is not the mechanism leading to an increased radiosensitivity at low lomeguatrib concentrations it was hypothesized that cell death, i.e. apoptosis is responsible for the results.

The ultimate success of radiotherapy in treating cancers is due to the death of the tumor cells [40]. The radiobiological more accurate term for cell death is the “permanent loss of clonogenic capacity” [40] and highly depends on the DNA damage response.

Apoptosis is one of the cell death pathways which is highly regulated and occurs not only after e.g. radiation-induced DNA damages (intrinsic) but also upon external signals from the surroundings (extrinsic) [40; 78]. In order to activate apoptosis proapoptotic molecules need to be activated, or anti-apoptotic molecules need to be inhibited. Since intracellular apoptosis-controlling pathways are often deregulated in GBM new treatment options are investigated in order to restore apoptosis [78]. Here it was hypothesized that lomeguatrib enhances apoptosis. However, a decreased number of apoptotic cells were detected upon 1 μ M and 20 μ M lomeguatrib treatment in LN18 cells, while T98G and U118 did not show differences compared to the untreated controls. Upon 8 Gy irradiation induction of apoptosis was observed in all cell lines 48 hours after irradiation but no effect was observed upon the combined

treatment of radiation and lomeguatrib. Here, contradictory results were published first by Taspinar et al. [60] and Ugur et al. [56] who reported no effect upon 50 μM lomeguatrib in GBM cells, while Shi et al. [65] reported induction of apoptosis by lomeguatrib in pancreatic cancer cells. These deviations might be explained due to the different tumor entities, however, pancreatic cancer is also prominent for high radio- and chemoresistance and mechanisms to avoid apoptosis [79].

Since apoptosis is not the mechanism explaining the increased radiosensitivity after low dose lomeguatrib it can be hypothesized that lomeguatrib exhibits a radiosensitizing effect through other cell death pathways, such as autophagy, mitotic catastrophe, senescence, or necrosis.

As Shi et al. [65] reported induction of apoptosis by increased expression of Caspase-3 and Bax, which are both pro-apoptotic proteins [79], they also reported suppressed autophagy upon lomeguatrib treatment in pancreatic cancer cells. They observed a decrease in Bcl-2 (anti-apoptotic), Beclin1, and Atg5, which are essential components of the autophagosome [80]. Here, it might be interesting to investigate the difference to pancreatic cancer if autophagy is the responsible mechanism in GBM.

Mitotic catastrophe, however, is the leading cause of cell death upon ionizing radiation [81] and occurs post-mitotic. After activation of cell cycle checkpoints and completion of DNA repair via the DNA damage response some cells with unrepaired DNA lesions are still able to enter mitosis [81]. Some tumor cells are additionally deficient in apoptosis pathway and cell cycle checkpoints and therefore enter mitosis with DNA lesions [82]. These lesions include chromosome aberrations such as dicentric and acentric fragments, and ring chromosomes [40]. Since chromosomes with one or more centromeres cannot be separated during metaphase, these cells will die from mitotic catastrophe eventually. If, however, these cells omit the mitotic checkpoint and complete mitosis with a tetraploid DNA content a giant polyploidy cell with the remaining acentric fragment forming micronuclei will be formed [82]. Genetic material,

however, will be lost upon next mitosis, which will ultimately result in cell death via delayed apoptosis, delayed senescence, or delayed necrosis [82].

4.8 Migration is suppressed upon high dose lomeguatrib and irradiation

GBM is characterized by extensive migration and invasion into the surrounding healthy brain tissue [5] contributing to the high probability of recurrence and relapse. Infiltration occurs via preexisting structures such as blood vessels and myelinated nerve fibers and depends on the stiffness of the extracellular matrix (ECM) [83]. Therefore, GBM with high invasive potential produces large amounts of collagen, fibronectin, and laminin promoting stiffness of the ECM required for cell migration [83; 84]. Upon hypoxia or nutrient depletion glioma cells tend to migrate (“Go”), while they proliferate (“Grow”) if sufficient amounts of oxygen and nutrients are available. This principle is called “Go or Grow” [83]. Other factors contribute to the “Go or Grow” principle as well, such as miRNAs [85], transcription factors [86], and also ionizing radiation [87].

Increased migration potential upon low LET as used during radiotherapy is still a negative side effect yet to overcome. As previously reported, ionizing radiation increases migration of GBM cell lines in vitro [88-92]; here we could show increased migration in LN18 and U118 cells upon 8 Gy ionizing radiation, but not in T98G cells although this was published earlier [88; 89]. As Shi et al. demonstrated in pancreatic cancer cells migration as well as invasion behavior was suppressed after lomeguatrib treatment [65]. This finding is partially in accordance with the results of this work. Here, a significant increase in migration was observed in LN18 cells upon 20 μ M lomeguatrib treatment compared to the untreated control. Interestingly, migration was significantly decreased when 20 μ M lomeguatrib was combined with 8 Gy ionizing

radiation (Figure 3.24). However, 1 μM lomeguatrib had no effect on migration behavior. Similar results were observed in U118 cells; no change in migration was observed upon 1 μM or 20 μM (except after 24 hours migration was significantly decreased) lomeguatrib compared to the untreated control (Figure 3.26 a). The combination of lomeguatrib and irradiation did not reveal any significant differences to the irradiate control samples, except after 24 hours migration was significantly decreased upon 1 μM lomeguatrib (Figure 3.26 b).

In the T98G cell line, no migration behavior was detected in any of the tested samples although reported otherwise [88; 89] and therefore, no effect of lomeguatrib was observable (Figure 3.25). Differences in the results may be explained due to the application of different assays (transwell assay or wound healing), chemoattractants, or serum starvation.

Cell migration is an important process during embryonic development and tissue homeostasis but also leads to cancer and promotes metastases [93]. Migration is a complex process involving five stages: polarization, protrusion, cell-matrix adhesion, ECM degradation, and retraction [94]. Polarization is the preparation of the leading edge with membrane proteins to form protrusions, which require actin polymerization for movement, followed by adhesion of the protrusion to the ECM via integrins to generate traction [94]. Matrix metalloproteinases (MMPs) degrade the ECM to enable further migration and final retraction of the cells' trailing edge [94]. MMPs are hereby the important players for carcinogenesis; secreted by tumor cells MMPs degrade interstitial matrix releasing cytokines to promote tumor movement also in surrounding tumor cells [95]. MMP-2 and MMP-9 e.g. activate latent transforming growth factor (TGF)- β , which enhances invasion and migration by upregulation of integrin $\alpha\text{v}\beta\text{3}$, stimulates ROS production, and suppresses PTEN (tumor suppressor gene) [83]. Differential expression of MMPs [96] and TGF- β [97] among cell lines might explain the differences in migration behavior and different responses upon inhibitor treatment.

Other factors influencing migration also involve growth factors, chemoattractants, miRNAs, transcription factors, or mutations [84]. Internal factors vary between cell lines since every cell line has its unique mutation pattern and unique expression of miRNAs contributing to the observed differences in migration.

4.9 Lomeguatrib does not affect tumor growth *in vivo*

In order to further investigate the effects of MGMT inhibition upon radiotherapy a subcutaneous xenograft mouse model was used. Mice were injected with lomeguatrib 24 hours before irradiation to ensure MGMT inhibition at the time of irradiation. Middleton et al. [37] and Clemons et al. [58] reported extensive MGMT depletion in all tested host tissues including the kidneys, liver, lung, and bone marrow already two hours after a single i.p. dose of 20 mg kg⁻¹ lomeguatrib. Complete inactivation of MGMT in a subcutaneous MCF-7 xenograft was observed two to eight hours after administration [58]. In the brain, MGMT depletion was 24 % only, but 100 % in a subcutaneous melanoma tumor [37]. Based on these publications the dose of 20 mg kg⁻¹ i.p. was chosen and based on previous Western blot findings a duration of 24 hours before irradiation was chosen. MGMT depletion in the tumors or other tissues was not further investigated.

Also, Hu et al. reported significantly reduced MGMT activity in T98G and U87MG derived subcutaneous tumors after daily administration of 8 mg kg⁻¹ lomeguatrib for three weeks [98].

Here, tumor growth delay was investigated in mice subcutaneously injected with LN18 and U118 cells and irradiated at 0 Gy, 5 Gy, or 15 Gy ionizing radiation 24 hours after lomeguatrib treatment. First, significant differences in tumor growth were detected between mice irradiated at the Gulmay and mice irradiated at the SARRP. This might be due to the different energies of the devices (200 kV at the Gulmay vs.

220 kV at the SARRP) as well as the difference in beam orientation. At the SARRP, which allows for high precision and targeted irradiation, two beams were applied from opposing directions to the delineated tumor. In contrast, imaging was not possible at the Gulmay and the dose was delivered in a single beam.

Also, a significant difference between caliper and ultrasound measurements was observed in the LN18 tumors, only. This is due to the fact that tumor cells were injected too deep under the skin into the muscles of the mice. Therefore, caliper measurements revealed smaller tumors compared to ultrasound measurements.

No significant tumor growth delay was detected upon lomeguatrib treatment compared to the sodium chloride treated mice in either cell line. Also, no tumor growth delay was observed upon 5 Gy or 15 Gy irradiation in any of the implanted cell lines, although tumor quadrupling times were higher in both cell lines upon irradiation. Interestingly, LN18 showed higher tumor quadrupling times after 5 Gy irradiation as after 15 Gy, but U118 revealed opposing results with higher tumor quadrupling times after 15 Gy irradiation.

The differences in tumor growth delay among the two cell lines might root in the different radiosensitivity of the cell lines in vitro. However, U118 is a radiosensitive cell line with a D50 of $1.62 \text{ Gy} \pm 0.14 \text{ Gy}$, while LN18 is an intermediate radioresistant cell line with a D50 of $2.27 \text{ Gy} \pm 0.24 \text{ Gy}$. Therefore, opposing results would have been expected and do not explain the difference in tumor growth delay times. Since the mechanism behind the radioresistance of GBM is not fully understood it is impossible to explain the results from the tumor growth delay experiment. It can be hypothesized that migration might be important since both cell lines have shown differential initial migration behavior. Further, invasion is a crucial process in GBM as well and might contribute to tumor resistance not only to radiation but also to other treatments, such as chemo- and inhibitor therapy.

Also, lomeguatrib did not reveal any significant effect on tumor growth delay in either cell line, which is in accordance with the results from Clemons et al. [58] and Hu et al. [98] who both reported no effect on tumor growth upon 20 mg kg⁻¹ respectively 8 mg kg⁻¹. Here it was shown, that in contrast to the findings from the in vitro experiments lomeguatrib in combination with irradiation did not show a favorable effect in vivo.

However, MGMT inhibition was only assumed but not proven during this thesis after lomeguatrib administration. Therefore, insufficient MGMT inhibition might be a reason for the inconclusive results. As seen from the in vitro results low concentrations of lomeguatrib revealed opposing results to high concentration lomeguatrib treatments. As a direct translation of in vitro concentrations to in vivo concentrations is almost impossible the already published lomeguatrib concentration was administered during this thesis. It is possible that the concentration was too low or too high to observe the hypothesized effects or the treatment duration was too short and consequently, MGMT inhibition was insufficient.

5. Conclusion and Outlook

The overall aim of this thesis was to investigate the role of MGMT in radiation therapy. The highly specific and potent MGMT inhibitor lomeguatrib was used to inhibit MGMT expression in MGMT promoter unmethylated cell lines, i.e. MGMT expressing cell lines *in vitro*, as well as in xenograft tumors *in vivo*.

It is of great importance to mention that this is the first work investigating the MGMT inhibitor lomeguatrib in combination with irradiation *in vitro* as well as *in vivo*.

First, it was demonstrated that lomeguatrib significantly inhibited MGMT protein expression in the three tested cell lines with different radiosensitivity. Already low concentrations resulted in significantly reduced MGMT expression rather shortly after administration. Interestingly, lomeguatrib exhibited different effects at different concentrations; low concentration (1 μM) resulted in increased radiosensitivity while higher concentrations (20 μM) resulted in increased radioresistance in all cell lines. This observation was shown in other cellular processes as well, such as a reduced radiation-induced G2/M arrest upon 20 μM but no change upon 1 μM . However, apoptosis, induction of DNA double-strand breaks as well as DNA damage repair were not altered by lomeguatrib.

While LN18 and U118 cells showed opposing results in the migration assay as well as in the *in vivo* experiments, similar results were shown in the colony-forming assay, cell cycle, and apoptosis analysis. In contrast, T98G, which was the most radioresistant cell line, showed opposing results to the previously mentioned cell lines when they showed similar results. E.g. DSB repair foci were increased in T98G cells upon 1 μM and 20 μM , while LN18 and U118 showed no response. Also, T98G cells were injected subcutaneously into NMRI nude mice but no tumor growth was

observed while LN18 and U118 cells rapidly developed tumors. Also, no migration was observed in T98G, while LN18 and U118 cells showed high migratory potential.

Since the three tested cell lines with initial different radiosensitivity showed different outcomes in almost every experiment the underlying molecular differences of the cell lines need to be further investigated, as well as the individual mutation patterns. E.g. differential p53 expression greatly influences the cell cycle and different miRNA expression patterns might be responsible for different migration behavior. Future experiments need to investigate the underlying mechanisms contributing to the different results upon different lomeguatrib concentrations and need to optimize *in vivo* dosage, timing, and possible fractionated radiotherapy.

Still, this study gives new insights on the dose-dependent effects of lomeguatrib in combination with ionizing radiation, which might be beneficial in the treatment of MGMT promoter unmethylated GBM patients.

6. References

1. Stewart, B., & Wild, C. P. (2019). World cancer report 2014. *Public Health*, 16; 511-519.
2. Siegel, R. L., Miller, K. D., & Jemal, A. (2020). Cancer statistics, 2020. *CA: A Cancer Journal for Clinicians*, 70(1), 7-30.
3. Louis, D. N., Ohgaki, H., Wiestler, O. D., Cavenee, W. K., Burger, P. C., Jouvett, A., Scheithauer, B. W., & Kleihues, P. (2007). The 2007 WHO classification of tumours of the central nervous system. *Acta neuropathologica*, 114(2), 97-109.
4. Louis, D. N., Perry, A., Reifenberger, G., Von Deimling, A., Figarella-Branger, D., Cavenee, W. K., Ohgaki, H., Wiestler, O. D., Kleihues, P., & Ellison, D. W. (2016). The 2016 World Health Organization classification of tumors of the central nervous system: a summary. *Acta neuropathologica*, 131(6), 803-820.
5. Furnari, F. B., Fenton, T., Bachoo, R. M., Mukasa, A., Stommel, J. M., Stegh, A., Hahn, W. C., Ligon, K. L., Louis, D. N., & Brennan, C. (2007). Malignant astrocytic glioma: genetics, biology, and paths to treatment. *Genes & development*, 21(21), 2683-2710.
6. Ohgaki, H., & Kleihues, P. (2013). The definition of primary and secondary glioblastoma. *Clinical cancer research*, 19(4), 764-772.
7. Ohgaki, H., Dessen, P., Jourde, B., Horstmann, S., Nishikawa, T., Di Patre, P.-L., Burkhard, C., Schüler, D., Probst-Hensch, N. M., & Maiorka, P. C. (2004). Genetic pathways to glioblastoma: a population-based study. *Cancer research*, 64(19), 6892-6899.
8. Watanabe, K., Tachibana, O., Sato, K., Yonekawa, Y., Kleihues, P., & Ohgaki, H. (1996). Overexpression of the EGF receptor and p53 mutations

- are mutually exclusive in the evolution of primary and secondary glioblastomas. *Brain pathology*, 6(3), 217-223.
9. Fujisawa, H., Reis, R. M., Nakamura, M., Colella, S., Yonekawa, Y., Kleihues, P., & Ohgaki, H. (2000). Loss of heterozygosity on chromosome 10 is more extensive in primary (de novo) than in secondary glioblastomas. *Laboratory investigation*, 80(1), 65-72.
 10. Ohgaki, H., & Kleihues, P. (2007). Genetic pathways to primary and secondary glioblastoma. *The American journal of pathology*, 170(5), 1445-1453.
 11. Parsons, D. W., Jones, S., Zhang, X., Lin, J. C.-H., Leary, R. J., Angenendt, P., Mankoo, P., Carter, H., Siu, I.-M., & Gallia, G. L. (2008). An integrated genomic analysis of human glioblastoma multiforme. *science*, 321(5897), 1807-1812.
 12. Nakamura, M., Yang, F., Fujisawa, H., Yonekawa, Y., Kleihues, P., & Ohgaki, H. (2000). Loss of heterozygosity on chromosome 19 in secondary glioblastomas. *Journal of Neuropathology & Experimental Neurology*, 59(6), 539-543.
 13. Ueki, K., Ono, Y., Henson, J. W., Efird, J. T., von Deimling, A., & Louis, D. N. (1996). CDKN2/p16 or RB alterations occur in the majority of glioblastomas and are inversely correlated. *Cancer research*, 56(1), 150-153.
 14. Henson, J. W., Schnitker, B. L., Correa, K. M., von Deimling, A., Fassbender, F., Xu, H. J., Benedict, W. F., Yandell, D. W., & Louis, D. N. (1994). The retinoblastoma gene is involved in malignant progression of astrocytomas. *Annals of Neurology: Official Journal of the American Neurological Association and the Child Neurology Society*, 36(5), 714-721.
 15. Beier, D., Hau, P., Proescholdt, M., Lohmeier, A., Wischhusen, J., Oefner, P. J., Aigner, L., Brawanski, A., Bogdahn, U., & Beier, C. P. (2007). CD133+

- and CD133— glioblastoma-derived cancer stem cells show differential growth characteristics and molecular profiles. *Cancer research*, *67*(9), 4010-4015.
16. Zakaria, J., & Prabhu, V. C. (2017). Cortical mapping in the resection of malignant cerebral gliomas. *Exon Publications*, 263-280.
 17. Verger, A., & Langen, K.-J. (2017). PET Imaging in glioblastoma: Use in clinical practice. *Exon Publications*, 155-174.
 18. Fernandes, C., Costa, A., Osório, L., Lago, R. C., Linhares, P., Carvalho, B., & Caeiro, C. (2017). Current standards of care in glioblastoma therapy. *Exon Publications*, 197-241.
 19. Li, Y. M., Suki, D., Hess, K., & Sawaya, R. (2016). The influence of maximum safe resection of glioblastoma on survival in 1229 patients: can we do better than gross-total resection? *Journal of neurosurgery*, *124*(4), 977-988.
 20. Tan, A. C., Ashley, D. M., López, G. Y., Malinzak, M., Friedman, H. S., & Khasraw, M. (2020). Management of glioblastoma: State of the art and future directions. *CA: A Cancer Journal for Clinicians*, *70*(4), 299-312.
 21. Fabian, D., Guillermo Prieto Eibl, M. d. P., Alnahhas, I., Sebastian, N., Giglio, P., Puduvalli, V., Gonzalez, J., & Palmer, J. D. (2019). Treatment of glioblastoma (GBM) with the addition of tumor-treating fields (TTF): a review. *Cancers*, *11*(2), 174.
 22. Stupp, R., Taillibert, S., Kanner, A., Read, W., Steinberg, D. M., Lhermitte, B., Toms, S., Idbaih, A., Ahluwalia, M. S., & Fink, K. (2017). Effect of tumor-treating fields plus maintenance temozolomide vs maintenance temozolomide alone on survival in patients with glioblastoma: a randomized clinical trial. *Jama*, *318*(23), 2306-2316.
 23. Newlands, E., Stevens, M., Wedge, S., Wheelhouse, R. T., & Brock, C. (1997). Temozolomide: a review of its discovery, chemical properties, pre-

-
- clinical development and clinical trials. *Cancer treatment reviews*, 23(1), 35-61.
24. Denny, B. J., Wheelhouse, R. T., Stevens, M. F., Tsang, L. L., & Slack, J. A. (1994). NMR and molecular modeling investigation of the mechanism of activation of the antitumor drug temozolomide and its interaction with DNA. *Biochemistry*, 33(31), 9045-9051.
25. Barciszewska, A.-M., Gurda, D., Głodowicz, P., Nowak, S., & Naskręt-Barciszewska, M. Z. (2015). A new epigenetic mechanism of temozolomide action in glioma cells. *PLoS One*, 10(8).
26. Zhang, J., FG Stevens, M., & D Bradshaw, T. (2012). Temozolomide: mechanisms of action, repair and resistance. *Current molecular pharmacology*, 5(1), 102-114.
27. Kolodner, R. D., & Marsischky, G. T. (1999). Eukaryotic DNA mismatch repair. *Current opinion in genetics & development*, 9(1), 89-96.
28. Pegg, A., & Byers, T. (1992). Repair of DNA containing O6-alkylguanine. *The FASEB journal*, 6(6), 2302-2310.
29. Tano, K., Shiota, S., Collier, J., Foote, R. S., & Mitra, S. (1990). Isolation and structural characterization of a cDNA clone encoding the human DNA repair protein for O6-alkylguanine. *Proceedings of the National Academy of Sciences*, 87(2), 686-690.
30. Hegi, M. E., Diserens, A.-C., Gorlia, T., Hamou, M.-F., De Tribolet, N., Weller, M., Kros, J. M., Hainfellner, J. A., Mason, W., & Mariani, L. (2005). MGMT gene silencing and benefit from temozolomide in glioblastoma. *New England Journal of Medicine*, 352(10), 997-1003.
31. Pegg, A. E., Boosalis, M., Samson, L., Moschel, R. C., Byers, T. L., Swenn, K., & Dolan, M. E. (1993). Mechanism of inactivation of human O6-

- alkylguanine-DNA alkyltransferase by O6-benzylguanine. *Biochemistry*, 32(45), 11998-12006.
32. Dolan, M. E., Moschel, R. C., & Pegg, A. E. (1990). Depletion of mammalian O6-alkylguanine-DNA alkyltransferase activity by O6-benzylguanine provides a means to evaluate the role of this protein in protection against carcinogenic and therapeutic alkylating agents. *Proceedings of the National Academy of Sciences*, 87(14), 5368-5372.
33. McElhinney, R. S., Donnelly, D. J., McCormick, J. E., Kelly, J., Watson, A. J., Rafferty, J. A., Elder, R. H., Middleton, M. R., Willington, M. A., & McMurry, T. B. H. (1998). Inactivation of O 6-alkylguanine-DNA alkyltransferase. 1. Novel O 6-(hetarylmethyl) guanines having basic rings in the side chain. *Journal of medicinal chemistry*, 41(26), 5265-5271.
34. Dolan, M. E., Mitchell, R. B., Mummert, C., Moschel, R. C., & Pegg, A. E. (1991). Effect of O6-benzylguanine analogues on sensitivity of human tumor cells to the cytotoxic effects of alkylating agents. *Cancer research*, 51(13), 3367-3372.
35. Quinn, J. A., Desjardins, A., Weingart, J., Brem, H., Dolan, M. E., Delaney, S. M., Vredenburgh, J., Rich, J., Friedman, A. H., & Reardon, D. A. (2005). Phase I trial of temozolomide plus O6-benzylguanine for patients with recurrent or progressive malignant glioma. *J Clin Oncol*, 23(28), 7178-7187.
36. Quinn, J. A., Jiang, S. X., Reardon, D. A., Desjardins, A., Vredenburgh, J. J., Rich, J. N., Gururangan, S., Friedman, A. H., Bigner, D. D., & Sampson, J. H. (2009). Phase II trial of temozolomide plus o6-benzylguanine in adults with recurrent, temozolomide-resistant malignant glioma. *Journal of Clinical Oncology*, 27(8), 1262.
37. Middleton, M. R., Kelly, J., Thatcher, N., Donnelly, D. J., McElhinney, R. S., McMurry, T. B. H., McCormick, J. E., & Margison, G. P. (2000). O6 -

- (4 - bromothenyl) guanine improves the therapeutic index of temozolomide against A375M melanoma xenografts. *International journal of cancer*, 85(2), 248-252.
38. Watson, A. J., Sabharwal, A., Thorncroft, M., McGown, G., Kerr, R., Bojanic, S., Soonawalla, Z., King, A., Miller, A., & Waller, S. (2010). Tumor O6-methylguanine-DNA methyltransferase inactivation by oral lomeguatrib. *Clinical cancer research*, 16(2), 743-749.
39. Hall, E. J., & Giaccia, A. J. (2006). *Radiobiology for the Radiologist* (Vol. 6). Lippincott Williams & Wilkins.
40. Joiner, M. C., & van der Kogel, A. J. (2018). *Basic clinical radiobiology*. CRC press.
41. Lieber, M. R., Ma, Y., Pannicke, U., & Schwarz, K. (2003). Mechanism and regulation of human non-homologous DNA end-joining. *Nature reviews Molecular cell biology*, 4(9), 712-720.
42. San Filippo, J., Sung, P., & Klein, H. (2008). Mechanism of eukaryotic homologous recombination. *Annu. Rev. Biochem.*, 77, 229-257.
43. Voshart, D. C., Wiedemann, J., van Luijk, P., & Barazzuol, L. (2021). Regional Responses in Radiation-Induced Normal Tissue Damage. *Cancers*, 13(3), 367.
44. Bettstetter, M., Dechant, S., Ruemmele, P., Vogel, C., Kurz, K., Morak, M., Keller, G., Holinski-Feder, E., Hofstaedter, F., & Dietmaier, W. (2008). MethyQESD, a robust and fast method for quantitative methylation analyses in HNPCC diagnostics using formalin-fixed and paraffin-embedded tissue samples. *Laboratory investigation*, 88(12), 1367-1375.
45. Kirstein, A., Schilling, D., Combs, S. E., & Schmid, T. E. (2021). Lomeguatrib Increases the Radiosensitivity of MGMT Unmethylated Human

-
- Glioblastoma Multiforme Cell Lines. *International Journal of Molecular Sciences*, 22(13), 6781. <https://www.mdpi.com/1422-0067/22/13/6781>
46. Ostrom, Q. T., Gittleman, H., Farah, P., Ondracek, A., Chen, Y., Wolinsky, Y., Stroup, N. E., Kruchko, C., & Barnholtz-Sloan, J. S. (2013). CBTRUS statistical report: Primary brain and central nervous system tumors diagnosed in the United States in 2006-2010. *Neuro-oncology*, 15(suppl_2), ii1-ii56.
47. Dungey, F. A., Löser, D. A., & Chalmers, A. J. (2008). Replication-dependent radiosensitization of human glioma cells by inhibition of poly (ADP-Ribose) polymerase: mechanisms and therapeutic potential. *International Journal of Radiation Oncology* Biology* Physics*, 72(4), 1188-1197.
48. Jue, T. R., Nozue, K., Lester, A. J., Joshi, S., Schroder, L. B., Whittaker, S. P., Nixdorf, S., Rapkins, R. W., Khasraw, M., & McDonald, K. L. (2017). Veliparib in combination with radiotherapy for the treatment of MGMT unmethylated glioblastoma. *Journal of translational medicine*, 15(1), 61.
49. Robins, H. I., Zhang, P., Gilbert, M. R., Chakravarti, A., de Groot, J. F., Grimm, S. A., Wang, F., Lieberman, F. S., Krauze, A., & Trotti, A. M. (2016). A randomized phase I/II study of ABT-888 in combination with temozolomide in recurrent temozolomide resistant glioblastoma: an NRG oncology RTOG group study. *Journal of neuro-oncology*, 126(2), 309-316.
50. Bajan, S., & Hutvagner, G. (2020). RNA-Based Therapeutics: From Antisense Oligonucleotides to miRNAs. *Cells*, 9(1), 137.
51. Hong, D. S., Kang, Y.-K., Borad, M., Sachdev, J., Ejadi, S., Lim, H. Y., Brenner, A. J., Park, K., Lee, J.-L., & Kim, T.-Y. (2020). Phase 1 study of MRX34, a liposomal miR-34a mimic, in patients with advanced solid tumours. *British journal of cancer*, 1-8.

-
52. Kirstein, A., Schmid, T. E., & Combs, S. E. (2020). The role of miRNA for the treatment of MGMT unmethylated glioblastoma multiforme. *Cancers*, *12*(5), 1099.
53. Aasland, D., Reich, T. R., Tomicic, M. T., Switzeny, O. J., Kaina, B., & Christmann, M. (2018). Repair gene O6 - methylguanine - DNA methyltransferase is controlled by SP1 and up - regulated by glucocorticoids, but not by temozolomide and radiation. *Journal of neurochemistry*, *144*(2), 139-151.
54. Yoshino, A., Ogino, A., Yachi, K., Ohta, T., Fukushima, T., Watanabe, T., Katayama, Y., Okamoto, Y., Naruse, N., & Sano, E. (2010). Gene expression profiling predicts response to temozolomide in malignant gliomas. *International journal of oncology*, *36*(6), 1367-1377.
55. Christmann, M., Nagel, G., Horn, S., Krahn, U., Wiewrodt, D., Sommer, C., & Kaina, B. (2010). MGMT activity, promoter methylation and immunohistochemistry of pretreatment and recurrent malignant gliomas: a comparative study on astrocytoma and glioblastoma. *International journal of cancer*, *127*(9), 2106-2118.
56. Ugur, H. C., Taspinar, M., Ilgaz, S., Sert, F., Canpinar, H., Rey, J. A., Castresana, J. S., & Sunguroglu, A. (2014). Chemotherapeutic resistance in anaplastic astrocytoma cell lines treated with a temozolomide-lomeguatrib combination. *Molecular biology reports*, *41*(2), 697-703.
57. Reinhard, J., Eichhorn, U., Wiessler, M., & Kaina, B. (2001). Inactivation of O6 - methylguanine - DNA methyltransferase by glucose - conjugated inhibitors. *International journal of cancer*, *93*(3), 373-379.
58. Clemons, M., Kelly, J., Watson, A. J., Howell, A., McElhinney, R., McMurry, T., & Margison, G. P. (2005). O 6-(4-bromothienyl) guanine reverses

- temozolomide resistance in human breast tumour MCF-7 cells and xenografts. *British journal of cancer*, 93(10), 1152-1156.
59. St-Coeur, P.-D., Poitras, J. J., Cuperlovic-Culf, M., & Touaibia, M. (2015). Investigating a signature of temozolomide resistance in GBM cell lines using metabolomics. *Journal of neuro-oncology*, 125(1), 91-102.
60. Taspinar, M., Ilgaz, S., Ozdemir, M., Ozkan, T., Oztuna, D., Canpinar, H., Rey, J. A., Sunguroğlu, A., Castresana, J. S., & Ugur, H. C. (2013). Effect of lomeguatrib–temozolomide combination on MGMT promoter methylation and expression in primary glioblastoma tumor cells. *Tumor Biology*, 34(3), 1935-1947.
61. Diserens, A., De Tribolet, N., Martin-Achard, A., Gaide, A., Schnegg, J., & Carrel, S. (1981). Characterization of an established human malignant glioma cell line: LN-18. *Acta neuropathologica*, 53(1), 21-28.
62. Oraiopoulou, M.-E., Tampakaki, M., Tzamali, E., Tamiolakis, T., Makatounakis, V., Vakis, A. F., Zacharakis, G., Sakkalis, V., & Papamatheakis, J. (2019). A 3D tumor spheroid model for the T98G Glioblastoma cell line phenotypic characterization. *Tissue and Cell*, 59, 39-43.
63. Zhang, Y., Zhao, W., Zhang, H. J., Domann, F. E., & Oberley, L. W. (2002). Overexpression of copper zinc superoxide dismutase suppresses human glioma cell growth. *Cancer research*, 62(4), 1205-1212.
64. Signorell, R. D., Papachristodoulou, A., Xiao, J., Arpagaus, B., Casalini, T., Grandjean, J., Thamm, J., Steiniger, F., Luciani, P., & Brambilla, D. (2018). Preparation of PEGylated liposomes incorporating lipophilic lomeguatrib derivatives for the sensitization of chemo-resistant gliomas. *International journal of pharmaceutics*, 536(1), 388-396.

-
65. Shi, Y., Wang, Y., Qian, J., Yan, X., Han, Y., Yao, N., & Ma, J. (2020). MGMT expression affects the gemcitabine resistance of pancreatic cancer cells. *Life sciences*, *259*, 118148.
66. Pawlik, T. M., & Keyomarsi, K. (2004). Role of cell cycle in mediating sensitivity to radiotherapy. *International Journal of Radiation Oncology* Biology* Physics*, *59*(4), 928-942.
67. Adeberg, S., Bernhardt, D., Harrabi, S. B., Nicolay, N. H., Hörner-Rieber, J., König, L., Repka, M., Mohr, A., Abdollahi, A., & Weber, K.-J. (2017). Metformin enhanced in vitro radiosensitivity associates with G2/M cell cycle arrest and elevated adenosine-5'-monophosphate-activated protein kinase levels in glioblastoma. *Radiology and oncology*, *51*(4), 431.
68. Patties, I., Kallendrusch, S., Böhme, L., Kendzia, E., Oppermann, H., Gaunitz, F., Kortmann, R.-D., & Glasow, A. (2019). The Chk1 inhibitor SAR-020106 sensitizes human glioblastoma cells to irradiation, to temozolomide, and to decitabine treatment. *Journal of Experimental & Clinical Cancer Research*, *38*(1), 1-16.
69. Iliakis, G., Wang, Y., Guan, J., & Wang, H. (2003). DNA damage checkpoint control in cells exposed to ionizing radiation. *Oncogene*, *22*(37), 5834-5847.
70. Taylor, W. R., & Stark, G. R. (2001). Regulation of the G2/M transition by p53. *Oncogene*, *20*(15), 1803-1815.
71. O'Farrell, P. H. (2001). Triggering the all-or-nothing switch into mitosis. *Trends in cell biology*, *11*(12), 512-519.
72. Kastan, M. B., & Bartek, J. (2004). Cell-cycle checkpoints and cancer. *nature*, *432*(7015), 316-323.
73. Giacinti, C., & Giordano, A. (2006). RB and cell cycle progression. *Oncogene*, *25*(38), 5220-5227.

-
74. Network, C. G. A. R. (2008). Comprehensive genomic characterization defines human glioblastoma genes and core pathways. *nature*, *455*(7216), 1061.
75. Wank, M., Schilling, D., Reindl, J., Meyer, B., Gempt, J., Motov, S., Alexander, F., Wilkens, J., Schlegel, J., & Schmid, T. (2018). Evaluation of radiation-related invasion in primary patient-derived glioma cells and validation with established cell lines: Impact of different radiation qualities with differing LET. *Journal of neuro-oncology*, *139*(3), 583-590.
76. Paull, T. T., Rogakou, E. P., Yamazaki, V., Kirchgessner, C. U., Gellert, M., & Bonner, W. M. (2000). A critical role for histone H2AX in recruitment of repair factors to nuclear foci after DNA damage. *Current Biology*, *10*(15), 886-895.
77. Short, S. C., Martindale, C., Bourne, S., Brand, G., Woodcock, M., & Johnston, P. (2007). DNA repair after irradiation in glioma cells and normal human astrocytes. *Neuro-oncology*, *9*(4), 404-411.
78. Valdés-Rives, S. A., Casique-Aguirre, D., Germán-Castelán, L., Velasco-Velázquez, M. A., & González-Arenas, A. (2017). Apoptotic signaling pathways in glioblastoma and therapeutic implications. *BioMed research international*, *2017*.
79. Westphal, S., & Kalthoff, H. (2003). Apoptosis: targets in pancreatic cancer. *Molecular cancer*, *2*(1), 1-14.
80. Menon, M. B., & Dhamija, S. (2018). Beclin 1 phosphorylation—at the center of autophagy regulation. *Frontiers in cell and developmental biology*, *6*, 137.
81. Castedo, M., Perfettini, J.-L., Roumier, T., Andraeu, K., Medema, R., & Kroemer, G. (2004). Cell death by mitotic catastrophe: a molecular definition. *Oncogene*, *23*(16), 2825-2837.

-
82. Eriksson, D., & Stigbrand, T. (2010). Radiation-induced cell death mechanisms. *Tumor Biology*, *31*(4), 363-372.
83. Armento, A., Ehlers, J., Schötterl, S., & Naumann, U. (2017). Molecular mechanisms of glioma cell motility. *Exon Publications*, 73-93.
84. Demuth, T., & Berens, M. E. (2004). Molecular mechanisms of glioma cell migration and invasion. *Journal of neuro-oncology*, *70*(2), 217-228.
85. Møller, H. G., Rasmussen, A. P., Andersen, H. H., Johnsen, K. B., Henriksen, M., & Duroux, M. (2013). A systematic review of microRNA in glioblastoma multiforme: micro-modulators in the mesenchymal mode of migration and invasion. *Molecular neurobiology*, *47*(1), 131-144.
86. Dhruv, H. D., McDonough Winslow, W. S., Armstrong, B., Tuncali, S., Eschbacher, J., Kislin, K., Loftus, J. C., Tran, N. L., & Berens, M. E. (2013). Reciprocal activation of transcription factors underlies the dichotomy between proliferation and invasion of glioma cells. *PLoS One*, *8*(8), e72134.
87. Von Essen, C. (1991). Radiation enhancement of metastasis: a review. *Clinical & experimental metastasis*, *9*(2), 77-104.
88. Steinle, M., Palme, D., Misovic, M., Rudner, J., Dittmann, K., Lukowski, R., Ruth, P., & Huber, S. M. (2011). Ionizing radiation induces migration of glioblastoma cells by activating BK K⁺ channels. *Radiotherapy and Oncology*, *101*(1), 122-126.
89. Serafim, R. B., da Silva, P., Cardoso, C., Di Cristofaro, L. F. M., Netto, R. P., de Almeida, R., Navegante, G., Storti, C. B., de Sousa, J. F., & de Souza, F. C. (2021). Expression profiling of glioblastoma cell lines reveals novel extracellular matrix-receptor genes correlated with the responsiveness of glioma patients to ionizing radiation. *Frontiers in oncology*, *11*.
90. Palumbo, S., Tini, P., Toscano, M., Allavena, G., Angeletti, F., Manai, F., Miracco, C., Comincini, S., & Pirtoli, L. (2014). Combined EGFR and

- autophagy modulation impairs cell migration and enhances radiosensitivity in human glioblastoma cells. *Journal of cellular physiology*, 229(11), 1863-1873.
91. Bou-Gharios, J., Assi, S., Bahmad, H. F., Kharroubi, H., Araj, T., Chalhoub, R. M., Ballout, F., Harati, H., Fares, Y., & Abou-Kheir, W. (2021). The potential use of tideglusib as an adjuvant radio-therapeutic treatment for glioblastoma multiforme cancer stem-like cells. *Pharmacological Reports*, 73(1), 227-239.
92. Wild-Bode, C., Weller, M., Rimmer, A., Dichgans, J., & Wick, W. (2001). Sublethal irradiation promotes migration and invasiveness of glioma cells: implications for radiotherapy of human glioblastoma. *Cancer research*, 61(6), 2744-2750.
93. Horwitz, R., & Webb, D. (2003). Cell migration. *Current Biology*, 13(19), R756-R759.
94. De Ieso, M. L., & Yool, A. J. (2018). Mechanisms of aquaporin-facilitated cancer invasion and metastasis. *Frontiers in chemistry*, 6, 135.
95. Polacheck, W. J., Zervantonakis, I. K., & Kamm, R. D. (2013). Tumor cell migration in complex microenvironments. *Cellular and Molecular Life Sciences*, 70(8), 1335-1356.
96. Hagemann, C., Anacker, J., Ernestus, R.-I., & Vince, G. H. (2012). A complete compilation of matrix metalloproteinase expression in human malignant gliomas. *World journal of clinical oncology*, 3(5), 67.
97. Tritschler, I., Gramatzki, D., Capper, D., Mittelbronn, M., Meyermann, R., Saharinen, J., Wick, W., Keski - Oja, J., & Weller, M. (2009). Modulation of TGF - β activity by latent TGF - β - binding protein 1 in human malignant glioma cells. *International journal of cancer*, 125(3), 530-540.

98. Hu, Y. H., Jiao, B. H., Wang, C. Y., & Wu, J. L. (2021). Regulation of temozolomide resistance in glioma cells via the RIP2/NF - κ B/MGMT pathway. *CNS neuroscience & therapeutics*, 27(5), 552-563.

List of Figures

Figure 1.1: Development of GBM.....	2
Figure 1.2: Treatment scheme for Glioblastoma multiforme.	5
Figure 1.3: Temozolomide mode of action.	7
Figure 1.4: Mode of action of temozolomide in the presence of MGMT.....	8
Figure 1.5: Compton process.	11
Figure 1.6: Photoelectric process and characteristic x-ray production.	12
Figure 1.7: Direct and indirect effects of radiation.....	13
Figure 1.8: Non-homologous end-joining.	14
Figure 1.9: Homologous recombination.....	15
Figure 2.1: PCR amplification curve.	26
Figure 3.1: Colony-forming assay (CFA) to compare survival fractions after pre- and post-plating.....	34
Figure 3.2: Colony-forming assay (CFA) of six established human glioblastoma cell lines.	36
Figure 3.3: Western Blot analysis of all parental cell lines.....	38
Figure 3.4: Western Blot analysis of LN18, T98G, and U118 cell lines.....	39
Figure 3.5: Western Blot quantification of LN18, T98G, and U118 cell lines.	40
Figure 3.6: Cell survival after lomeguatrib treatment.	42
Figure 3.7: Cell cycle distribution after lomeguatrib treatment.	42
Figure 3.8: Western Blot analysis after combined irradiation and lomeguatrib treatment.....	43
Figure 3.9: CFA of LN18 cells treated with 0 μ M, 1 μ M, and 20 μ M lomeguatrib.	44
Figure 3.10: Colony-forming assay of T98G with 1 μ M or 20 μ M lomeguatrib.....	45
Figure 3.11: Colony-forming assay of U118 with 1 μ M and 20 μ M lomeguatrib. ..	46

Figure 3.12: Cell cycle distribution in LN18 cells. 48

Figure 3.13: Cell cycle distribution after lomeguatrib and radiation treatment in T98G cells..... 49

Figure 3.14: Cell cycle distribution after lomeguatrib and radiation treatment in U118 cells..... 50

Figure 3.15: γ H2AX foci in LN18 cells. 51

Figure 3.16: Exemplary figures of γ H2AX foci staining in LN18 cells..... 52

Figure 3.17: γ H2AX foci in T98G cells..... 53

Figure 3.18: Exemplary figures of γ H2AX foci staining in T98G cells. 54

Figure 3.19: γ H2AX foci in U118 cells..... 55

Figure 3.20: Exemplary figures of γ H2AX foci staining in U118 cells. 56

Figure 3.21: Apoptosis after lomeguatrib and radiation treatment in LN18 cells.. 57

Figure 3.22: Apoptosis after lomeguatrib and radiation treatment in T98G cells. 58

Figure 3.23: Apoptosis after lomeguatrib and radiation treatment in U118 cells.. 58

Figure 3.24: Relative wound closure LN18 cells. 59

Figure 3.25: Relative wound closure T98G cells..... 60

Figure 3.26: Relative wound closure U118 cells..... 61

Figure 3.27: Relative tumor growth of LN18 tumors *in vivo* after irradiation and caliper measurement. 64

Figure 3.28: Relative tumor growth of LN18 tumors *in vivo* after irradiation and ultrasound measurement..... 65

Figure 3.29: Relative tumor growth of LN18 tumors *in vivo* after irradiation. 67

Figure 3.30: Relative tumor growth of U118 tumors *in vivo* after irradiation..... 70

Figure 3.31: Relative tumor growth of LN18 and U118 tumors *in vivo*. 72

Figure 3.32: Relative tumor growth of LN18 and U118 tumors *in vivo*. 73

List of Tables

Table 2.1: Characteristics of established human glioblastoma multiforme cell lines.	18
Table 2.2: Primer for MethyQESD.....	24
Table 2.3: Settings for qPCR.....	25
Table 2.4: Preparation of BSA standard dilution series.	27
Table 3.1: D50 values.	35
Table 3.2: Radiobiological parameters of the established human glioblastoma cell lines.	37
Table 3.3: MGMT promoter methylation.....	38
Table 3.4. Doubling times of glioblastoma cell lines.....	41
Table 3.5: Linear-quadratic parameters.....	47
Table 3.6: Tumor growth of LN18 tumors.	62
Table 3.7: Difference in tumor growth of LN18 tumors irradiated at Gulmay or SARRP.....	63
Table 3.8: Calculated p-values for caliper vs. ultrasound measurement.....	66
Table 3.9: Tumor growth delay of LN18 tumors.....	68
Table 3.10: Tumor growth of U118 tumors.	68
Table 3.11: Tumor growth delay of U118 tumors.....	69
Table A.1: Calculated p-values from cell cycle FACS analysis.	109
Table A.2: Calculated p-values from migration assay.	110
Table A.3: Calculated p-values from migration assay.	110

Appendix

Table A.1: Calculated p-values from cell cycle FACS analysis. Calculated applying Student's t-test. p-values in bold are statistically significant. Table reprint from [45].

cell line	comparison	p-value		
		G1	G2/M	S
LN18	0 Gy 0 μ M - 0 Gy 1 μ M	0.7216	0.2716	0.5557
	0 Gy 0 μ M - 8 Gy 0 μ M	< 0.0001	< 0.0001	0.0957
	0 Gy 1 μ M - 8 Gy 1 μ M	< 0.0001	0.0002	0.3799
	8 Gy 0 μ M - 8 Gy 1 μ M	0.6659	0.9615	0.6854
	0 Gy 0 μ M - 0 Gy 20 μ M	0.8523	0.9020	0.9125
	0 Gy 0 μ M - 8 Gy 0 μ M	0.0025	0.0003	0.0849
	0 Gy 20 μ M - 8 Gy 20 μ M	0.0100	0.0374	0.6565
	8 Gy 0 μ M - 8 Gy 20 μ M	0.0332	0.0085	0.0687
T98G	0 Gy 0 μ M - 0 Gy 1 μ M	0.8923	0.3786	0.8771
	0 Gy 0 μ M - 8 Gy 0 μ M	0.0580	0.0003	0.1098
	0 Gy 1 μ M - 8 Gy 1 μ M	0.0419	0.0002	0.0510
	8 Gy 0 μ M - 8 Gy 1 μ M	0.7003	0.9021	0.8021
	0 Gy 0 μ M - 0 Gy 20 μ M	0.6737	0.0140	0.1019
	0 Gy 0 μ M - 8 Gy 0 μ M	0.0006	0.0024	0.9001
	0 Gy 20 μ M - 8 Gy 20 μ M	0.0025	0.0001	0.1456
	8 Gy 0 μ M - 8 Gy 20 μ M	0.0342	0.0511	0.9310
U118	0 Gy 0 μ M - 0 Gy 1 μ M	0.1068	0.7759	0.8115
	0 Gy 0 μ M - 8 Gy 0 μ M	< 0.0001	< 0.0001	0.0007
	0 Gy 1 μ M - 8 Gy 1 μ M	< 0.0001	< 0.0001	0.0041
	8 Gy 0 μ M - 8 Gy 1 μ M	0.6896	0.0941	0.0532
	0 Gy 0 μ M - 0 Gy 20 μ M	0.2950	0.0545	0.6297
	0 Gy 0 μ M - 8 Gy 0 μ M	0.0047	0.0006	0.2414
	0 Gy 20 μ M - 8 Gy 20 μ M	0.0124	0.0019	0.1552
	8 Gy 0 μ M - 8 Gy 20 μ M	0.0809	0.2753	0.7805

Table A.2: Calculated p-values from migration assay. Calculated applying Student's t-test compared to the relative initial area (0 h). p-values in bold are statistically significant.

cell line	time point	0 Gy			8 Gy		
		0 μ M	1 μ M	20 μ M	0 μ M	1 μ M	20 μ M
LN18	6 h	0.7305	0.0063	0.0549	0.6121	0.4098	0.9972
	24 h	0.0385	0.2289	<0.0001	0.1332	0.6353	0.2025
	30 h	0.0262	0.1352	0.0015	0.0167	0.3219	0.1346
	48 h	0.0458	0.1494	0.0001	0.0288	0.0177	0.0929
T98G	6 h	0.1794	0.0620	0.9388	0.4388	0.9864	0.9970
	24 h	0.2691	0.6208	0.0655	0.9880	0.4590	0.0105
	30 h	0.0788	0.6823	0.0659	0.8503	0.4443	0.0081
	48 h	0.0979	0.2985	0.1526	0.3844	0.7570	0.0005
U118	6 h	0.0200	0.0079	0.0030	0.0027	0.0076	0.0001
	24 h	0.0071	0.0038	0.0042	0.0015	0.0011	0.0045
	30 h	0.0017	0.0043	0.0104	0.0074	0.0627	< 0.0001
	48 h	0.0019	0.0007	0.0186	0.0132	0.0126	0.0422

Table A.3: Calculated p-values from migration assay. Calculated applying Student's t-test compared to the relative initial area (0 h). p-values in bold are statistically significant.

dose	time point	comparison	LN18	T98G	U118
0 Gy	6 h	0 μ M vs. 1 μ M	0.1974	0.0868	0.9725
		0 μ M vs. 20 μ M	0.5113	0.7358	0.6716
	24 h	0 μ M vs. 1 μ M	0.5498	0.9731	0.9638
		0 μ M vs. 20 μ M	0.0063	0.1553	0.0238
	30 h	0 μ M vs. 1 μ M	0.4850	0.9813	0.6255
		0 μ M vs. 20 μ M	0.0075	0.4845	0.3734
	48 h	0 μ M vs. 1 μ M	0.4699	0.9495	0.4396
		0 μ M vs. 20 μ M	0.0037	0.4064	0.5125
8 Gy	6 h	0 μ M vs. 1 μ M	0.5093	0.9056	0.1200
		0 μ M vs. 20 μ M	0.7461	0.8321	0.0944
	24 h	0 μ M vs. 1 μ M	0.4434	0.3814	0.0264
		0 μ M vs. 20 μ M	0.2944	0.5151	0.7733
	30 h	0 μ M vs. 1 μ M	0.3822	0.2449	0.5004
		0 μ M vs. 20 μ M	0.1929	0.8852	0.1343
	48 h	0 μ M vs. 1 μ M	0.4017	0.1765	0.2011
		0 μ M vs. 20 μ M	0.0980	0.2300	0.040

Publications

Kirstein, A., Schilling, D., Combs, S. E., & Schmid, T. E. (2021). Lomeguatrib Increases the Radiosensitivity of MGMT Unmethylated Human Glioblastoma Multiforme Cell Lines. *International Journal of Molecular Sciences*, *22*(13), 6781.

Kirstein, A., Schmid, T. E., & Combs, S. E. (2020). The role of miRNA for the treatment of MGMT unmethylated glioblastoma multiforme. *Cancers*, *12*(5), 1099.

Acknowledgments

My deepest gratitude goes to my supervisor Prof. Thomas Schmid for giving me the opportunity to carry out this exciting project in his laboratory. I am very thankful for all the encouraging discussions, guidance, continuous support, and excellent supervision.

I would like to thank my second supervisor, Prof. Björn Menze, for being part of my thesis committee and for the nice meetings and the helpful discussions and ideas.

Also, I want to thank Prof. Klaus Trott, Prof. Stephanie Combs, and Prof. Mike Atkinson for introducing me into the fascinating world of Radiobiology.

Special thanks to Dr. Daniela Schilling for her expertise, steady encouragement, and critical review of my data.

Further, I am deeply grateful to Dr. Sophie Dobiasch for her excellent expertise and support especially during the *in vivo* experiments.

Thank you to PD Dr. Omid Azimzadeh for saving my Western Blots and to Dr. Stefan Bartzsch for supporting me with the data analysis.

I would like to thank all lab members for their technical and intellectual support and the great time I had in the lab.

With all my heart, I am especially thankful for my family for their loving and encouraging support.